NTIA-REPORT-79-24

# Investigation of Digital Microwave Communications in a Strong Meteorological Ducting Environment

R. W. Hubbard

**U.S. DEPARTMENT OF COMMERCE**
**Juanita M. Kreps, Secretary**

Henry Geller, Assistant Secretary
for Communications and Information

August 1979

## Preface

This study was conducted with the support and cooperation of the Capabilities Development Department, Pacific Missile Test Center (PMTC) Point Mugu, California 93042 under MIPR No. N6312678MP31106.

TABLE OF CONTENTS

LIST OF FIGURES

# INVESTIGATION OF DIGITAL MICROWAVE COMMUNICATIONS IN A STRONG METEOROLOGICAL DUCTING ENVIRONMENT

R. W. Hubbard*

This report describes an experiment conducted over a LOS microwave link off the coast of southern California. The objective was to determine the effect of known anomalous propagating conditions, caused by persistent temperature inversions in the atmosphere, on a wideband digital communications system. A channel probe was used to measure the effective impulse response of the transmission channel, and bit-error-rate (BER) measurements were made on the same probe test signal. In addition, a dual receiver was used to investigate the application of angle diversity on the reception of signals in this propagation environment.

The results of the experiment indicate that the test link should, if properly configured, support digital transmission at a mission rate on the order of 50 Mb/s. Recommendations for implementing a digital system for the specific link are given in the conclusions.

Key words: Angle diversity; channel characterization; digital microwave communications; impulse response

## 1. INTRODUCTION

Wideband digital communication links in the microwave frequency band are rapidly being implemented in both commercial and military networks. However, in many areas of the world with differing atmospheric conditions, the performance of these systems has been found to be less than ideal. The performance is degraded from the theoretical primarily due to various forms of frequency selective fading, or multipath. A number of examples have recently been cited

*The author is with the Institute for Telecommunication Sciences, National Telecommunications and Information Administration, U.S. Department of Commerce, Boulder, Colorado 80303.

in the literature by Barnett (1978), Anderson et al. (1978), Dougherty & Hartman (1977), and Samson et al. (1976). Performance results similar to those above are discussed by Hubbard (1978) in relation to the measured channel impulse response function. The latter can be measured using a pseudo-random noise (PN) probe that is described by Linfield et al. (1976).

Because of the performance anomalies that have been observed, there is a new caution among potential users of these digital communication systems, and manufacturers of microwave digital radios are actively seeking adaptive techniques to overcome the problems. In order to be successful, however, additional information is needed in order to characterize the transmission channel, and a detailed assessment of the impact on various modulation techniques should be undertaken. It is in this vein that the experiment described in this report was conducted. It is a first step toward assessing the propagation and transmission characteristics of a particular microwave link for wideband digital communications.

## 2. BACKGROUND

The Pacific Missile Test Center (PMTC) of the U.S. Navy at Pt. Mugu, CA, operates a number of microwave communication links in direct support of mission activities. These links carry both data and voice information critical to range test programs. The microwave links are part of a complex communication network (PMTC, 1976) linking Pt. Mugu centers to the Channel Islands and other range facilities. Personnel at PMTC who are responsible for both the planning and operational aspects of the microwave links have been studying the alternatives for improving the performance and increasing the capacity of the system. A likely alternative to the present systems is to shift eventually to an all-digital communications system, which should improve tandem link performance and provide greater capacity and flexibility. This alternative presents a significant problem or question to resolve because of anamolous

propagation conditions that develop along the California coast at certain times of the year. The question is "What form of digital transmission should be used, and at what rates?" This question forms the background for the experiment discussed in this report.

The PMTC personnel have had many years of experience with their current microwave links that use analog systems, and they are well aware of propagation factors that have degraded these systems in the past. For example, strong temperature inversions are known to build up consistently off and along the coast line near Pt. Mugu in the months of August and September. These inversions cause superrefractive layers, either elevated or surface based, that lead to ducting and/or trapping conditions for microwave signals. These conditions can be overcome to a great extent through the use of both frequency and space diversity systems. However, the resultant fading observed in the propagated signals can be a result of either power fading or multipath fading (or both) under these particular atmospheric conditions. Multipath causes frequency selective fading across the transmission bandwidth, and is generally more detrimental to a digital signal than to its analog counterpart. The problem is compounded by the fact that a digital system degrades very rapidly beyond some threshold level, whereas an analog system is characterized by a more gradual or so-called "graceful" degradation curve.

It is therefore very important to understand and evaluate the potential transmission degradation expected for a digital communications link. The PMTC personnel recognized this fact in their planning phases, and initiated the project discussed in this report. A decision was made to measure the transmission quality of one of the longer over-water links at PMTC during the most dominant period of propagation anomalies. The measurements were conducted by the Institute for Telecommunication Sciences (ITS), National Telecommunications and Information

Administration (NTIA), U.S. Department of Commerce, in Boulder, CO. The objective of the project was to develop sufficient information about the link to guide PMTC personnel in making their decisions regarding digital transmission rates.

## 3. EXPERIMENT DESIGN

The experiment conducted by ITS was planned to provide three pieces of information about the particular microwave link. These are:

1. Characterization based on the impulse response of the transmission channel.*
2. Bit-error-rate (BER) performance under various channel conditions.
3. Evaluate possible performance improvement using a form of angle diversity at the receiving antennas.

### 3.1 Link Description

The test link for the experiment operates between Laguna Peak (LP) near the PMTC to San Nicholas Island (SNI), approximately 65 miles (104.6 km) offshore. The existing microwave system is implemented for transmission in one direction only from SNI to LP, using 10-ft (3-m) parabolic antennas in all locations. Frequency diversity is used at the transmitter on 7.17 and 7.47 GHz, each with a power of 5 watts. The receiver terminal at LP is configured for vertical space diversity reception, with the antennas spaced approximately 125 ft (38 m) apart on the tower.

The elevation at SNI is 912 ft (278 m), and at LP it is 1400 ft (426.7 m) above msl. The transmitting antenna at SNI is 70 ft (21.3 m) above the surface. The lower antenna at LP is approximately 30 ft (9 m) above the surface. The lower antenna is just above a sloping ridge in the immediate foreground, and the terrain from the site slopes steeply to the coast line. Two photographs of the LP site, taken from the beach at Pt. Mugu and

*Transmission channel is used here to connote the microwave propagation path, including the terminal antennas.

a close-up below the tower, are shown in Figure 1. We have not included a profile plot of the link, as it is entirely over water beyond the LP terminal shown in Figure 1.

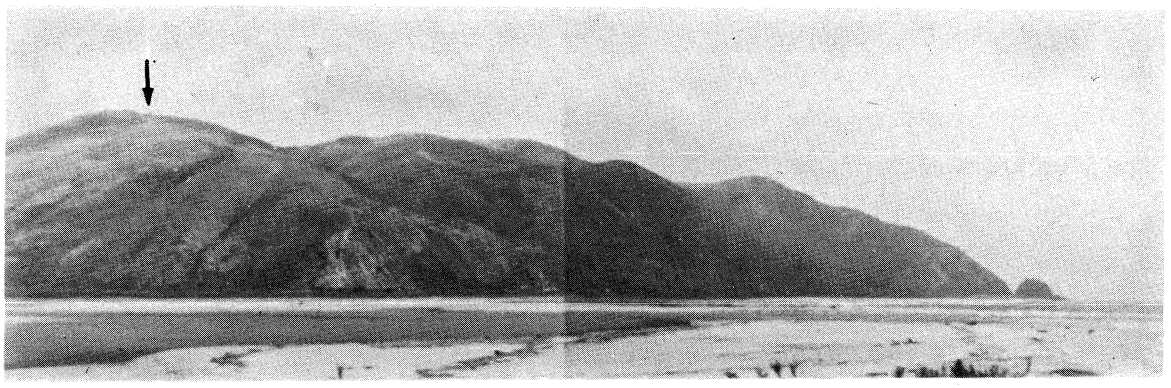

Figure 1. The Laguna Peak (LP) receiver terminal.

## 3.2 Impulse Response Measurements

The instrumentation used for the impulse response measurements was the ITS channel probe mentioned previously, implemented for BPSK operation at three transmission rates of 10 Mb/s, 50 Mb/s and 150 Mb/s. The highest data rate is used to provide a 6 ns resolution to the impulse response measurements. The lower rates were included primarily for making bit-error-rate (BER) measurements over the link, using the same PN code as used for the impulse response measurements. The impulse resolutions for these data rates are 100 ns and 20 ns respectively. However, as will be seen in the data section of this report, the 50 Mb/s transmission rate provided very useful data, when the impulse response and BER were measured simultaneously.

The channel probe was operated at 8.6 GHz, and was duplexed over the existing microwave link with the PMTC microwave signals. The duplexers were installed in the antenna feed lines at both terminals, using waveguide to coax adapters and short sections of low-loss cable. The channel 1 ports of the duplexers are designed to pass 7.15 to 7.7 GHz signals, and the channel 2 port is relatively narrowband for the 8.6 GHz probe test signal. At least 50 dB of isolation between the two ports is provided, and no interference to the PMTC operating frequencies was experienced.

A simplified block diagram of the channel probe is shown in Figure 2. The PN code used 511 bits per sequence ($2^9$-1). The final power amplifier stage of the transmitter is a TWT amplifier capable of up to 20 watts output. However, the power output for these experiments was held to one watt (30 dBm). The receiver for the system is a dual channel instrument (only one channel is shown in Figure 2), so that the impulse response could be simultaneously measured over both receiving antennas. The maximum PN clock rate is 150 MHz, providing an impulse resolution of approximately 6.7 ns. However, the operation of the system is such that the measurement is performed in a millisecond time frame with an equivalent

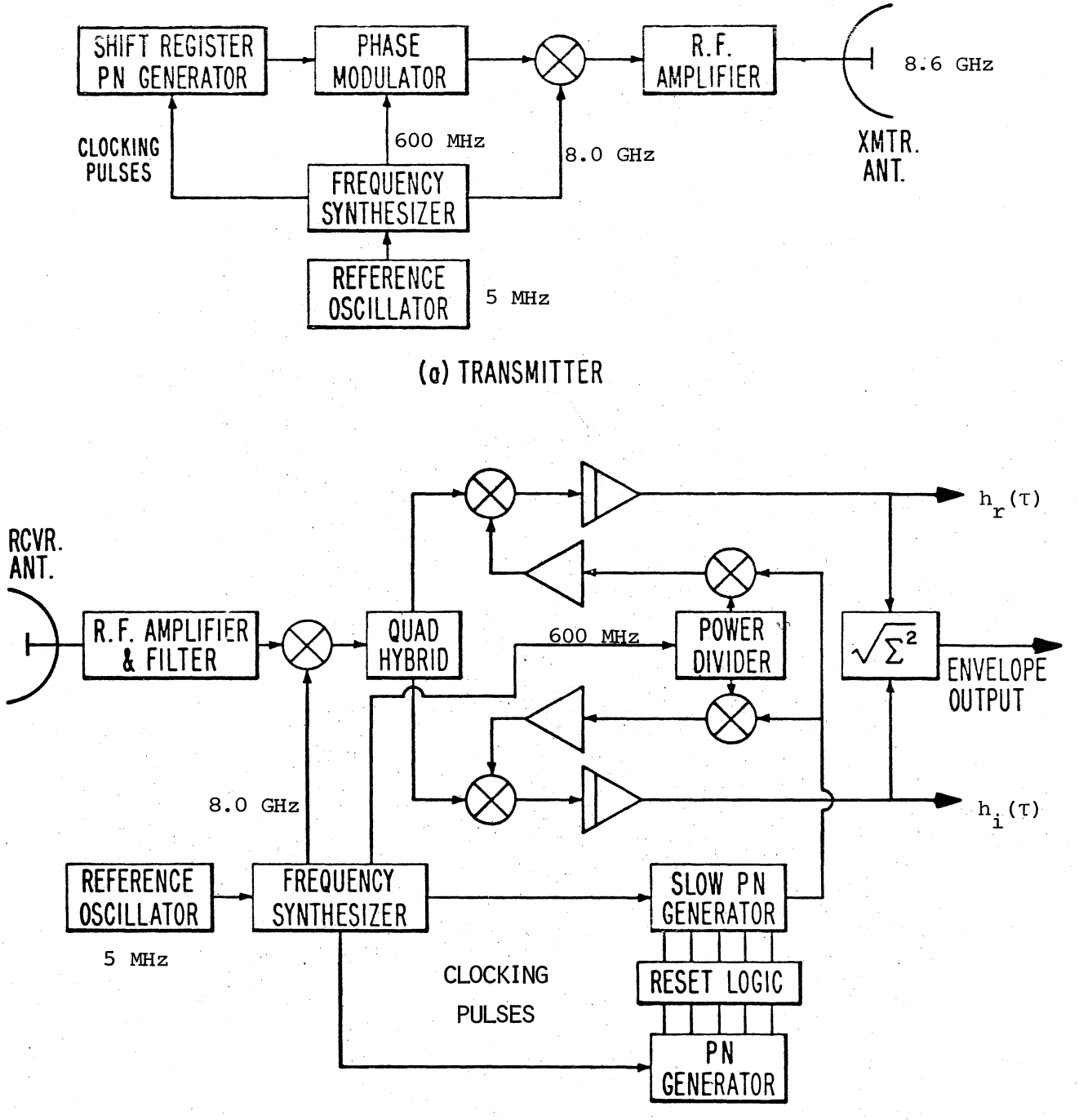


Figure 2. Simplified block diagram of the PN Channel Probe. The receiver is dual channel; only one channel is shown.

resolution in the nanosecond range. This process is described in Linfield et al. (1976). The processing rate in the receiver is variable; i.e., from 1 to 50 impulses per second can be selected. This rate is chosen by the operator to be commensurate with channel variability. For this experiment it was found that 2 responses per second were adequate to keep pace accurately with changes in the channel, and to provide good resolution within the primary response. The window length in this case is 500 ms, corresponding to 3.4 μsec (511 × 6.66 ns) in total delay resolution. Two lower clock rates were also used in the experiment, primarily for the BER performance measurements described below. At the lower rates of 10 and 50 MHz, resolution is lost in the impulse function, but the transmission rate is more typical of the desired digital system at PMTC. The 50 MHz rate (as seen later) did provide significant impulse data however. All three rates provide impulse data that can be conveniently recorded on analog magnetic tape for later playback and analysis. During the measurements, the impulse responses measured for both transmission paths (space diversity) were continuously monitored on a storage oscilloscope. A polaroid scope camera was also used to record the responses periodically.

The receiver of the probe is designed to be self calibrating. A PN modulated signal identical to that of the transmitter is generated in the rf portion of the receiver at a fixed and known level. In the calibrate mode, this signal is fed to both receiver channels through accurate step attenuators for a calibration up to 70 dB in dynamic range. Both the received signal level (RSL), measured at the 600 MHz IF of the system, and the magnitude of the impulse response are calibrated at the same time with this signal.

The probe transmitter is equipped for remote control, using a touch-tone signal system over a voice channel. In the case of the PMTC, a circuit was provided through other radio facilities from LP to SNI. Touch-tone codes are provided for the following operations:

1. Transmitter (TWT):ON-OFF
2. PN code or cw operation
3. Selection of PN clock rate (10, 50 or 150 MHz).

Thus, once installed, the transmitter was left unattended by ITS personnel, and controlled remotely from the LP receiver site.

3.3 Error Rate Measurements

Prior to the PMTC measurements, the probe receiver was modified from its original configuration to include a digital data detector and a phase-locked loop (PLL) on one receiver channel. The PN code used in the test signal to derive the power impulse function was detected and compared in a bit-error-rate system with the locally generated code. A commercial instrument was used for these measurements which was capable of clocking up to 150 MHz. The clock for the error detector was derived from the 5-MHz reference oscillator of the receiver shown in Figure 2. In addition, the reference oscillator was phase locked to the received signal, dividing down from the 600 MHz IF for the locking loop.

Since a bi-phase modulation is used in the probe transmitter for the PN code, the error performance is relative to a bi-phase transmission mode. No signal conditioning was used in the receiver detection scheme, and the signal-to-noise ratio (S/N) was not ideal. As a result, the error rate was not as low as desired for a clear channel (no multipath). However, since relative performance of the digital transmission with respect to the channel response was the primary objective, the measurement scheme proved adequate. The error performance achieved for back-to-back operation is noted in the data section of this report for reference purposes.

As noted previously, it was anticipated that the measurements would be continued during December 1978. However, the ducting conditions did not develop during that month, and our measurements were limited to those obtained during August and September 1978. In the period between September and December,

the receiver detector was improved so that the December BER measurements would have been more direct rather than relative.

3.4 Angle Diversity Measurements

Following the approach used by Hartman and Smith (1975), the experiment was configured to include a tilted-beam antenna measurement to investigate the fading distribution with angle diversity. As was shown in the cited report, under certain multipath conditions the fading range on a microwave link can be significantly reduced using this technique.

For this portion of the experiment, a second dual-channel receiver was used at LP. The two receiver channels could be tuned to either of the PMTC operating frequencies. Two parabolic antennas, each 4 ft (1.2 m) in diameter were mounted side-by-side, on the tower at LP at approximately the same height as the lower antenna for the operating receivers. To establish a baseline for the data on this system, both antennas were originally aligned for maximum RSL and the signal was recorded for some period of time. The two received signals were nearly identical in this configuration, and the receiver gains were adjusted to provide as nearly identical calibration ranges as possible. A signal generator was used to perform the calibrations at the operating frequency. Low-loss foam-flex cable was used between the receivers and the antennas.

After the baseline data had been obtained, one of the antennas was tilted upward to the point that a nominal 2 dB loss in signal level was received on that particular channel. When a multipath signal is received with sufficient difference in the vertical angle of arrival with respect to the more direct path, the tilted antenna pattern provides some magnitude discrimination for a multipath signal arriving from below the more direct path (say from a surface reflection). This was the case in the experiment reported by Hartman and Smith (1975). However, as will be seen from the data section, the multipath observed over the SNI-LP link is not generally due to surface reflection. Thus the angle diversity was not particularly advantageous in this case.

Both individual events and distribution functions of the data are presented in Section 4 and in the Appendix. Plans had been made (for the December 1978 measurements) to tip one antenna downward to verify our results more conclusively. However, as noted above, no measurements were performed in December.

## 4. SUMMARY OF RESULTS

The measurements began on 20 August 1978 after equipment installation and check-out. Arrangements were made with PMTC personnel to obtain radiosonde data taken daily at both Pt. Mugu and at SNI. In addition, a forecast statement was issued by the Navy each day which described the expected meteorological conditions. These data were used to schedule measurement periods. The measurements continued through 18 September 1978. At that time the marine layer, the dominant factor in the propagation mechanism, began to subside. The experiment was stopped, with expectation of continuing during December 1978 as noted previously.

Specific examples of the data analyses for the experiment are presented in this summary and in the Appendix to this report.

In this section we will present a summary of our results, and a discussion of the data analyses that lead to the conclusions given in Section 5.

### 4.1 Meteorological Conditions

During the measurement period in August and the first few days of September 1978, the meteorological conditions relative to the microwave path consistently included either an elevated ducting layer, or ducting conditions that begin near the surface. Typically, the refractive index profile from both Pt. Mugu and SNI consisted of a subrefractive or near zero lapse rate (N/kft) for the first few hundred feet above the surface, and a superrefractive (or ducting) layer, extending to heights near 4000 ft (1219 m). In many cases the ducting layer appeared continuous. Other profiles indicated that the layer was broken into two or more sections. A brief summary of the

profiles most relevant to the radio data are given in Table 1. It should be noted from this table that both terminals of the microwave link were frequently within the noted duct.

4.2. Impulse Response Data

During periods when strong refractive layering or ducting was present over the path, the impulse response data indicated strong multipath conditions. For example, Figure 3 shows two examples of the measured power impulse response of the channel. These responses were photographed directly from the storage oscilloscope during the measurements. The top part of the figure (a) illustrates a clear channel (no multipath) condition, while part (b) shows a very strong multipath component with a delay time of nearly 10 ns. These responses were measured with the highest resolution of the probe system, at a clock rate of 150 MHz. Thus, the base width of the response for a clear channel would be approximately 13.3 ns as shown in Figure 3(a). In general, the delay time of a multipath component can be measured as the difference between the two (or more) peaks in the response. This difference, however, can be misleading for delays shorter than the resolution due to the relative phase of the multipath and the more direct signal. In these cases, the base width of the response will indicate the delay difference when compared with the clear channel width.

There are two distinct ways in which the power impulse response function can be viewed. First, the resultant pulse can be viewed as the actual pulse that would be seen by a receiver if a 6.67 ns impulse had been transmitted. In other words, it displays the distribution of the power in the received pulse as a function of delay time. Thus we note for the response in Figure 3(b) that the pulse has been spread (by the multipath) so that it would extend into the adjacent bit-time had the transmission rate for a digital system actually been 150 Mb/s (the rate for this particular response measurement). The second way of viewing the response is in the more classical sense that it is the equivalent of the impulse response of the

Table 1. Summary of Refractive Index Profile Data.

| DATE (1978) | STATION | TIME | REFRACTIVITY CONDITIONS: |
|---|---|---|---|
| 8/21 | PM | 1633 | Duct: 750' to 1400'<br>Duct: 1500' to 2250' |
| | SNI | 1500 | Subref: 0 to 1000'<br>Stand: 1000' to 1750'<br>Duct: 1750' to 2750' |
| 8/22 | PM | 1545 | Stand: 0 to 1500'<br>Duct: 1500' to 3500' |
| | SNI | 1455 | Subref: 0 to 800'<br>Duct: 800' to 1700' |
| 8/23 | PM | 0500 | Subref: 0 to 400'<br>Duct: 400' to 1900'<br>Duct: 2600' to 3500' |
| | PM | 0915 | Stand: 0 to 1400'<br>Duct: 1400' to 3400' |
| | SNI | 0858 | Subref: 0 to 1000'<br>Duct: 1000' to 3600' |
| | PM | 1555 | Subref: 0 to 400'<br>Duct: 400' to 650'<br>1800' to 2100'<br>3200' to 3900' |
| 8/24 | PM | 0500 | Subref: 0 to 300'<br>Duct: 300' to 2300'<br>2600' to 3700' |
| | PM | 1024 | Stand: 0 to 1400'<br>Duct: 1400' to 1650'<br>2400' to 2800'<br>3250' to 3700' |
| | SNI | 0856 | Subref: 0 to 800'<br>Duct: 800' to 1500'<br>3600' to 3950' |
| | PM | 1553 | Stand: 0 to 600'<br>Duct: 600' to 3700' |
| | SNI | 1455 | Subref: 0 to 900'<br>Severe Duct: 900' to 1000' |
| 8/25 | PM | 0504 | Subref: 0 to 250'<br>Stand: 250' to 1050'<br>Duct: 1050' to 1700'<br>2200' to 2700'<br>3150' to 3600' |
| | PM | 1139 | Duct: 0 to 2400' |
| | SNI | 0900 | Subref: 0 to 1200'<br>Duct: 1300' to 4300' |
| | PM | 1605 | Stand: 0 to 1200'<br>Duct: 1200' to 2000' |
| | SNI | 1411 | Subref: 0 to 1000'<br>Duct: 1000' to 4000' |
| 8/28 | PM | 0507 | Subref: 0 to 250'<br>Duct: 250' to 3000' |
| | PM | 1040 | Stand: 0 to 500'<br>Duct: 500' to 2500' |
| | SNI | 0854 | Subref: 0 to 800'<br>Duct: 800' to 850' |
| | PM | 1657 | Duct: 0 to 1900' |
| | SNI | 1453 | Subref: 0 to 800'<br>Duct: 800' to 2200' |
| 8/29 | PM | 1557 | Stand: 0 to 900'<br>Duct: 900' to 1350'<br>Severe Duct: 1800' to 1950' |
| | SNI | 1455 | Subref: 0 to 1500'<br>Duct: 1500' to 5000' |
| 8/30 | PM | 1556 | Stand: 0 to 2000'<br>Severe Duct: 2200' to 2300'<br>Duct: 2450' to 2850' |
| | SNI | 1452 | Stand: 0 to 1750'<br>Duct: 1750' to 3100' |
| 8/31 | PM | 0509 | Stand: 0 to 1250'<br>Duct: 1250' to 1900' |
| | PM | 1058 | Stand: 0 to 1450'<br>Severe Duct: 1450' to 1650'<br>Duct: 1650' to 2950' |
| | SNI | 0904 | Stand: 0 to 1200'<br>Duct: 1200' to 3700' |
| | PM | 1549 | Stand: 0 to 1100'<br>Duct: 1250' to 2000'<br>2600' to 3200' |
| | SNI | 1458 | Stand: 0 to 1100'<br>Duct: 1350' to 3700' |
| 9/1 | PM | 0515 | Stand: 0 to 1350'<br>Severe Duct: 1350' to 2150' |
| | PM | 0910 | Stand: 0 to 1250'<br>Duct: 1250' to 1850' |
| | SNI | 0901 | Duct: 550' to 1000' |
| | PM | 1607 | Stand: 0 to 1200'<br>Severe Duct: 1200' to 2050' |
| | SNI | 1357 | Subref: 0 to 1500'<br>Severe Duct: 1500' to 1700' |
| 9/5 | PM | 0505 | Subref: 0 to 300'<br>Duct: 300' to 3150' |
| | SNI | 0846 | Duct: 0 to 500'<br>Stand: 500' & above |
| | PM | 1550 | Stand: 0 to 7000' |
| | SNI | 1518 | Stand: 0 to 7000' |
| 9/6 | PM | 1004 | Duct: 0 to 1000'<br>Stand: 1000' to 5000' |
| | SNI | 0851 | Subref: 0 to 500'<br>Stand: 500' & above |
| | PM | 1546 | Duct: 0 to 500'<br>Stand: 500' & above |
| | SNI | 1434 | Subref: 0 to 500'<br>Stand: 500' & above |
| 9/7 | PM | 0000 | Super: 0 to 1850'<br>Subref: 1850' to 2400'<br>Duct: 2400' to 2850' |
| | SNI | 0005 | Super: 0 to 1450'<br>Stand: 1450' to 3400'<br>Duct: 3400' to 4000' |
| 9/8 | PM | 0505 | Duct: 0 to 2400' |
| 9/12 - 18 | All | | Minor ducting above 2400' |

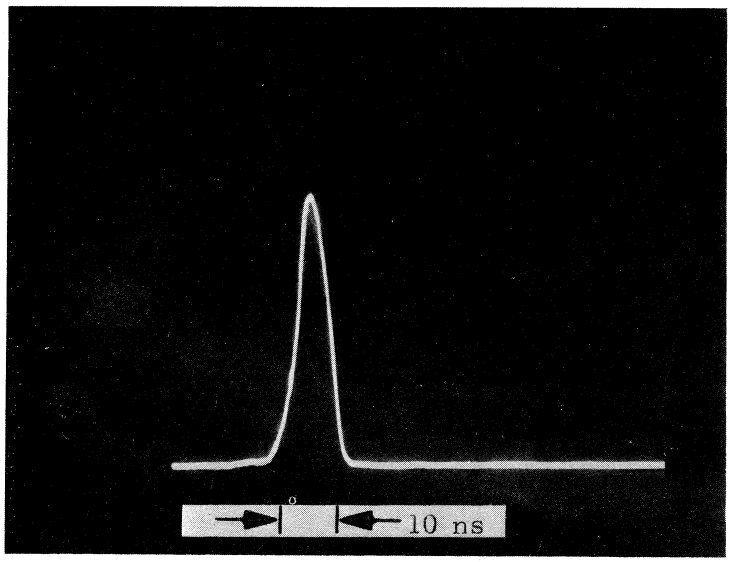


(a) Clear channel response; impulse width is 13.3 ns.

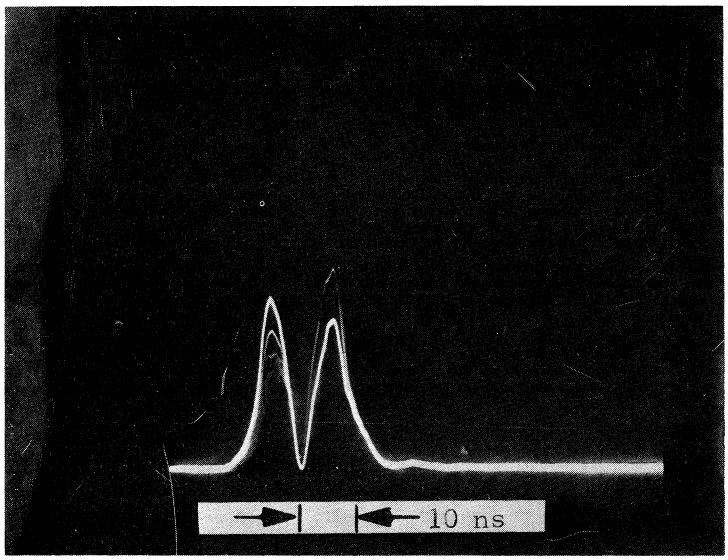


(b) Response with a multipath component delayed 10 ns.

Figure 3. Examples of the power impulse response measured over the SNI-LP link with a PN clock rate of 150 MHz.

channel (filter). Each peak in the response represents signal energy received over the link that has propagated over a different path, and the delay time is directly equivalent to the path length difference. For a time delay of 1 ns, the path length difference is almost 1 ft (actually 0.984 ft/ns). Thus, the measured delay can be used to define an ellipsoid on a plot of the propagation path that will bound the region for the multipath component. This concept is particularly useful if the multipath is a result of a point reflection, but is of no value in the case of refractive multipath. However it can be used to investigate possible reflections from meteorological boundaries. An example of this is presented in Appendix A.

As a simple example of the application of these data to the question of digital transmission performance in a given channel, we consider the response shown in Figure 3(b). We noted above that if this channel were used to transmit digital information at a rate of 150 Mb/s, the performance would be degraded by the channel since one bit is spread to the adjacent bit-time, which results in intersymbol interference. However, if the transmission rate were on the order of 50 Mb/s (one bit-time of 20 ns), the delay spread of 10 ns in the response does not result in intersymbol interference. The received pulse is merely distorted by the multipath, and in most instances it would be interpreted correctly by the receiver. This view of the multipath situation is over simplified, but is a useful concept for initial evaluation of the channel. Obviously, the prolonged performance must be based on a statistical summary of the response; how frequently does the multipath exist and how does it vary with time?

The impusle response may also be used to develop a frequency domain view of the transmission channel (Rummler, 1978). This concept is frequently convenient, as most communication engineers are more familiar with frequency functions than their equivalent time domain functions. Also, the frequency domain concept of the transmission channel is used in recent

literature concerning the performance of digital communication systems. Some of this literature is referenced in the Introduction. The frequency transfer function of a channel or device is derived from the Fourier transform of its impulse response. Other statistics of the channel characteristics may be derived from various operations on the impulse response, as presented in a paper by Gallager (1964). For example, the familiar frequency correlation function is the Fourier transform of the power impulse function measured by the channel probe. Examples of this transform are included in the paper by Hubbard (1977), where the results show the coherent bandwidth of the channel. Transforming a delta-function impulse response on a theoretical basis provides a very useful method of analyzing the channel behavior, and determining some limiting performance values. For example, if we use the response information of Figure 3(b), where there is an initial (direct) response and a multipath component of nearly equal magnitude at a delay of 10 ns, we can construct the corresponding frequency transfer function assuming the impulse function to be composed of a delta function at a delay $\tau_o = 0$ and another at $\tau_1 = 10$ ns. The transform is sketched in Figure 4. The nulls in the frequency response function are separated by

$$\Delta f_n = \frac{1}{\tau} = \frac{1}{10 \text{ ns}} = 100 \text{ MHz}, \qquad (1)$$

and the frequency of the nulls are found from

$$f_n = \frac{n}{2\tau} \qquad (2)$$

where n is a series of either even or odd integers depending on the relative phase of the multipath component. If the multipath is derived from a reflection with an associated phase reversal the series is even, and the first null of the transfer function will occur at $f_n = 1/\tau$. If the multipath is derived in the channel from refraction, or diffraction, then the delayed signal does not undergo a phase reversal and the series becomes odd. The first null of the transfer function

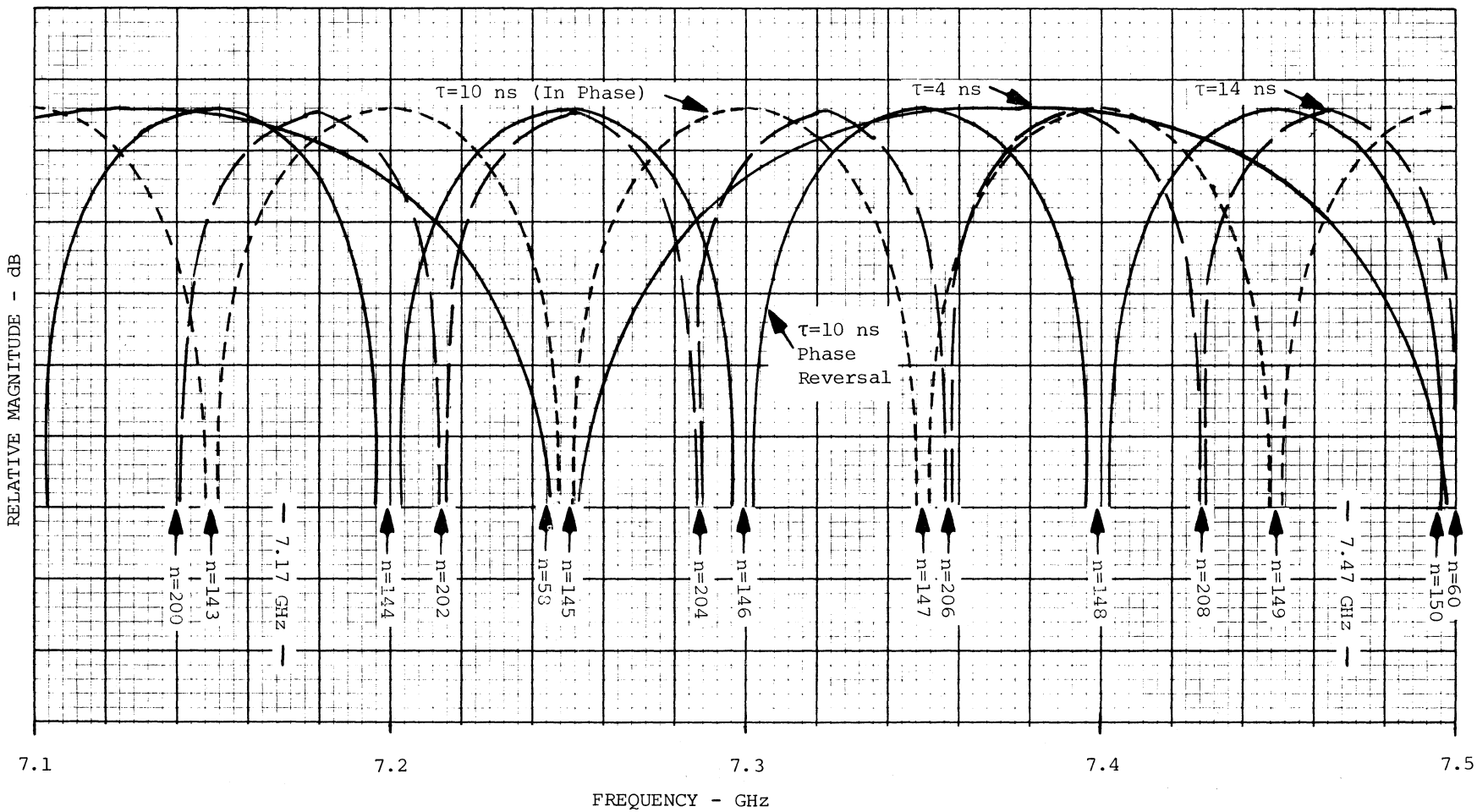


Figure 4. The theoretical frequency transfer function for a channel with a multipath component equal in magnitude to the direct component, at the delay times indicated.

in this case will fall at $f_n = 1/2\tau$. Both of these conditions are depicted in the functions in Figure 4 for a delay of 10 ns. The first case is shown as the solid-line function, and the second with the short dashed curve. Phase relationships between these extremes result in a shift of the nulls along the frequency axis with a slight change in their separation. This concept is important to our later conclusions for the SNI-LP path.

Another important concept to visualize is the effect of changing time-delays in the multipath channel. For example, we are assuming for the moment that the functions depicted in Figure 4 are representative of a nominal (observed) delay of 10 ns. However, as seen from the data below, the relatively stable delay over the link ranged in value from around 4 ns to as long as 14 ns. The theoretical transfer functions for delays of these values are also sketched in Figure 4. It is difficult to convey the dynamics of the channel using these static descriptions. However, using the on-site observations and the analysis of the data summarized in the Appendix, we can discuss system performance aspects and reach some conclusions. The delay magnitudes of 4 and 14 ns are representative of the "worst case" conditions observed. The first important consideration is to note that with a delay component of 14 ns, the coherence bandwidth of the channel could become relatively narrow compared to the required bandwidth for a 50 Mb/s (nominal) mission bit stream; the theoretical transfer function seen in Figure 4 has a null-to-null width $\Delta f_n = 71.4$ MHz for this case. Obviously the mission bit-stream spectra would suffer some in-band distortion at either of the two operating frequencies (noted in the figure) for the PMTC system, even when the channel conditions remain fairly static as shown. However, as discussed later in this report, there are techniques under development for digital microwave systems to combat adaptively these in-band distortions. The most severe problem for system performance would occur whenever a deep null of the channel transfer function "moves" across the signal passband. Thus, we must

consider the dynamics of the channel, and the following paragraphs summarize our analysis and results. Details of the analysis are given in the Appendix.

The "worst case" conditions observed during the experiment occurred on 31 August 1978 at a time when a fairly strong ducting-type refractive layer existed between the SNI and LP terminals. The radiosonde data indicated that the layer extended over the entire length of the propagation path, with a steeper, more defined trapping gradient near the LP terminal and a broken gradient toward the SNI terminal. The refractivity profiles for these conditions are shown in Figure 5, as measured during the morning hours. Note that the layer thickness was about 200 ft (61 m) near the LP terminal, and that at least for a time, both terminals were probably embedded in the layer. The stability of the layer during the day can be assessed from the profile plots shown in Figure 6, which were obtained from the afternoon radiosonde launches. Note that the very strong ducting gradient at LP during the morning run has changed to some extent, and the profiles for the two ends of the path are more nearly the same. In addition, the morning and afternoon profiles from SNI are seen to be quite similar, indicating a fairly stable condition during the day.

Before discussing the channel dynamics in any detail, we wish to characterize the impulse response data for this particular date with the following statements:

1. The channel could be readily characterized with a two-path model most of the time.
2. Delays measured in the multipath structure remained relatively fixed for periods of minutes and longer.
3. Delay components were rarely observed to change in the space diversity channels at the same time.
4. The distribution of power in the impulse response changes slowly over periods of several seconds.

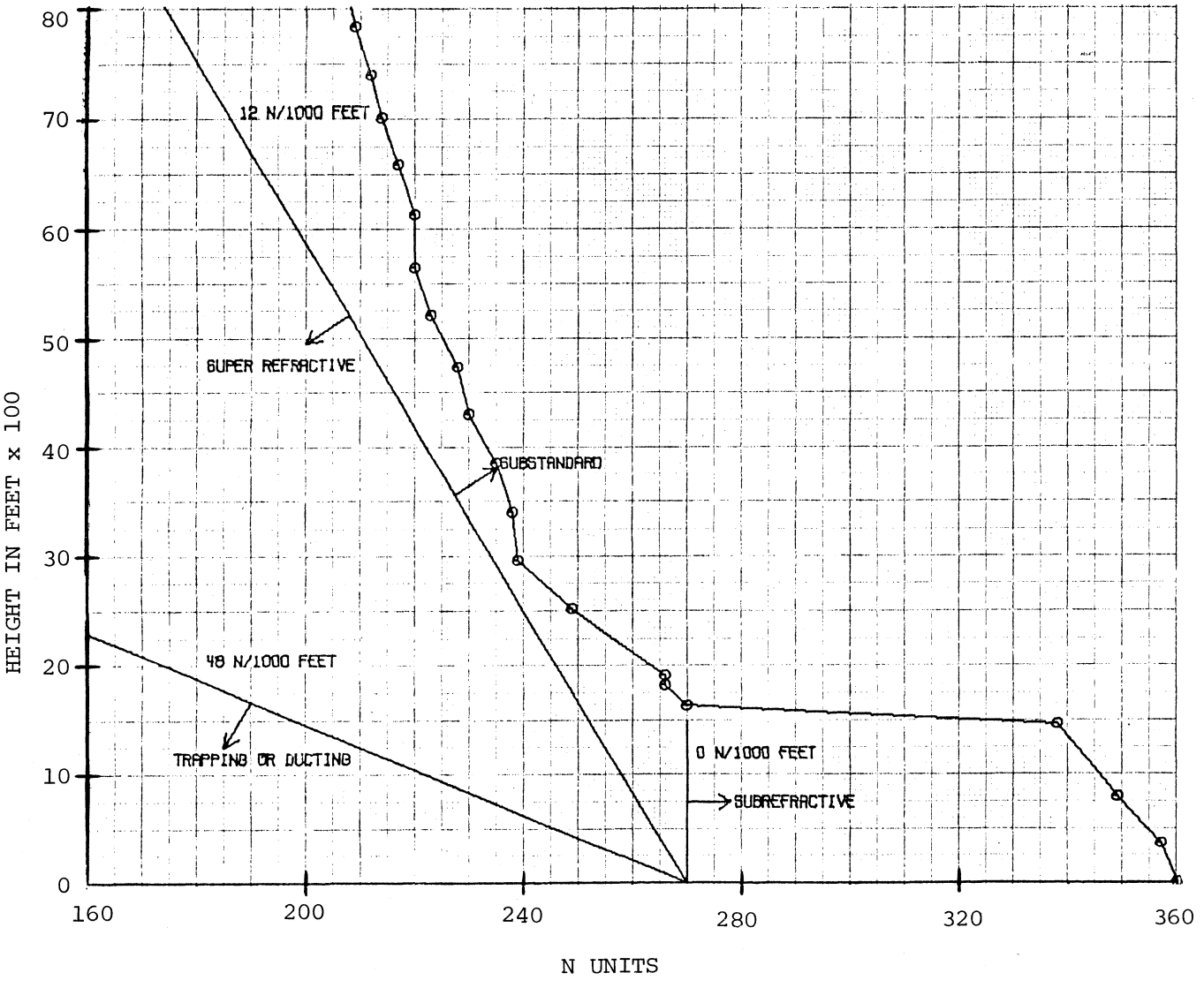


Figure 5(a). Refractive index profile for Pt. Mugu at 1058 PST, 31 August 1978.

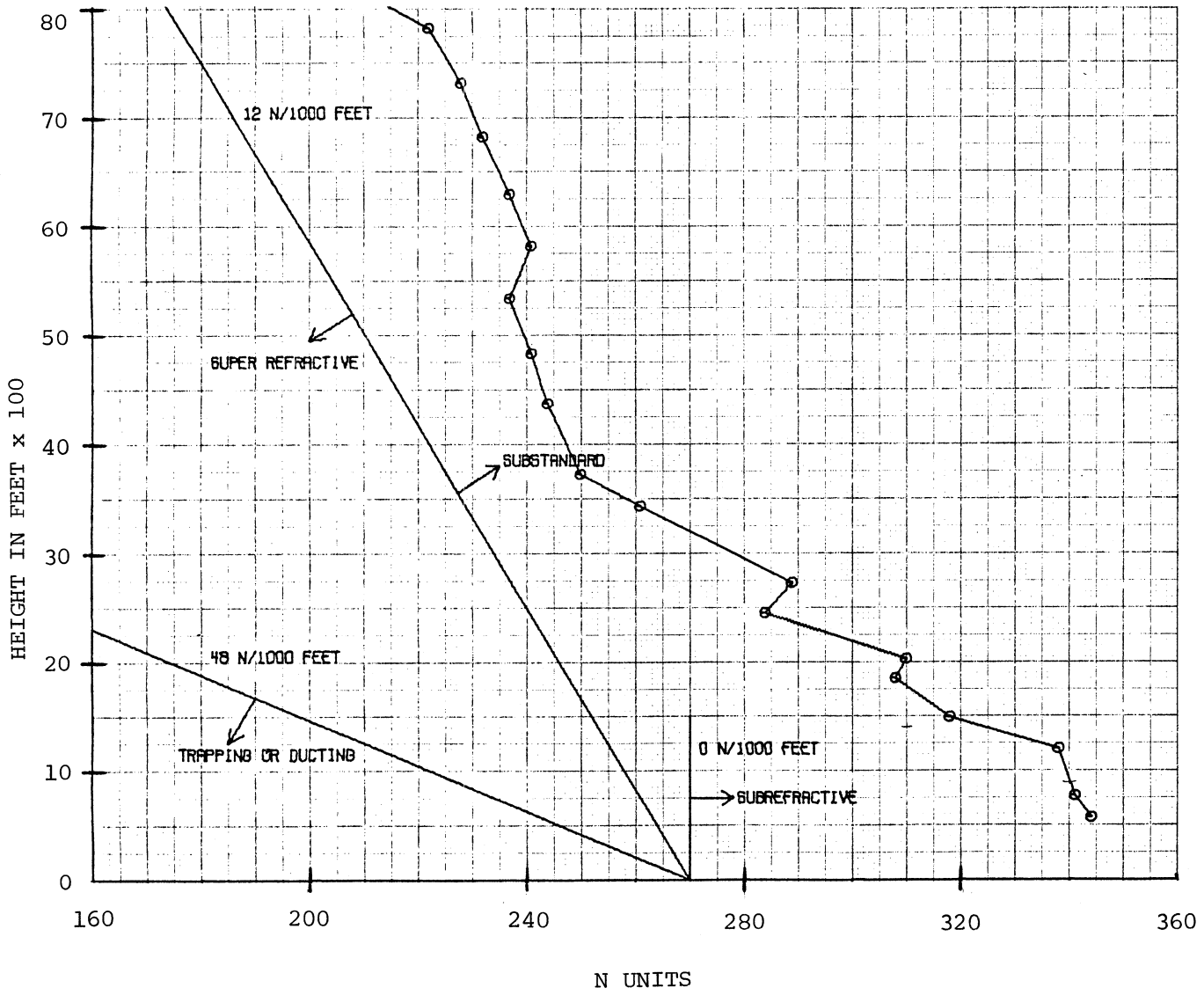


Figure 5(b). Refractive index profile for SNI at 0904 PST, 31 August 1978.

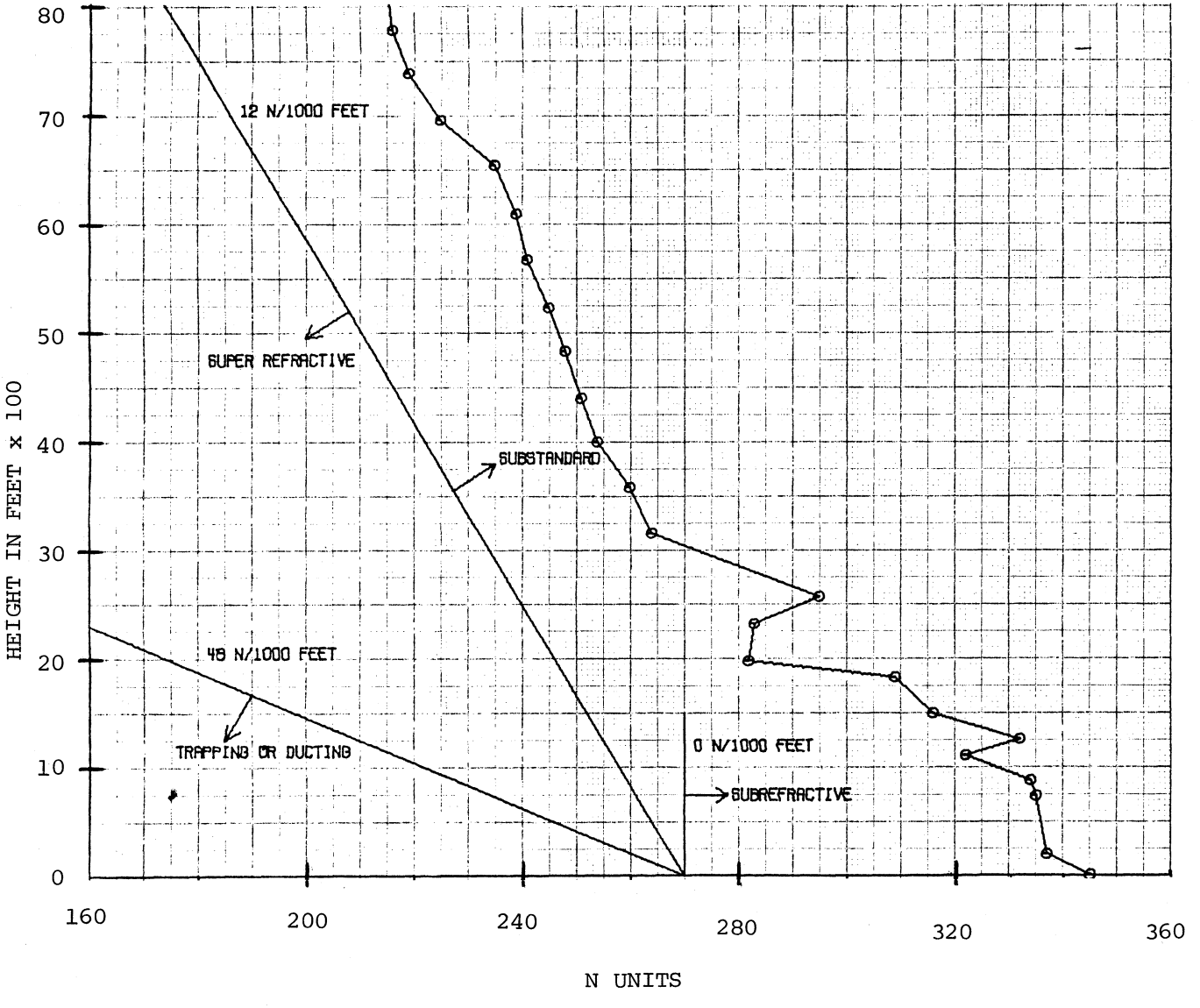


Figure 6(a). Refractive index profile for Pt. Mugu at 1549 PST, 31 August 1978.

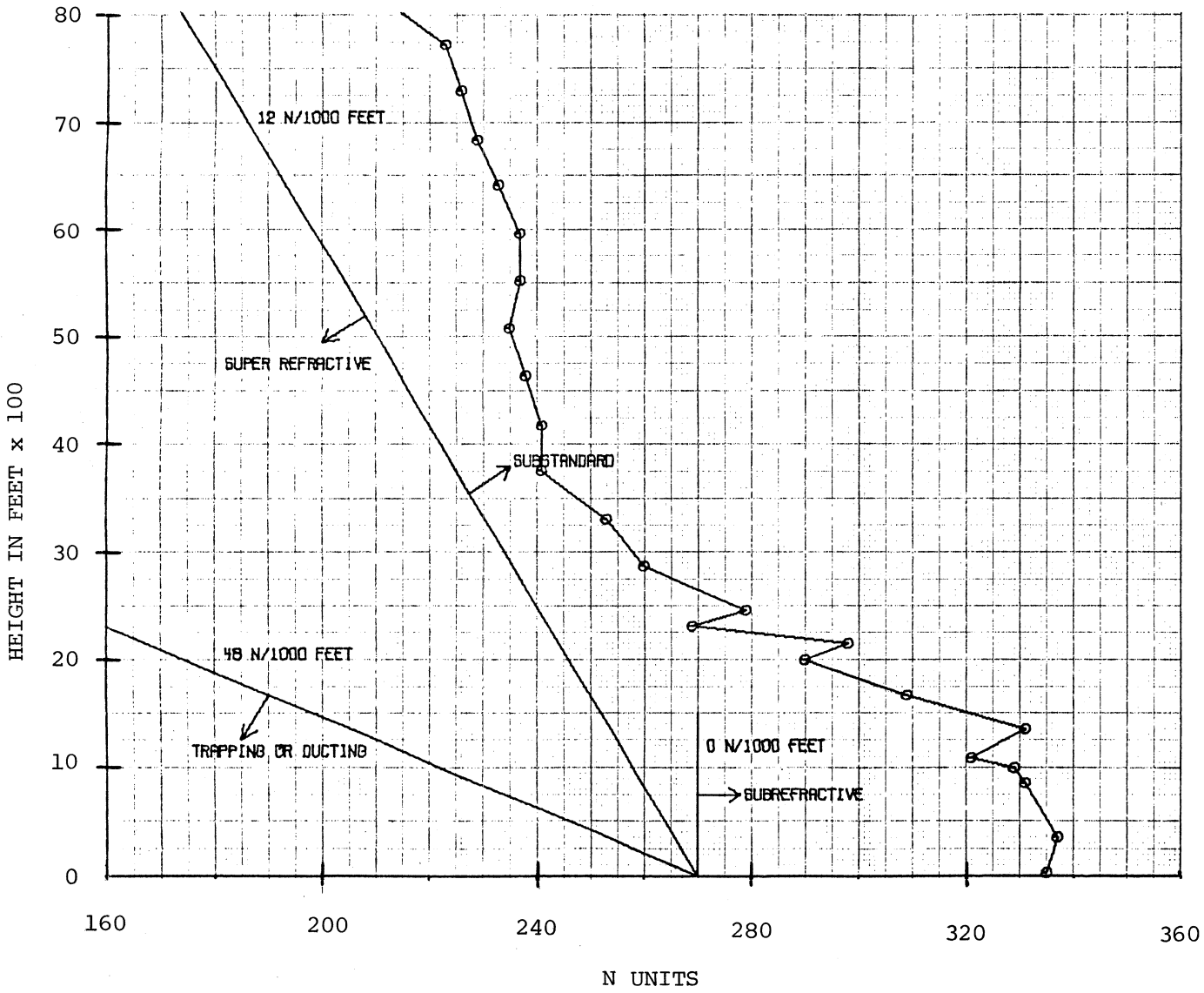


Figure 6(b). Refractive index profile for SNI at 1458 PST, 31 August 1978.

An example of the power distribution change is illustrated with the photograph of the measured response shown in Figure 7. This power impulse was measured at the 150 MHz clock rate, yielding a response width of 13.3 ns. As seen from the figure, two fairly equal signals were first observed with a relative delay time on the order of 14 ns. The sequence of responses are 500 ms apart in observation time, progressing from top to bottom of the figure. Note that the two components are initially of nearly equal magnitude, but that the first response begins to decay as the delayed response increases in magnitude. This dynamic change results in possibly the worst case for system performance, since the digital receiver would (perhaps) first be synchronized with the first response signal. As this response fades below threshold, the system would lose sync and be required to re-sync on the delayed signal. This condition would result in a period of high error during the response change and the re-acquisition time required in the receiver. Error performance measurements associated with this dynamic response will be shown in Section 4.3.

In the time domain, the above channel condition illustrates a sudden change in total path transmission time as the signal energy shifts from the initial response to the delayed response or vice versa. In the frequency domain it can be visualized as a collapse of the frequency transfer function, followed by a transient recovery of the function with a different total path transmission time. After the digital system has been able to re-sync to the dominant signal path, then only the relative path delays are important.

Referring again to Figure 4, the theoretical transfer function for the two-path model can be used to illustrate two additional forms of performance degradation. The first to be considered is the effect of a change in delay-time for the multipath component relative to the more direct signal. We note from the figure that as the delay-time changes, nulls in the transfer function will appear to move through the passband

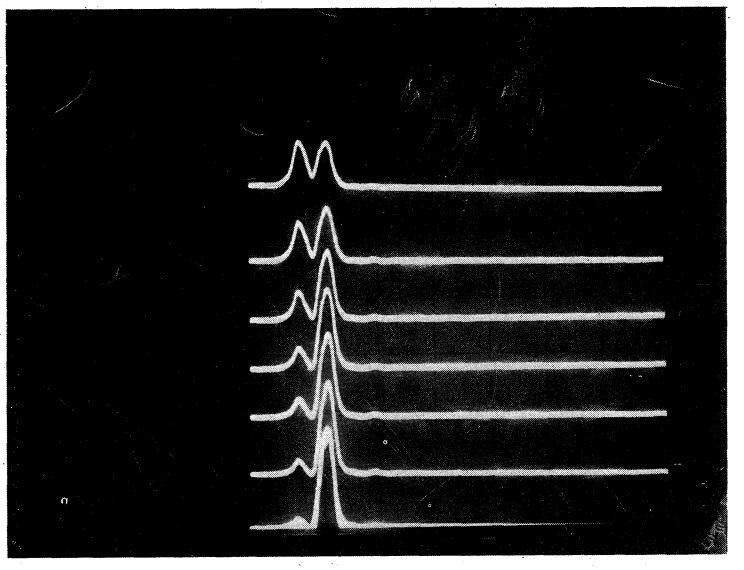

(a) Sequential responses, 500 ms apart from top to bottom.

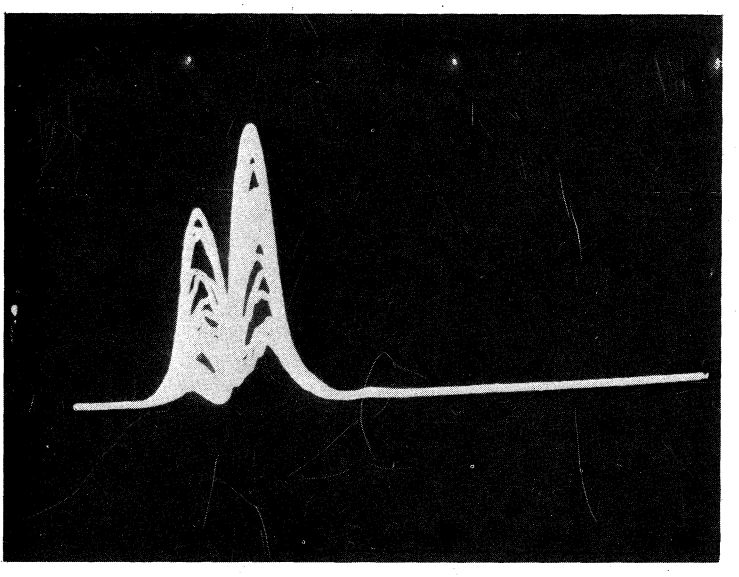

(b) Time-lapse photograph of the sequence in (a) on an expanded scale.

Figure 7. An example of the dynamic magnitude change between multipath components.

of the transmitted signal. The extreme of this example is to assume a change in delay from 14 ns to 4 ns in the figure. The concept on the frequency axis can be visualized by considering the transfer function baseline as a stretching rubber band with the cycloid shape of the function retained as it is stretched. The nulls become farther and farther apart, and a great many of them will move through the signal passband as the function is stretched. For example, we note from the figure that the first null (for $\tau$ = 14 ns) to move through a signal at 7.17 GHz is that labeled for n = 200, and the last one would be (for $\tau$ = 4 ns) where n = 58. Thus, in this case we would visualize a total of 71 nulls moving through the signal passband over the time required for the delay change from 14 to 4 ns. Similarly, 74 nulls would have been observed at the 7.47 GHz frequency for the same delay-time change. However, as the delay time changes so also does the relative phase of the two components, and thus the effect of any given null in the dynamic sense would be difficult to predict. It is clear that in-band distortions to the signal will occur, and notches will cause frequency selective fading.

The second change we wish to consider is one brought about by a relatively fixed delay time between the two components, but the relative phase slowly changes. Before discussing this situation, however, we should point out the manner in which phase information can be observed from the power impulse response measurements. For example, in the impulse measurements shown in Figure 7 we note that the delayed multipath is observed as an almost distinct response; i.e., it is delayed more than the resolution of the probe system. Thus, in this case the relative phase of the two components cannot be directly seen from the power impulse response; it can only be determined from the co- and quadrature correlation functions measured in the probe receiver. However, when the lower clock rates such as the 10 MHz and 50 MHz are used for the impulse measurements, the resolution is less and the relative phase is registered in the power impulse. For example, assume the delayed component with

a delay of 14 ns is observed in a measurement using the clock rate of 50 MHz. The resolution of the system for a distinct separate response for a multipath component is then 20 ns. A component with less delay than this will produce an impulse response that overlaps the more direct signal. If the delayed component is nearly in phase with the earlier one, the overall response will be broadened and the delay component will generally be seen as a distortion or with a distinct peak on the trailing edge of the response. If the delayed component approaches an out-of-phase condition, the power impulse will begin to split into two distinct pulses; i.e., with a notch developing within the resolution time. Examples of these two types of response are shown in Figure 8. Because of this characteristic the relative phase of the two components can be judged from individual responses, and delayed components less than the resolution time can usually be detected.

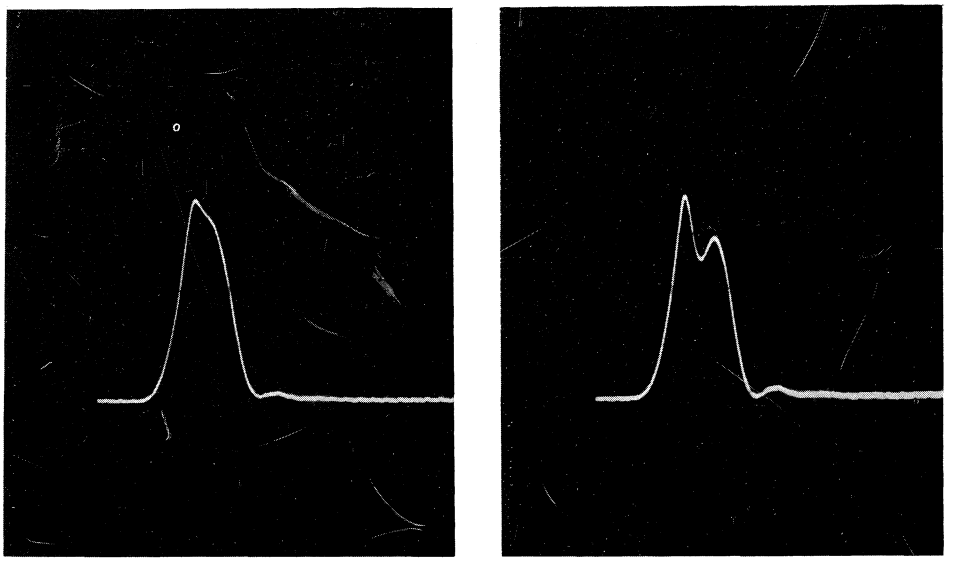

(a) Components near an in-phase relationship.

(b) Components approaching an out-of-phase relationship.

Figure 8. Examples of the power impulse response where the multipath component delay is within the resolution of the probe.

A change in relative phase between components can be transformed to the frequency transfer function as a shift of the function along the frequency axis. For example, in Figure 4 we have plotted the theoretical function for a delay of 10 ns when the two components are considered to be both in and out of phase with each other. Thus, a change in the relative phase with time will be visualized by a gradual shift in the one function toward the position of the other, and one null of the transfer function will move through the signal passband. This phenomenon seemed to be quite prevalent in the data for the SNI-LP measurements, i.e., the delay times were quite stable for periods of minutes and longer, but the relative phase could change many times during the period. Fading of the received signal level (RSL) could invariably be correlated with these phase changes, and the bit-error-rate (BER) performance measured on the probe signal (see Section 4.3) could be traced usually to an out-of-lock condition as the null moved through the signal passband. Examples of these data are presented below.

One other observation should be made before concluding this discussion. We note again from Figure 4 that multipath with shorter delays will produce fewer null frequencies in the transfer function, and thus fewer of them will impede the signal passband as the delay time changes by small degrees. However, we also note that the in-band distortion produced by a null resulting from a short delay time will be more severe; the attenuation of the signal components at a given level spans a broader frequency range. This characteristic might be summarized by observing that shorter path delays result in a lower probability of in-band distortions to a digital system, but that a null in the transfer function can produce significantly higher distortions for longer periods of time. Examples of this were observed many times in the SNI-LP link measurements, made possible only by the fact that the experiment permitted simultaneous observation of the impulse response of the channel,

the corresponding RSL, and the BER measure of the test signal bit stream.

It is almost impossible to convey to paper a complete description of the dynamics of the channel measurements, as it depends on a combination of the three pieces of information noted above. We have attempted in this section to illustrate the dynamic situation, based on the analysis and visual observations of the measurements. Examples to aid the reader have been presented, and more appear in later sections and the Appendix of this report. We have tried to include a sufficient sample and resumé of each of these three elements combined to demonstrate at least the results that have led to our conclusions for the SNI-LP link given in Section 5.

Before going to a discussion of the BER and RSL measurements, we wish to emphasize two important summary observations stated earlier in this section. All of the discussion and illustrations to this point have been relevant to a single propagation path; i.e., for a non diversity implementation. The SNI-LP path is, however, instrumented for both space and frequency diversity. The impulse response measurements were performed on both space diversity paths simultaneously. Results of these simultaneous observations bore heavily on our final conclusions. The measurements on each of the two paths were very similar. However, two distinctions could be made: first, the prevalence of multipath was higher for the lower receiving antenna at LP, and secondly, multipath with the same relative phase was only occasionally seen in both paths at the same time, and the dynamic changes were uncorrelated. The BER performance measures were scanned critically during these occasions and found to be acceptable on the monitored channel during the stable condition. The lack of correlation during impulse response changes indicates that good diversity performance can be expected. This conclusion is discussed in more detail in

Section 5. Statistical summaries of the impulse shape and width distributions are presented in the Appendix.

4.3 BER Performance vs. Channel Conditions

The limitations of the BER performance measurements for this experiment were pointed out in Section 3. A modification was made to the probe receiver to permit this measurement with a minimum of components. Prior to this modification, the PN code used for the impulse response test signal was not directly detected in the receiver. The minimum requirements for the BER feature consisted of providing a phase-lock loop on the receiver oscillator, a balanced-mixer detector for the recovery of the received PN code, and generation of a clock signal related to the received code for use with the error detector. The latter was a commercial instrument set so that the internal PN code length and format matched that generated in the probe system. The phase-lock loop (PLL) was closed between the received 600 MHz IF and the 5 MHz reference oscillator, and a data clock signal was generated from the PLL controlled oscillator. The PN code detection was made without benefit of any signal conditioning or shaping. In addition, the receiver was designed to restrict the signal bandwidth for only a PN clock rate at 150 MHz. The bandwidth was not restricted when measurements were made at the lower clock rates. As a result, the signal-to-noise ratios ($E/N_o$) for any of the data rates were not ideal. The back-to-back error performance at 150 Mb/s was on the order of $1 \times 10^{-6}$, and a decade better at the 50 Mb/s and 10 Mb/s rates.

However, it was not intended to perform any detailed BER measurements for statistical summaries in this experiment. The BER measure was primarily intended for use as a reference monitor of the channel performance in respect to the channel impulse function. For this application, the BER data were valuable on a relative basis, and for correlating various channel conditions. The prime objective was to characterize the transmission channel without regard to any particular

system or transmission mode. The BER measure is, however, representative of BPSK transmission in a nondiversity channel, since this is the modulation scheme used for the channel probe system.

To illustrate the application of these data with respect to the channel response functions and the RSL, we have chosen a few typical examples to present in this section. The data were taken from a period around 1300 in the afternoon of 31 August 1979, for which the refractive index profiles for the path spanning this time were given in Figures 5 and 6. This period was selected because it was representative of the "worst case" conditions found during the experiment, and it also embodied most of the channel conditions discussed in Section 4.2 with respect to the impulse response. Before presenting these data however, we wish to describe the recording and analysis features that are common to all of the figures presented.

The BER was recorded simultaneously with other data signals on a multi-channel chart recorder. Three channels of the recorder were used to register the BER count from the commercial error detector. The first two channels registered the first two significant figures (integer and decimal) of the BER, and the third channel registered the exponent value. These values were recorded as voltage level changes over a decade in each channel. The other data signals were the RSL for each channel of the probe receiver, the RSL for each channel of the tilted beam antenna experiment (discussed in the following section), and a time signal. The latter was derived from an IRIG Code B time-code generator which was used for precise timing on the associated magnetic tape recordings. The magnetic tape was used to record the impulse response data, the tilted beam data, and one RSL record from the Probe receiver. Thus, the timing signal and duplicate data provided a ready means of correlating the tape and chart records. A sample of the complete chart record is shown in Figure 9.

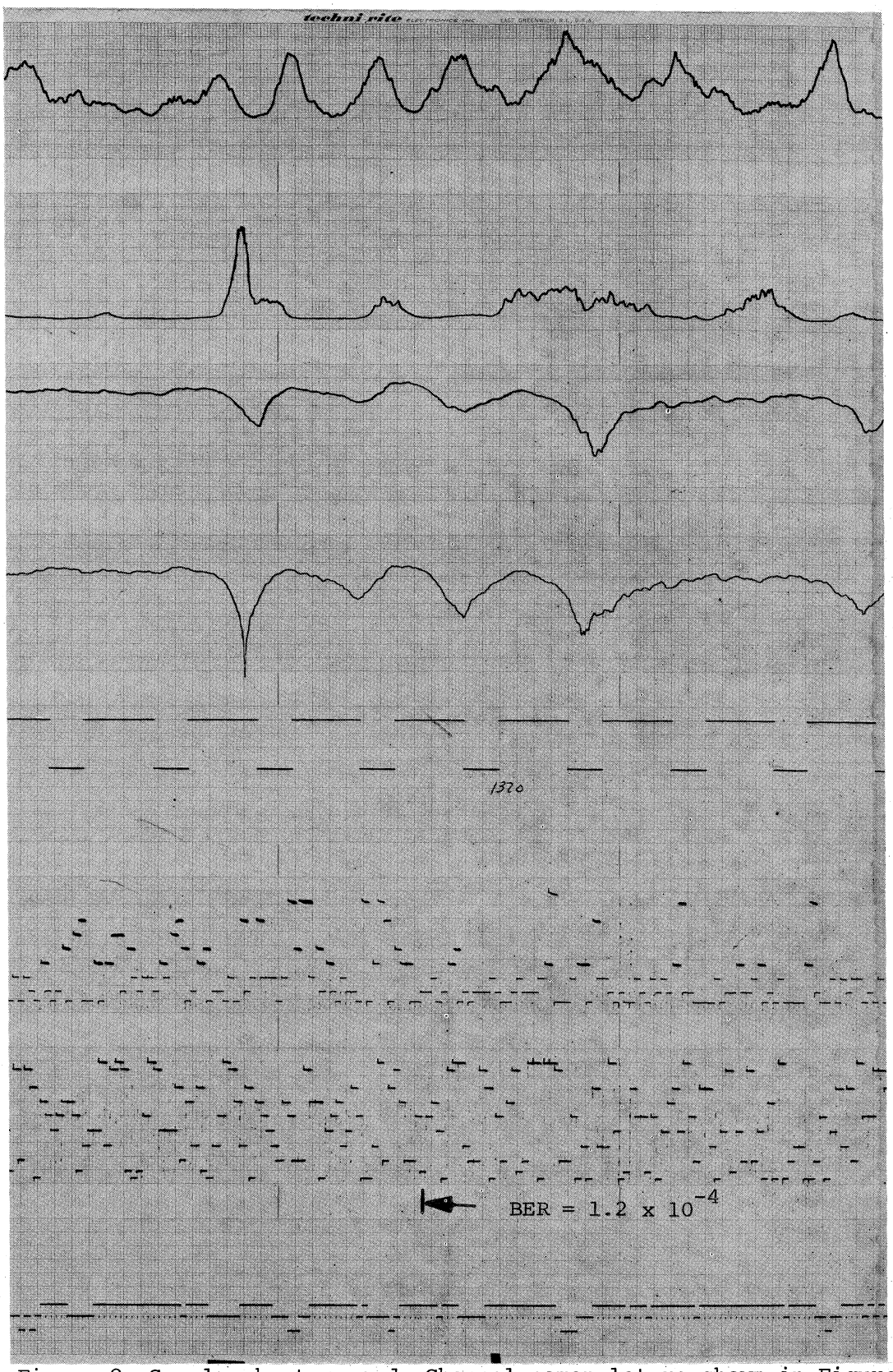


Figure 9. Sample chart record. Channel nomenclature shown in Figures 10 - 13.

The data in the following figures are blocked in 5-minute intervals. The impulse response for each probe receiver channel was reproduced from the magnetic tape and averaged over this interval in a digital time-series analyzer in the ITS laboratory. The result was then plotted on an X-Y recorder. At the same time, the impulse response during the interval was monitored on a storage oscilloscope, and a photograph(s) was made during the interval in order to depict the dynamic situation. These data were then compared with the RSL record and the BER data in each interval. The results are shown in the composite Figures 10 through 13.

The first 5-minute data interval is taken from 1255 to 1300, and the average of the impulse response for each diversity channel is shown in Figure 10(a). Both responses indicate a fairly clear-channel condition. Evidence of small magnitude multipath is seen only in the trailing edge of the two averages. A time-lapse photograph made from a magnetic tape playback for a 20 s interval at 1256 is shown in the lower half of the figure. This photo as well as others to follow were made by setting the scope sweep for an A + B display, and using the sync signal derived from the magnetic data tape. In this display, the time separation between the response from the lower receive antenna (left-hand response in the photo) and that from the upper antenna is due to the difference in the transmission time over the disparate length of waveguide between the antennas and the receiver.

The corresponding strip-chart record showing the RSL for both channels, and the BER record is shown in Figure 10(b). The RSL's during this period show moderate fading on the lower antenna signal (Ch. 1), and a fairly steady signal for the upper antenna (Ch. 2) with exception of the 8 to 10 dB fade just prior to 1300. The BER data were measured on the Ch. 1 signal only, so our comparisons between this performance monitor and the channel conditions are always with respect to Ch. 1. The fading in Ch. 1 is typical of slow power (or flat) fading, and the

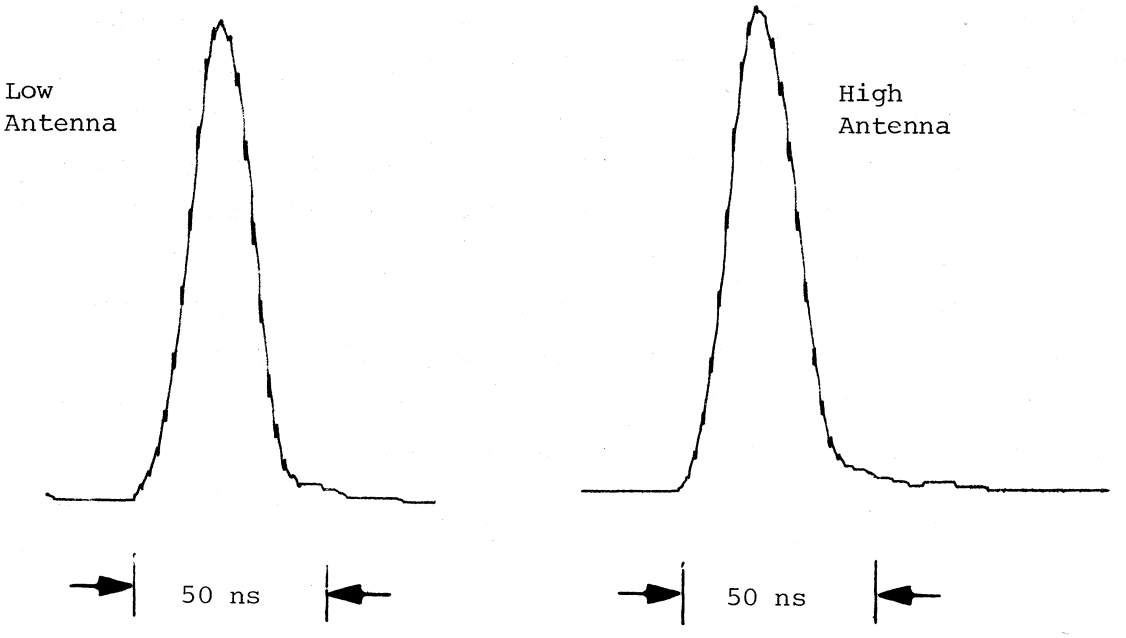


(a) Five-minute time averages.

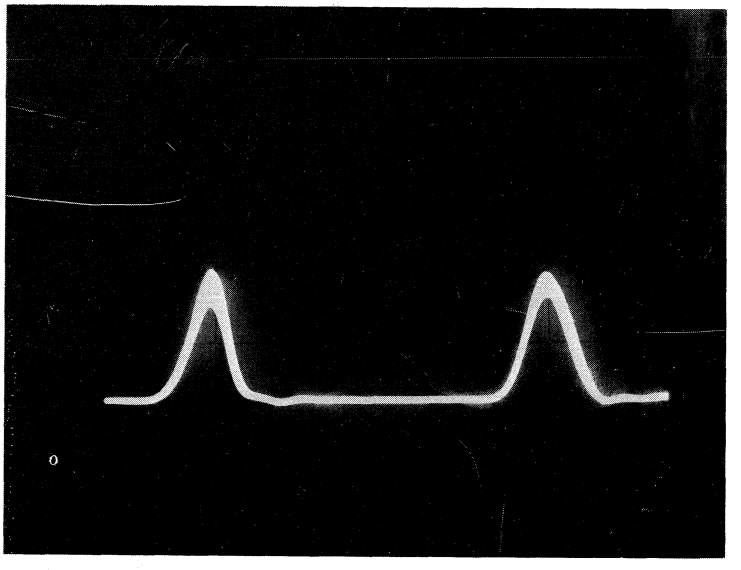

(b) Time-lapse photograph of 20 s period at 1256 PST.

Figure 10(a). The average power impulse response measured between 1255 and 1300 PST, 31 August 1978, at a PN clock rate of 50 MHz.

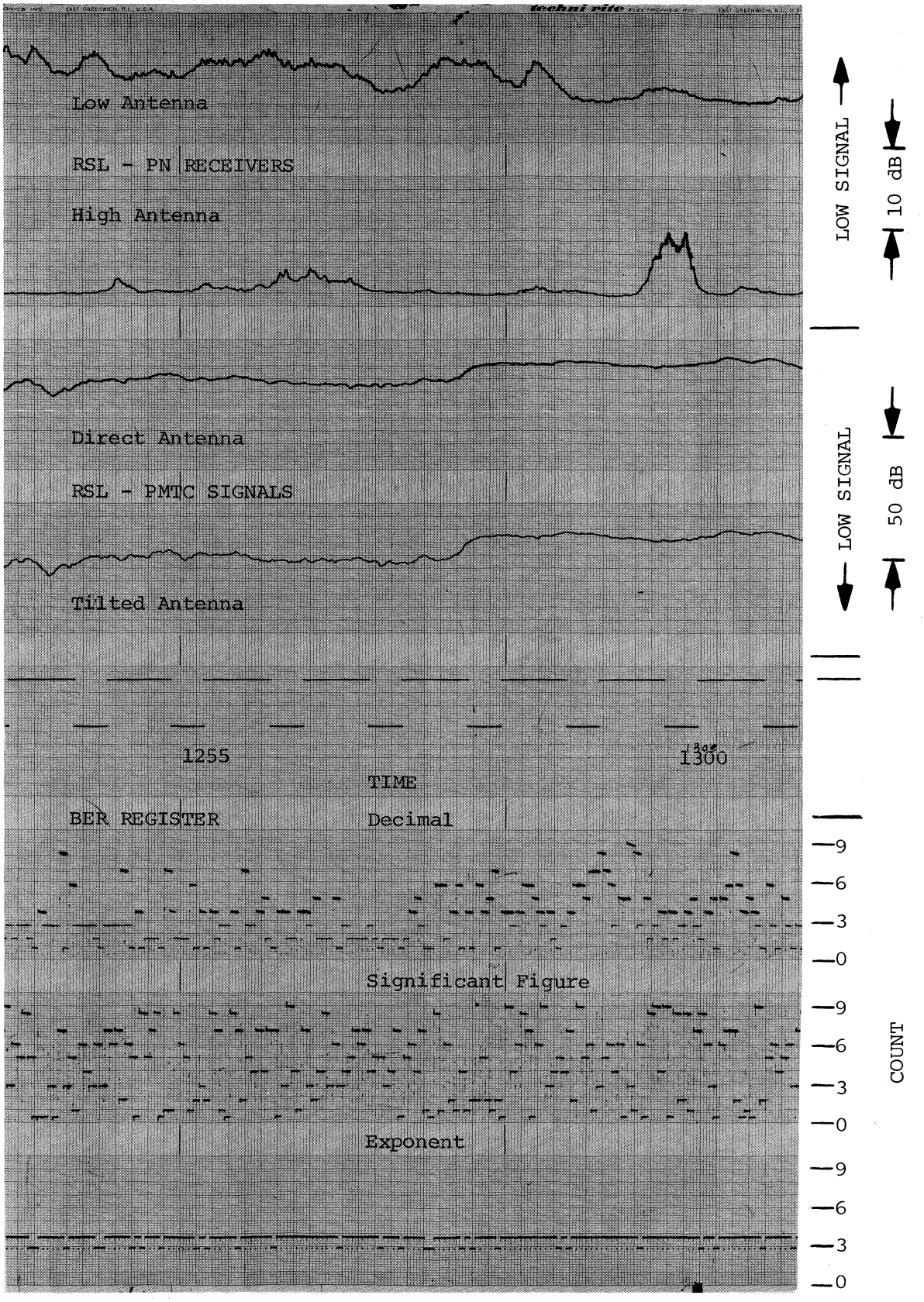


Figure 10(b). Strip chart record for 1255 - 1300 PST, 31 August 1978.

impulse data verify only short-delay multipath of relatively small magnitude. The channel conditions can be typified from Figure 4 by considering the transfer function for a component of short delay and slowly changing in either delay and/or relative phase. The fading is caused by the skirt attenuation of the transfer function that has a shallow slope over the signal pass band. The BER* is also quite stable over the period, ranging from a high of $8 \times 10^{-4}$ to a low of $2 \times 10^{-4}$. As we will see later in this discussion, the deeper fade in Ch. 2 prior to 1300 is typical of a relative shift in multipath where a null of the transfer function impinges on the signal passband with steeper slope. Note that as this condition appears in Ch. 2, the RSL in CH. 1 becomes more steady. This is more evident in the next data interval.

The data of Figure 11 are for the period 1300 to 1305. In the averages of the impulse response we see that Ch. 1 now displays a very strong and stable multipath component. The delay in the average response is seen to be about 10 ns. The high and stable RSL for the period also confirms the stability of the multipath. Measured at the 150 Mb/s rate, this impulse response would resemble that shown in Figure 7, where a more definite separation of the two components results from the higher resolution. Also the clear responses shown in Figure 10 would indicate the small scale multipath with the higher resolution measurements. However, we noted previously that the 50 Mb/s response was quite useful in our analyses, and Figure 11 is an example. The relative phase between the components is seen to be opposing as the cusp is developed within the resolution time.

The response for Ch. 2 has not changed significantly from the previous interval, but the RSL record indicates that the short-delay components in that channel have become less stable.

*For these comparisons we will generally ignore the decimal value, and read only the first significant figure and the exponent value from the chart record.

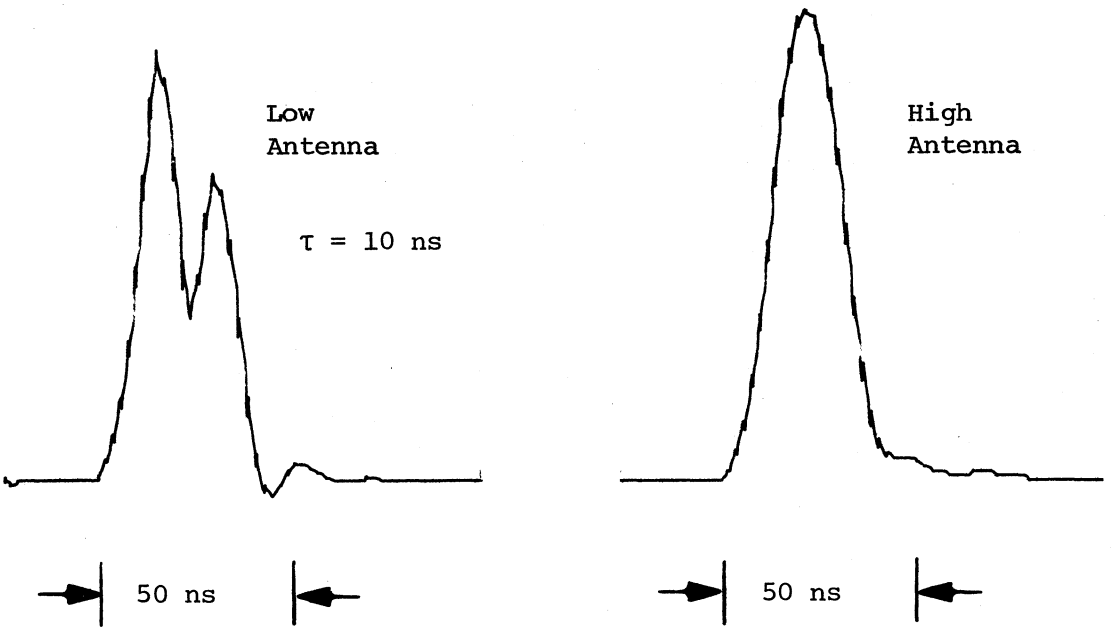


(a) Five-minute time averages.

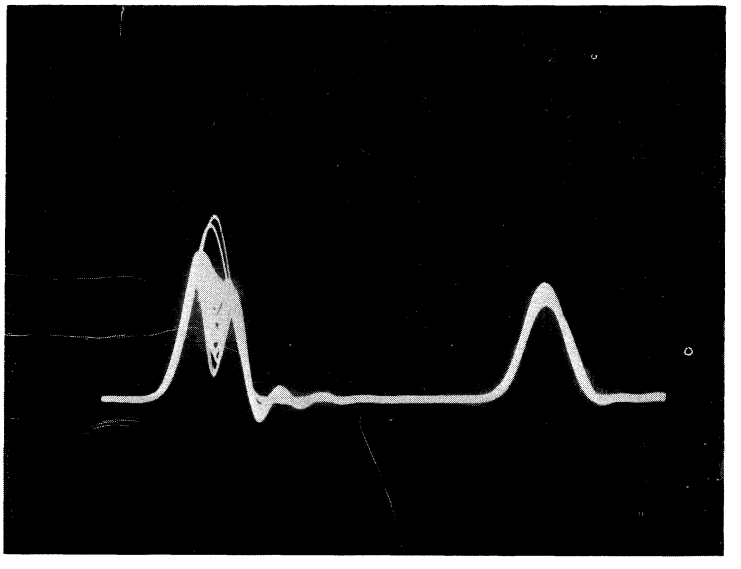

(b) Time-lapse photograph of 20 s period at 1304 PST.

Figure 11(a). The average power impulse response measured between 1300 and 1305 PST, 31 August 1978, at a PN clock rate of 50 MHz.

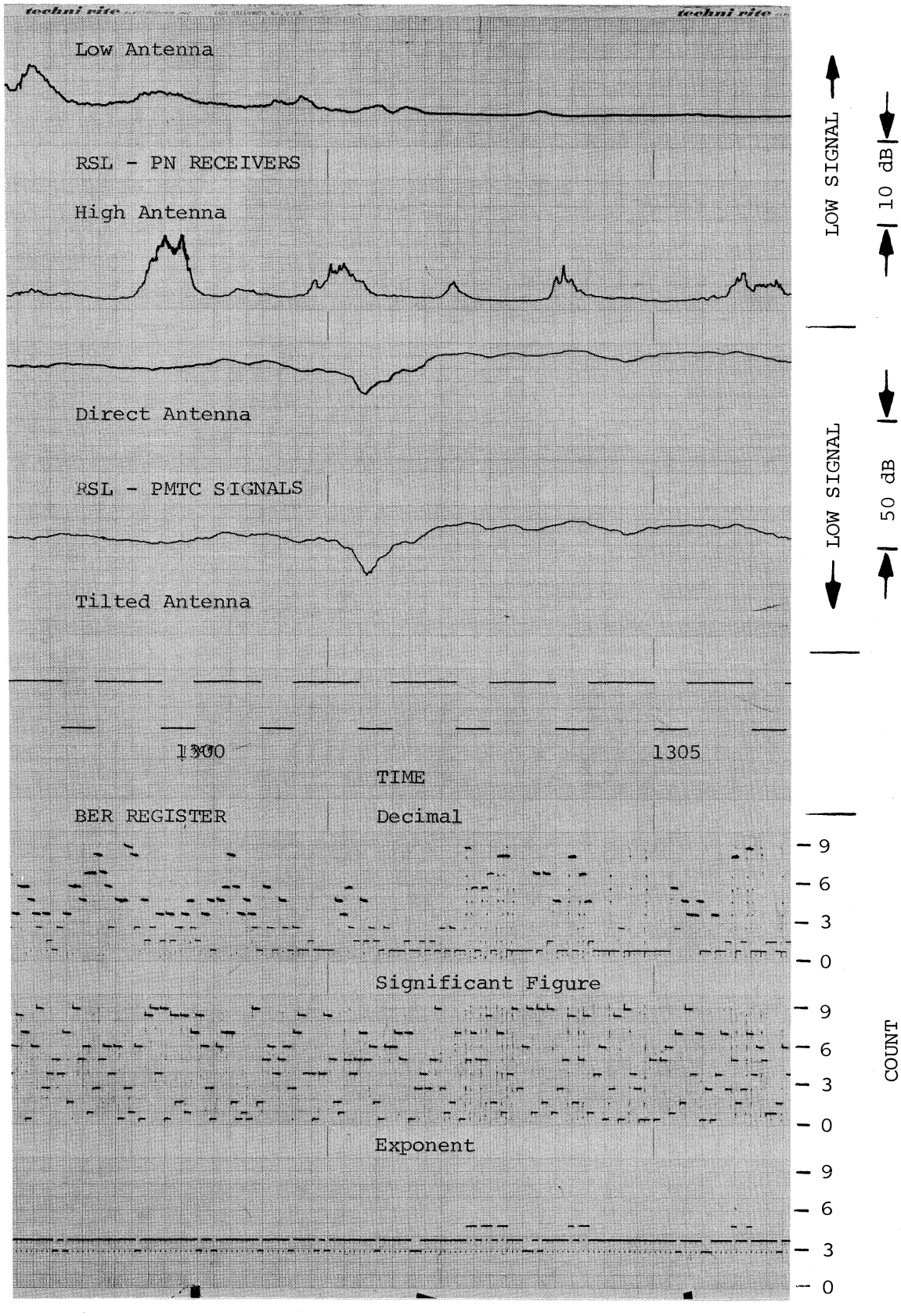


Figure 11(b). Strip chart record for 1300 - 1305 PST, 31 August 1978.

The photograph at the bottom of Figure 11(a) is a 20 s time lapse of the impulse data made at 1304. The dynamic change in relative phase between components in Ch. 1 is quite apparent, while only a slight distortion to the trailing edge of the Ch. 2 response is seen in the photo. The BER during this interval shown in Figure 11(b), is similar to the previous record with two exceptions. First, note that there are fewer intervals where the rate has dropped to the $10^{-3}$ level and those intervals are more random in the first few minutes of the block. Secondly, near 1303 we observe that the RSL in Ch. 1 has become very steady and the error rate has improved to values between 5 to 9 $\times$ $10^{-5}$ for short periods. The cause for the first observation is not tractable in any sense, but one can speculate on the probable cause. The impulse response between the two intervals in Ch. 1 indicates that a multipath component has gradually changed from a short delay to near 10 ns. As discussed in Section 3, the dynamics in the transfer function would cause a number of nulls to move across the signal pass-band. The resulting power notches in the received signal spectra will increase the error rate, and in-band distortions as the null begins to impinge add additional errors (see Barnett, 1978). We assume this change to be taking place during the time (1255 - 1303) when the RSL is increasing and becoming more steady. At around 1303 the delayed component is well established, and the relative phase was seen to be very stable at the time the best error performance was measured. This condition was directly observable in the data, where the impulse response remained stable and had the same general shape as the average shown in Figure 11(a). The photograph in the lower half of the figure was taken over a few seconds beginning at 1304. It indicates that the phase relationship began to change again with time, and the BER shown in Figure 11(b) returned to the pattern seen earlier in the interval. A few measures in the $10^{-5}$ range were still seen around 1305. One should note from this very short example the lack of correlation between RSL and

BER performance, a basic characteristic of multipath propagation. Also note that the multipath change in the two channels is not well correlated in any of these data displays.

The interval from 1305 to 1310 is depicted in Figure 12. The averages of the impulse functions are shown in the (a) part of the figure. The multipath in Ch. 1 is again seen to be quite stable, and the average delay-time has increased to approximately 12.5 ns. The first few minutes of the RSL record and the BER record in Figure 12(b) follow the characteristics from the previous interval until the deep fade in Ch. 1 just prior to 1308. At the null point of this RSL fade, the error detector lost synchronization and did not recover for several minutes (except momentarily around 1310). We discuss the details of this event later in this section. From the photograph of the Ch. 1 response in the lower half of Figure 12(a), we note that the relative phase is again changing somewhat more rapidly with time. For example, within the time-lapse display, we see individual functions typical of those for a near in-phase condition (broad top to the pulse) and several approaching an out-of-phase state (null within the resolution). This is again visualized in the frequency domain as a shift of the transfer function null along the frequency axis, with the associated in-band signal distortions. The BER is seen to step again between exponent values of $10^{-3}$ to $10^{-5}$ prior to entering the out-of-lock state caused by the variability of the multipath phase.

The data interval from 1310 to 1315 is shown in Figure 13. The average impulse response for Ch. 2 has not changed essentially throughout the total sequence. The Ch. 1 response average now indicates a multipath component with a stable delay of about 7.8 ns, and nearly in-phase with the earlier response. The time lapse photo at the bottom of the figure illustrates the development of this function, and also shows the relative stability at 1311. The RSL at this time is also stable, but the BER measure was lost becuase of the out-of-

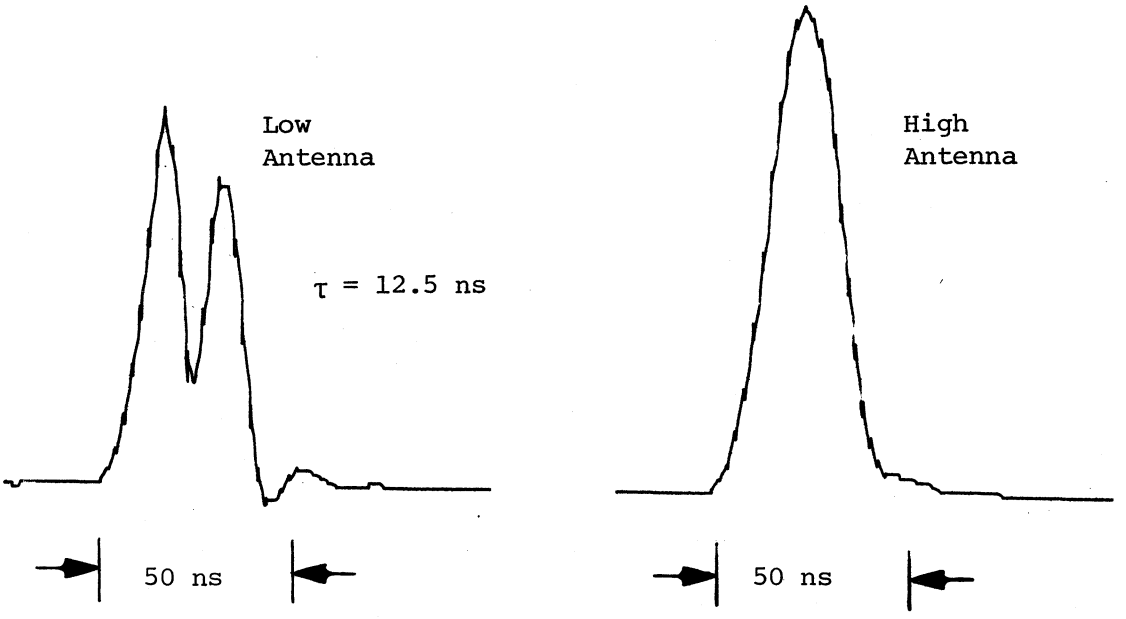


(a) Five-minute time averages.

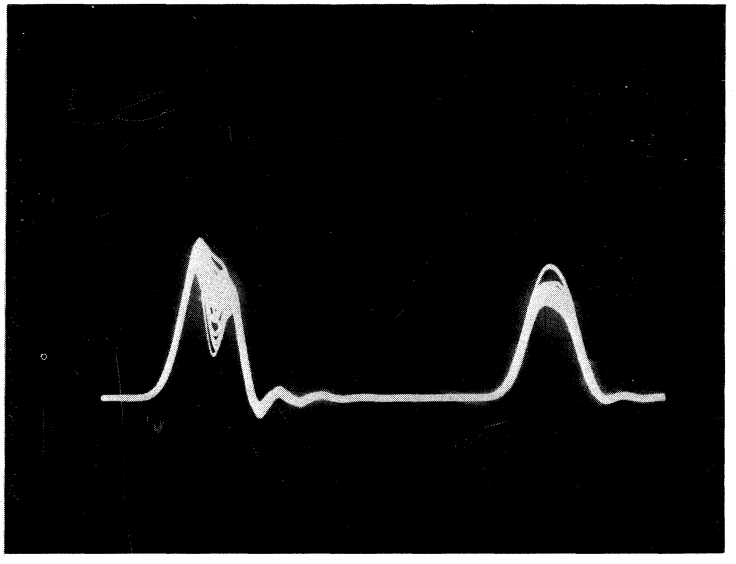

(b) Time-lapse photograph of 20 s period at 1307 PST.

Figure 12(a). The average power impulse response measured between 1305 and 1310 PST, 31 August 1978, at a PN clock rate of 50 MHz.

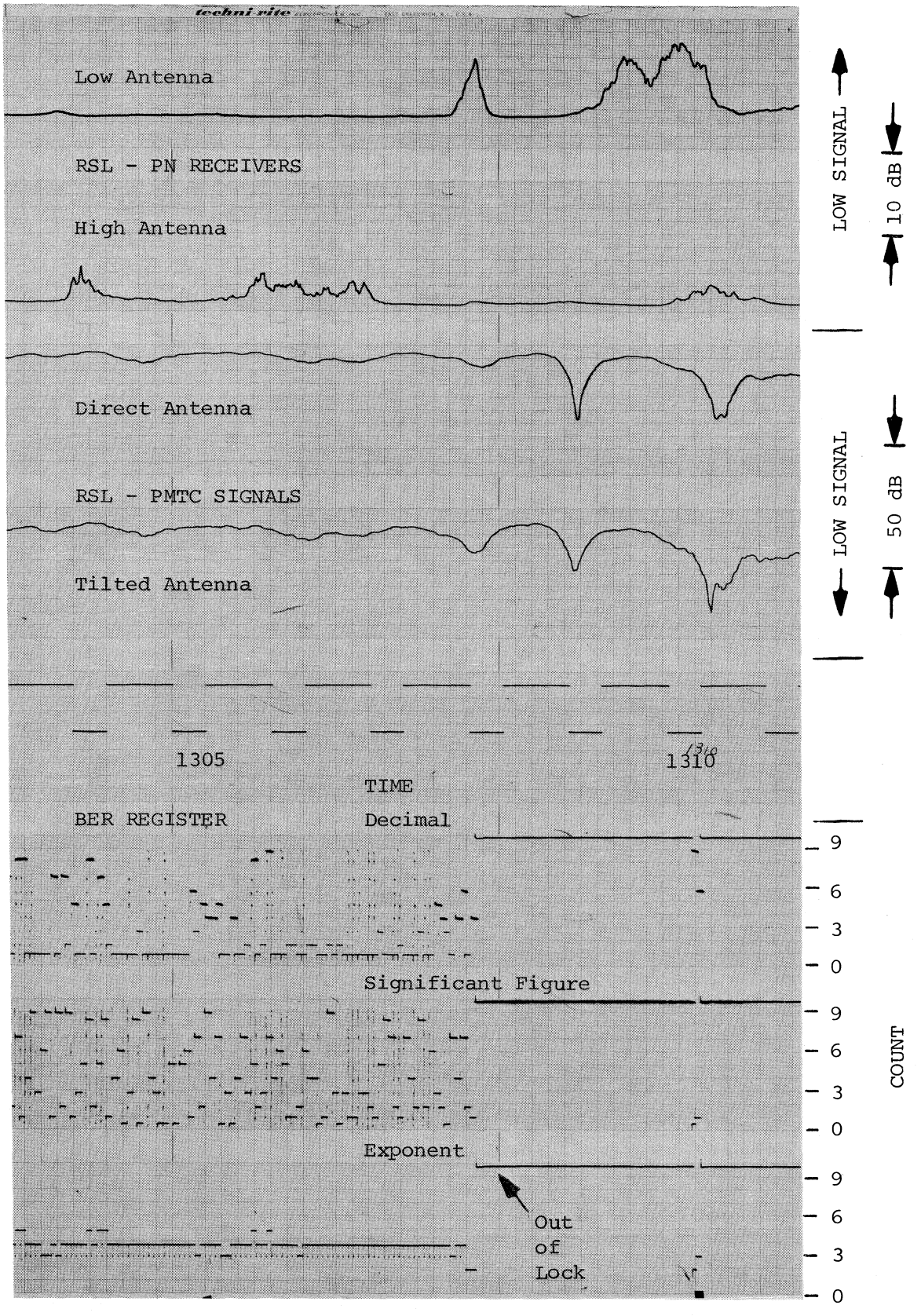


Figure 12(b). Strip chart record for 1305 - 1310 PST, 31 August 1978.

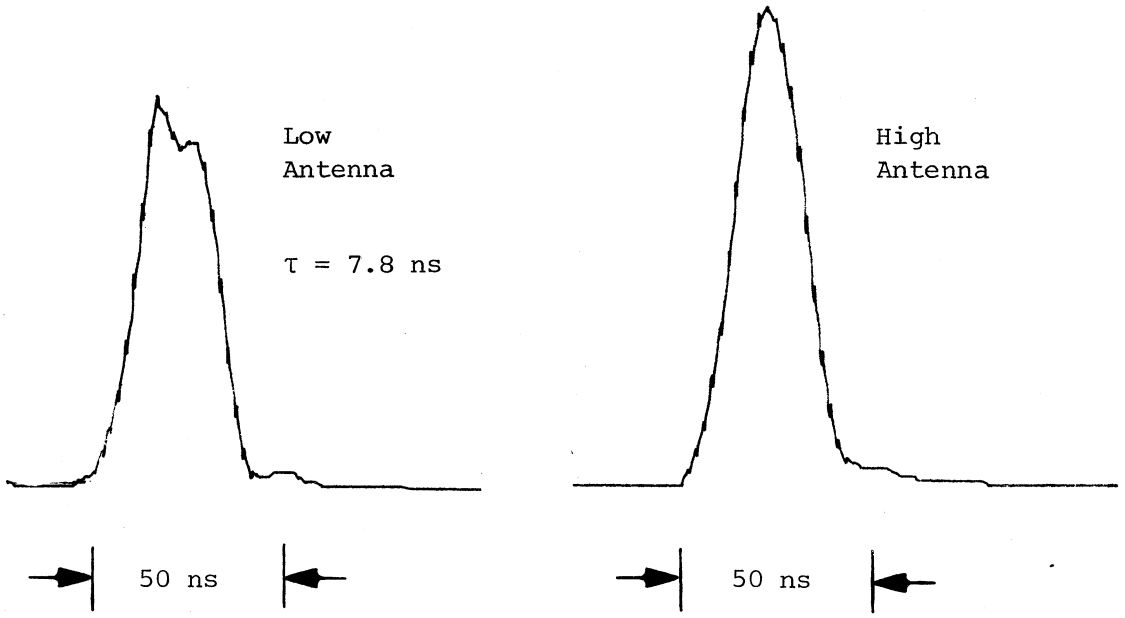


(a) Five-minute time averages.

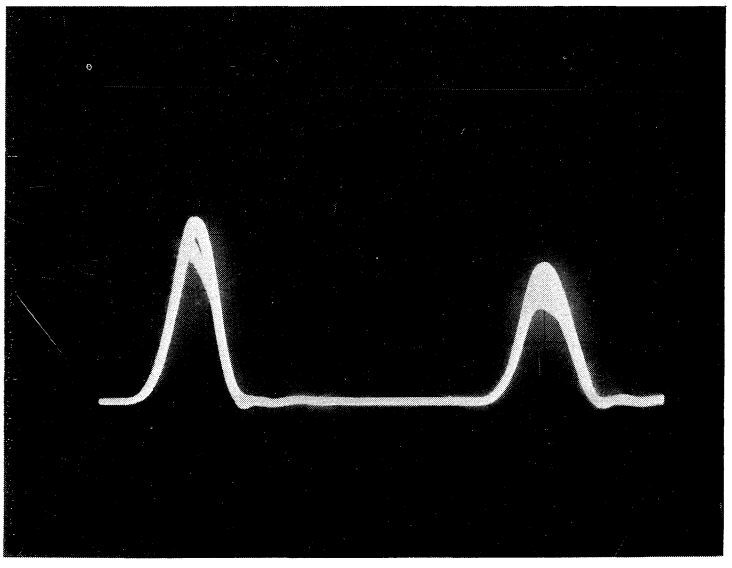

(b) Time-lapse photograph of 20 s period at 1311 PST.

Figure 13(a). The average power impulse response measured between 1310 and 1315 PST, 31 August 1978, at a PN clock rate of 50 MHz.

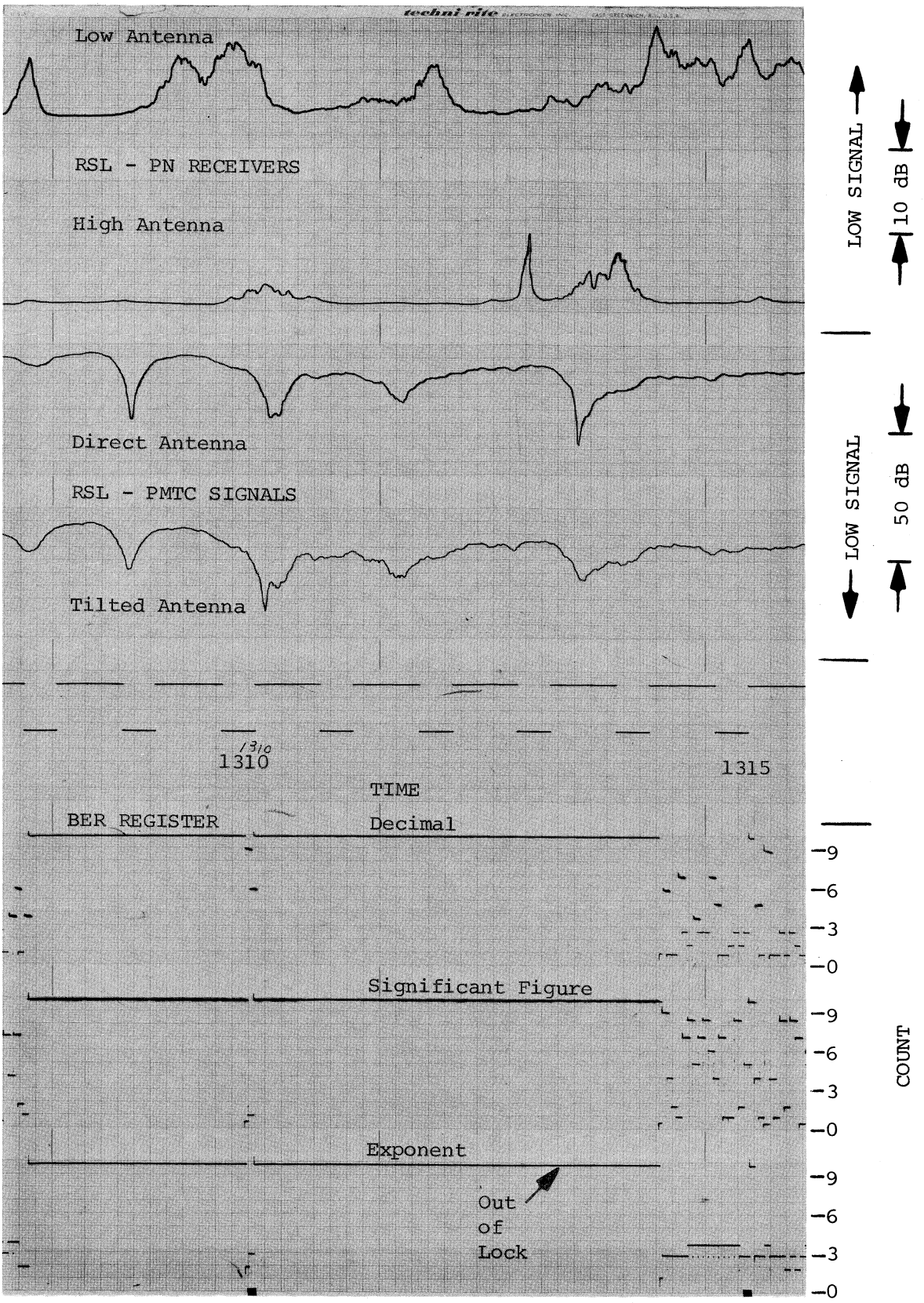


Figure 13(b). Strip chart record for 1310 - 1315 PST, 31 August 1978.

lock condition reached earlier. A note on this particular case is included in the discussion to follow.

We observe from Figure 13(b) that the RSL in Ch. 1 began to fade rather severely after 1311, and the BER detector re-synchronized on the data stream at 1314 during one of these fades. Even though the depth of some fades were several dB greater than the one observed at 1308 that caused the loss of sync, the BER performance was not greatly degraded over that during steady signal periods. Periodically, the BER fell to a few bits in $10^{-2}$ at the depths of the fades, but returned to $10^{-4}$ levels without loss of sync. The difference between the performance during these fades and others can be seen from the channel response functions presented below. Before presenting them however, we should note a characteristic of the bit error system. The data clock was derived from the PLL (as stated above) rather than from the received data. Thus when a change in the reference phase takes place within the PLL, the phase of the data could reverse creating a $\overline{\text{data}}$ (or inverted) bit stream to the error detector. This is the condition that was created by the first fade at 1308. A time-lapse photo of the impulse response at this time is shown in Figure 14(a). The dynamics are somewhat obscured in the photo, but referring to Figure 12(a) we can see that prior to 1308 the dominant signal path was the first response in the two-path function. At the time of the deep fade, the signal power slowly faded in the initial response and shifted to the delayed component, changing the phase reference of the PLL to that of the more dominant delayed signal. Thus the PLL tracked the change, and caused the phase of the data signal to reverse. In normal operation of the experiment, the operator of the probe manually changed the reference data stream in the error detector to reestablish the data sync. However, in this case the manual change was not made in order to follow the channel performance more directly.

The photograph shown in Figure 14(b) was made at the end of the interval where the data resynchronized at about 1314. At this time a reverse shift between the two components took place, and the dominant signal energy returned to the earlier component. In both (a) and (b) photographs there is also evidence that the total path changed in propagation time (or length) during the time-lapse. This can be seen in the shift in the envelope of the responses. The shift is greater in (b), and gives the impression that the delay between components in Ch. 1 is greater than it actually was. The photograph in part (c) of the figure was taken at 1310 where the error detector resynchronized for a few seconds, and then again went out of lock. The magnitude of the Ch. 1 response shows a power fade effect as well as the shift in energy between the two signal components.

The multipath fading continued with similar characteristics for the remainder of the afternoon, increasing somewhat in depth and rate in both channels. This can be seen in Figure 15 and 16 which are sections of the chart record following those periods discussed above. We see that the BER performance continues at about the same level, and with a pattern similar to that above. The error detector was however manually re-synchronized at the out-of-lock points seen in Figure 16. In order to show more of the dynamic multipath effects, we present additional time-lapse photographs of the impulse functions in Figure 17. The first photo in (a) illustrates that the Ch. 2 characteristics are similar to those discussed for Ch. 1. The data were recorded during a fade in Ch. 2 a few seconds past 1317 (see Figure 13b), and the response shows a shift in signal energy from one signal component to the other. Figure 17(b) shows that the fade in Ch. 1 at 1331 (Figure 15) was a power fade across the passband, and disturbed the BER count for a very short time at the bottom of the fade. The photo in (c) of the figure again illustrates the phase shift of signal energy in Ch. 1. At the same time, a minor change took

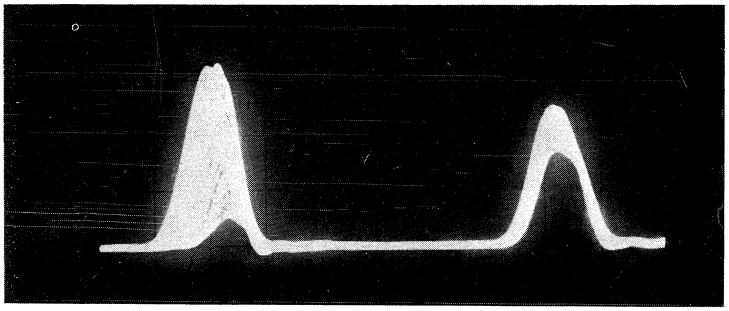

(a) Time-lapse response measured at 1308 PST, corresponding to the fade in Ch. 1 and the loss of synchronization in the data stream shown in Figure 12(b).

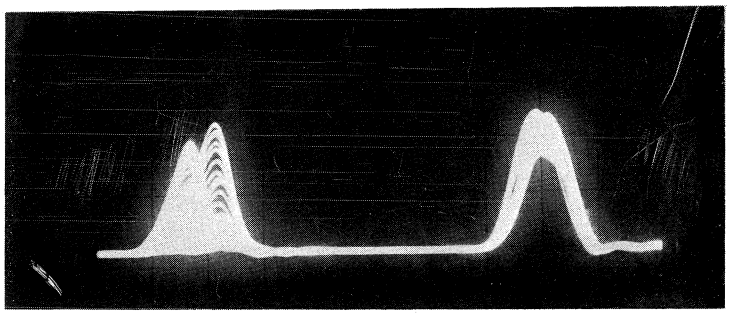

(b) Time-lapse response measured at 1314 PST, where the data stream resynchronized.

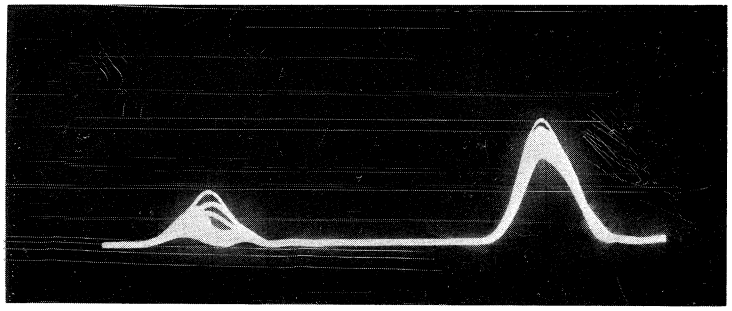

(c) Time-lapse response measured at 1310 PST, where the data stream resynchronized for a few seconds.

Figure 14. Time-lapse photographs of the power impulse response measured during the fading period in Ch. 1 beginning at 1308 PST, 31 August 1978.

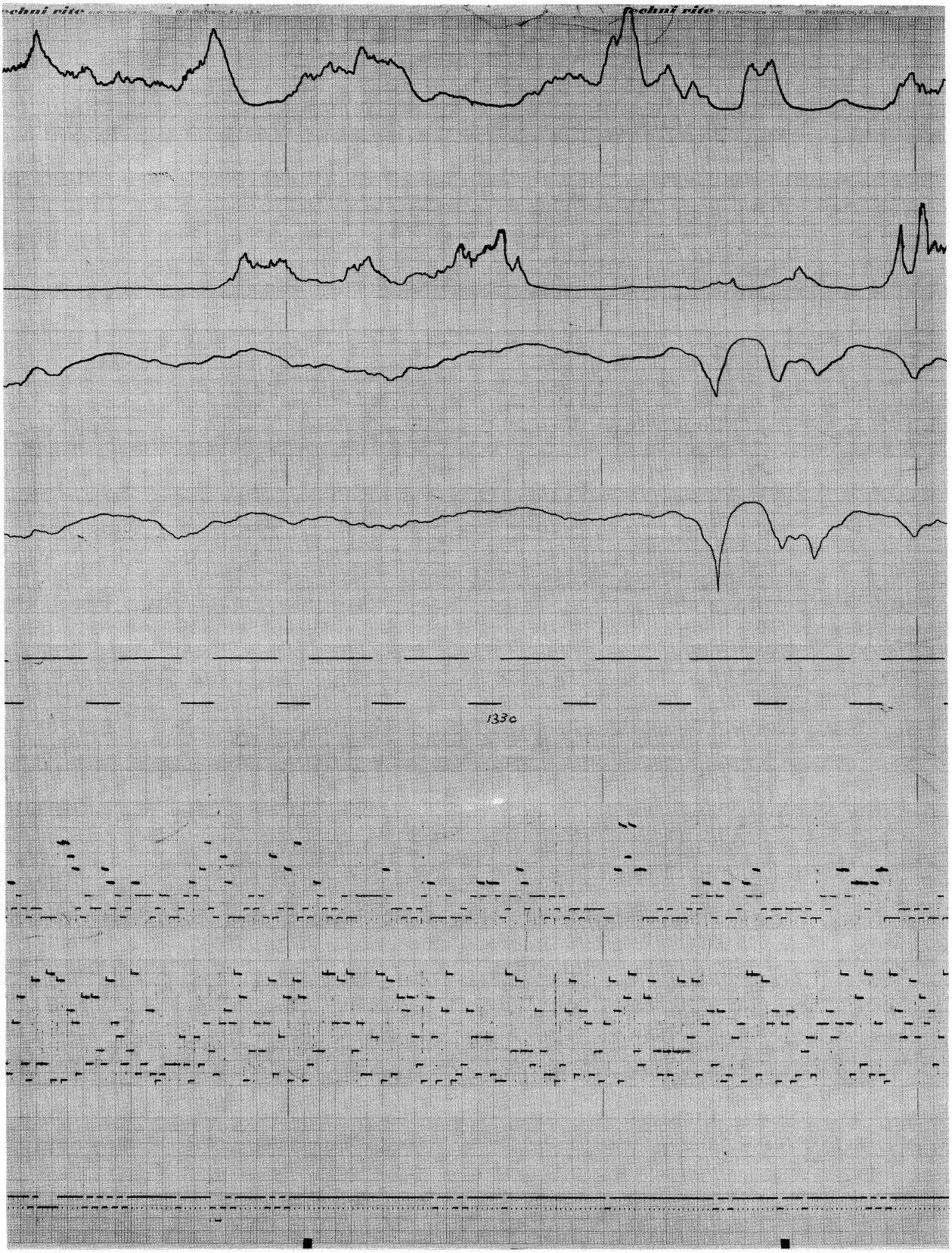


Figure 15. Strip chart record; nomenclature same as Figures 10 - 13.

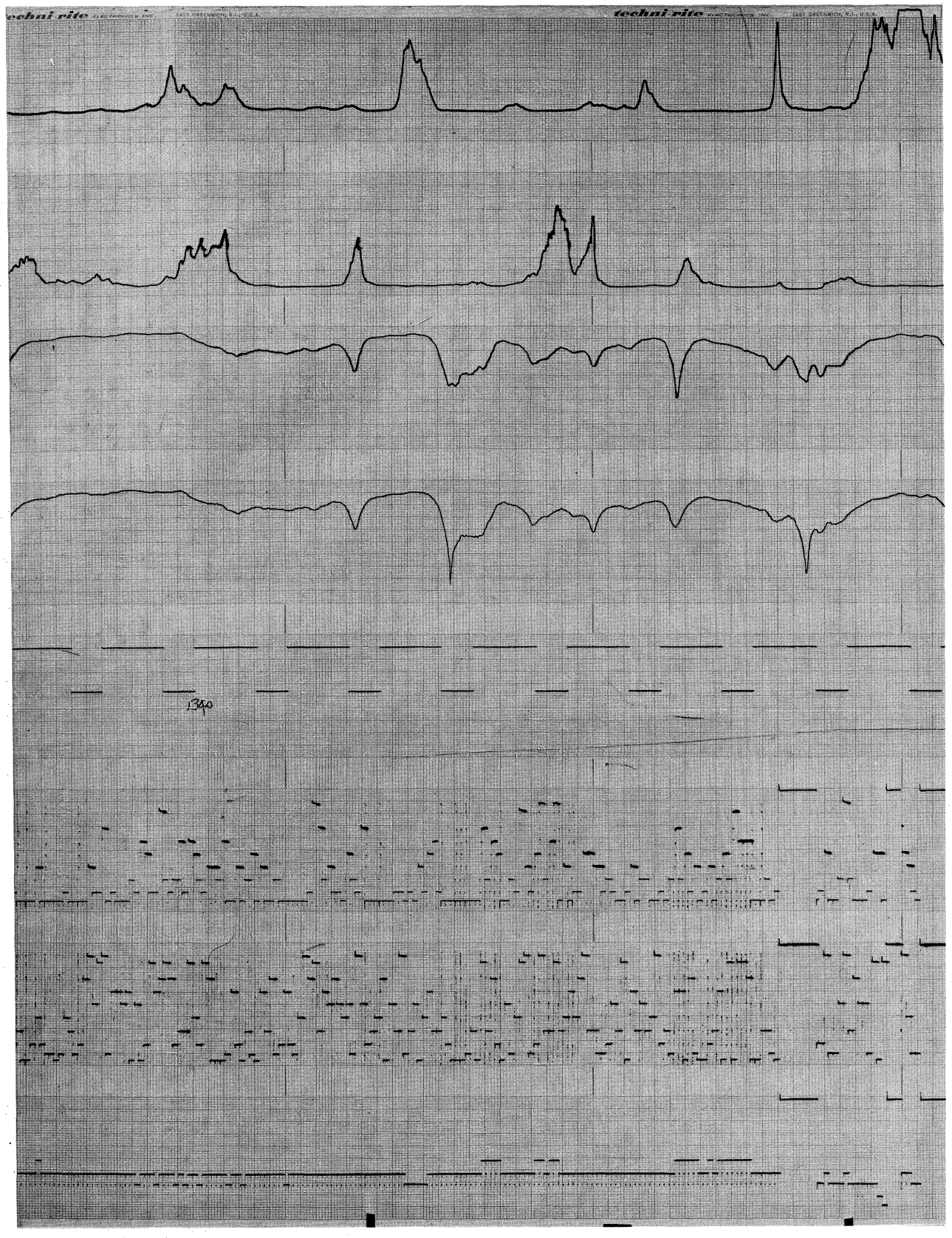


Figure 16. Strip chart record; nomenclature same as Figures 10 - 13.

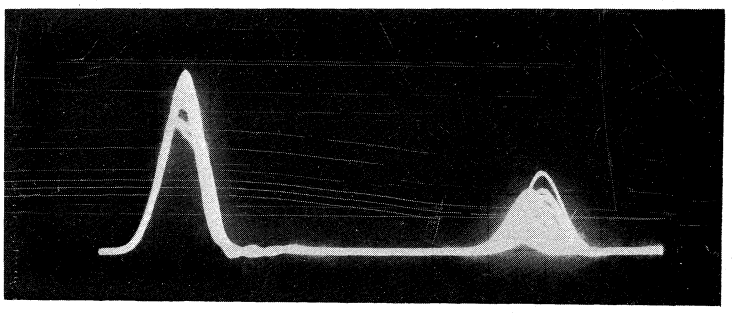

(a) Dynamic multipath measured in Ch. 2 (high antenna) at 1317 PST.

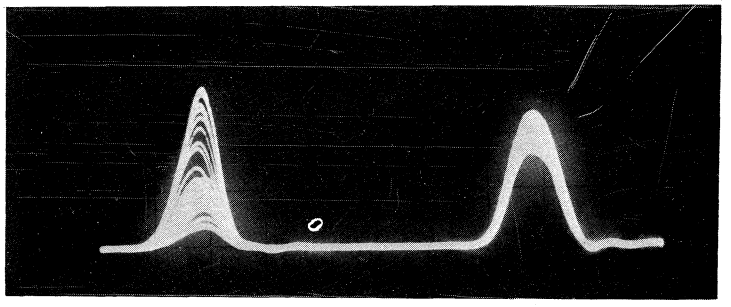

(b) A flat-fade response observed in Ch. 1 (low antenna) at 1331 PST.

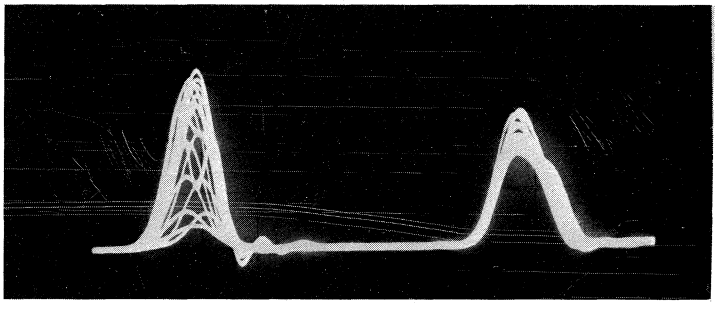

(c) Another example showing a power shift between components in Ch. 1, with only minor change in the Ch. 2 response at 1346 PST.

Figure 17. Time-lapse photographs of the power impulse response measured between 1317 and 1346 PST, 31 August 1978.

place in Ch. 2. This photo is for the data a few seconds after 1346 during a very sharp fade in Ch. 1. The data illustrate an important observation that was stated in Section 4.2; i.e., the multipath character of the diversity channels was similar, but rarely correlated in time. This is the desirable situation for effective space diversity and combined performance improvement.

To compare in some sense the BER performance in Ch. 2 (upper diversity receive Channel) with that in Ch. 1, the error detector system was switched to Ch. 2 around 1520 on the afternoon of 31 August. This change was accomplished by exchanging the IF signal cables from the rf head of the receiver to the two IF channels. Thus, the PLL and error detector followed the conditions from the upper antenna signal. The fading became more rapid and severe as the afternoon passed, but the BER performance remained essentially the same as that described above for Ch. 1. It was also possible to verify visually the same type of multipath effects. This switch in BER measurements was repeated several times throughout the experiment with the same result.

Most of the data obtained on 31 August were measured at the 50 Mb/s data rate in order to evaluate the BER performance characteristics. The resolution of the impulse response data is obviously not as high as the 150 Mb/s rate, but it can be seen from the above discussion that enough detail was available at the lower rate to permit some tractable comparisons. The meteorological conditions on the following day (1 September 1978) were very similar, and some of the data were recorded at the 150 Mb/s rate on that date. A discussion of these results is included in the Appendix. The results confirm the conclusions drawn on the basis of the example presented in this section at the lower clock rate.

## 4.4 Angle Diversity Measurements

The angle diversity measurements were made on the higher of the two operating frequencies of the PMTC microwave system (7.47 GHz), with the measurement apparatus as described in Section 3.4. The system was originally aligned for the lower frequency (7.17 GHz), but changed on 25 August 1978 to 7.47 GHz because of problems experienced by the Navy with the lower frequency transmitter.

The RSL levels for both receivers were initially recorded on chart paper only, and monitored for an extended period so that the receiver gains and calibrations on the two (aligned) antennas could be matched. One of the two antennas was later tilted for a nominal 2 dB loss in mean RSL. The data were then recorded on the magnetic tape system (as well as the strip chart recorder) beginning on 29 August 1978. Examples of the strip chart records can be seen in Figures 10 through 13 and Figures 15 and 16 in the previous section. They are the signal traces in Ch. 3 and Ch. 4 of these figures. Although the polarities of these signals are reversed from those for the two probe receiver channels (top two traces), the signal fading can be compared between the sets. With the exception of some of the sharper, deep fades seen in the 7.47 GHz signals, the fade range for the two frequencies is comparable. Since the probe system was operated at 8.6 GHz, the frequency separation is 1.13 GHz. This is almost 4 times the separation used between the PMTC frequency diversity channels. However, the separation between the two measured frequencies is not considered to be so large that some meaningful performance observations cannot be made. For example, just a scan of the records shown in the figures noted above will convey that the fading is not highly correlated in time between the two frequencies. If we assume that the multipath observed by the probe at 8.6 GHz is appropriate to a wide range of transmission frequencies, then we could expect a degree of spacial correlation for the two frequencies with some time lag between

the fading events. This cannot be verified easily however from the data. One can peruse the records and find some fade events that appear similar at the two frequencies, with time separation on the order of minutes, but the pattern is not consistent. There are of course two reasons that one would not expect this to prevail. First, the structure of the frequency transfer function changes with respect to a given operating frequency and thus the dynamic effects should be different. We rely on this fact for improvement in frequency diversity systems. In addition, we must keep in mind that the RSL for the probe signal is derived from a broadband transmission while that from the angle diversity measurement is from a relatively narrow band signal. Notches in the transfer function of the channel will produce fades of different character in the two records, even if the same dynamic multipath change is responsible for the fade. The important aspect in this comparison is the lack of correlation in time between the signals at the two frequencies; again a desirable result. It is actually a by-product of the experiment, but should not be overlooked.

Returning to the original objective for this part of the experiment, we wish to summarize the angle diversity data. Again looking back at the figures in the previous section, and scanning the two angle-diversity signals in the strip chart records, we can ascertain certain fades that are of less depth in the tilted-beam record (Ch. 4) than in the direct-beam record (Ch. 3). However, the reverse is also true on many occasions. Thus the final conclusion can only be drawn from a statistical summary. In general we have found that there is no statistical improvement. This is based on analyses of the magnitude distributions of the two RSL data records. The signals were played back from the magnetic tape recordings into the time-series analyzer mentioned previously. A probability density function (pdf) and a cumulative distribution (cd) function were developed in the process for both signal channels.

Examples of these results are shown in Figures 18 and 19. Figure 18 presents the pdf for each channel, which have been aligned on a relative power scale to match their peak magnitudes (the tilted antenna signal peak is in reality approximately 3 dB lower). There is no significant difference between these plots. The cumulative distributions are shown in Figure 19. They indicate that the tilted beam result is actually poorer than the direct antenna signal, as the probability of a lower RSL is higher in the tilted beam function than in its counterpart. If one matches the median signal levels for the distributions shown in Figure 19, it can be seen that the tilted antenna provides a very slight improvement. However, this example and others shown in the Appendix are not conclusive enough to warrant angle diversity as a viable option in configuration. In essence, the results suggest that the angle-of-arrival for multipath components in a refractive medium is a random variable. Thus, no fixed angular offset to the receiving antenna will provide significant improvement in fade margins.

Before concluding this discussion, one additional comment should be made regarding the angle diversity measurements. Even though the statistical analyses show relatively no improvement in the signal distributions, a distinct difference in character of some signal fades over the angle diversity paths was observed. Some of these may be seen in the RSL records (Ch. 3 and Ch. 4) of the figures presented in Section 4.3. In particular, we refer to Figures 10(b), 12(b), 13(b), and 16. In each of these figures, particular fades are seen that display different characteristics, indicating that either the multipath phase relationship or delay was not precisely correlated in both channels. Thus, as illustrated in Section 4.2, the effect on a digital bit stream could conceivably be different and uncorrelated. This conclusion cannot be verified from the measurements, however. The possibility was recognized during the data analysis, and plans were made to perform impulse response measurements on the angle-diversity

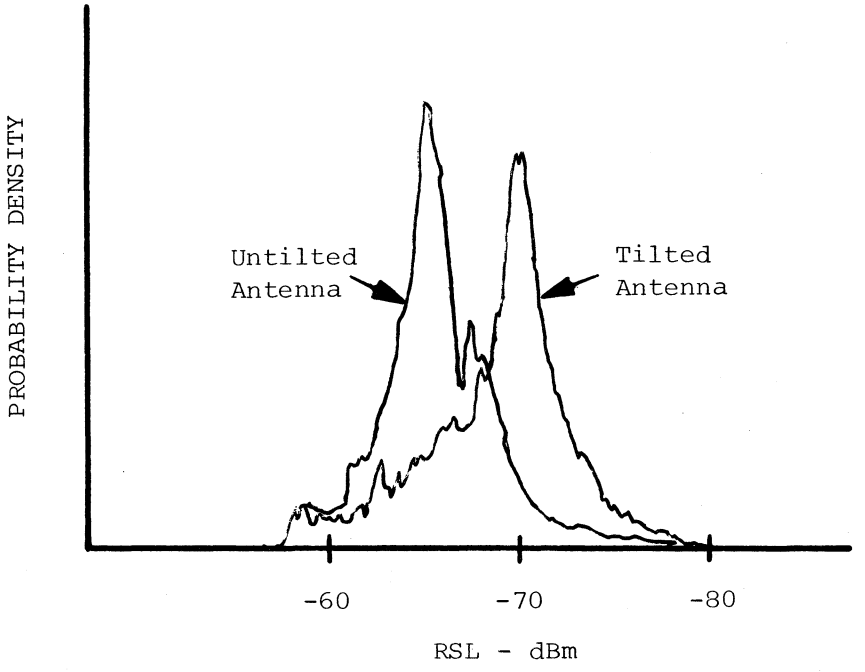


Figure 18. The probability density functions (pdf) for the tilted beam experiment, 1520 to 1730 PST on 30 August 1978.

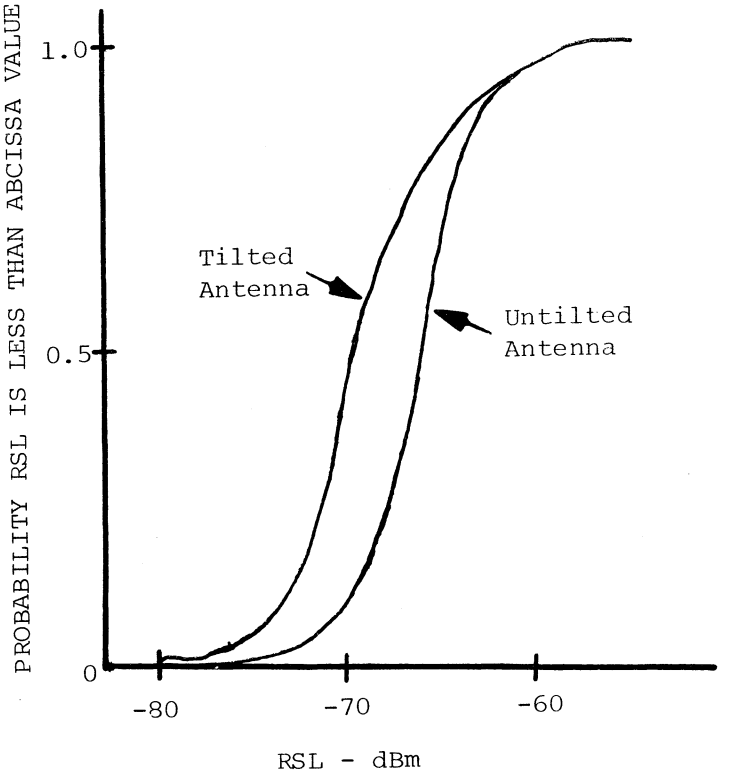


Figure 19. The cumulative probability functions for the data of Figure 18.

channels during December 1978. As pointed out previously, this portion of the experiment was not performed because the desired meteorological conditions did not develop. We mention this as a potential diversity technique only for completeness, and for future reference. If the technique has performance merit it can be conceivably implemented at lower cost than standard space diversity configurations.

## 5. CONCLUSIONS AND RECOMMENDATIONS

The results of the measurements summarized in this report permit some general conclusions to be reached, and specific recommendations to be made for a digital communication system at the PMTC. The conclusions and recommendations must be made on the assumption that the anomolous meteorological conditions encountered during the measurements are typical or representative of those normally found in the Pt. Mugu region. One reservation in this regard should be stated, based on information furnished by meteorologists at Pt. Mugu. It was pointed out to the ITS personnel that the marine layer which gives rise to the refractive structure was somewhat higher than normal during our experiment. For example, the layer height during August and September 1978 generally extended above the elevation of LP, which was considered to be unusual. However, a cursory comparison of refractive index profiles measured during the experiment with those measured in previous years (private communication) indicated that the refractive structure that would effect the microwave systems was quite similar. Some of the earlier data were obtained from airborne refractometer measurements between Vandenburg AFB and Santa Cruz Island in August of 1969. Therefore, we have assumed that the higher than normal marine layer does not have any significant impact on our results.

It is concluded that the SNI-LP link would not support a digital communication system operating with a mission bit stream on the order of 50 Mb/s, if configured for a single nondiversity

path. The multipath problem would be severe enough to cause unacceptable performance during most of the anomalous (ducting) season. The impulse response measurements show that the coherence bandwidth would not be adequate in the channel, and of course, the nondiversity power fading would be as severe as that known to degrade the present analog signals. The in-band distortion caused by the refractive multipath would frequently cause the BER to exceed threshold limits as reported by Barnett (1978). For example, Barnett's measurements have shown that BER's in excess of $10^{-3}$ were experienced over a non-diversity path when a power distortion (assumed linear) across the signal pass band was as small as 0.2 dB/MHz. These results were obtained on a 78 Mb/s, 8-PSK system, operating at 6 GHz over a 26.4 mile (42.48 km) test link. Transmission path distortions such as these have also been treated theoretically by Emshwiller (1978), and a method for estimating the fractional time of unacceptable performance in a LOS nondiversity link is given by this author for specific systems. Another estimate of nondiversity multipath outage time as a function of path length has been made in a paper by Prabhu and Greenstein (1979). Their results also illustrate the importance of the multipath degradation.

Comparing the real-time observations of BER performance and the multipath structure presented in Section 4, we conclude that significant performance improvement can be expected with the use of space diversity. Rarely in our measurements did we find the dynamic change in the multipath (that caused the worst case performance) occurring in the space diversity channels at the same time. This is <u>not</u> to say that the multipath did not exist in both channels at the same time; only that the dynamic changes were not correlated. Based on this observation, and on the improvement in performance reported by Anderson, et al. (1978) for a space diversity configuration, we conclude that space diversity will yield an acceptable level of performance in the SNI-LP channel with

proper single-link design. It should be noted that the results reported by Anderson, et al. were obtained using an adaptive phase combining technique at IF. It was beyond the scope of this experiment to consider the combining techniques for diversity systems. We thus restrict our consideration to the channel conditions, and conclude that any properly adjusted combining technique should be effective since the basic requirements for good space-diversity reception were inherent in the measurements. For example, if a switched type combiner is used, it also should be effective as long as it has been designed and adjusted for "hitless" operation with respect to the digital transmission stream.

The most restrictive frequency character in terms of the coherent bandwidth of the channel develops when the multipath delay approaches the 14 ns value. This was not a dominant condition however; delays of this magnitude were seen infrequently as shown in the delay distribution functions in the Appendix. In addition, this delay magnitude was practically never seen simultaneously in the space-diversity channels. It is interesting to note also, that this value of delay is quite close to the 13 ns value one would calculate for the maximum delay based on the path geometry and the 3 dB power points for the parabolic antenna patterns over this link.

Improvement of performance through frequency diversity was also noted as a distinct possibility in the discussion in Section 4. Although the experiment was not designed to evaluate specifically this aspect, the observation from the data is significant. Based on theoretical developments (Dougherty, 1967), the present frequency separation used on the SNI-LP link should provide a fade protection on the order of 24 dB. Within the frequency assignments used for other links in the PMTC network, the potential exists for much better diversity protection (greater frequency separations).

To summarize the above, it is concluded that the SNI-LP link will support a digital communication system with a

transmission bit-rate on the order of 50 Mb/s, if the system is configured using both the space and frequency diversity techniques presently used with proper combining. Space diversity alone would perhaps be adequate, but the frequency diversity should assure even better performance.

In addition to the diversity reception considerations, the above conclusion is also predicated on the assumption that some form of adaptive equalization (or compensation) should be an inherent feature of the digital microwave radio. We cannot evaluate this adaptive performance technique from our measurements, but we can consider it from the characterization of the measured channel and improvement results reported by others. It is readily seen from the channel response measurements that even with a space-diversity switched-combining technique, the in-band distortion to the 50 Mb/s transmission stream can become severe. For example, the linear distortion factor of 0.2 dB/MHz reported by Barnett (1978) can be several times higher in this channel when the multipath delay approaches the measured extreme of 14 ns. Thus, in order to protect the system under these conditions, an adaptive equalizer should be considered.

The expected performance improvement can be estimated from two recent experiments. The first of these has been reported in the literature by Anderson, et al. (1978). These authors report that a simple adaptive linear amplitude equalizer provides an improvement factor of about 2 when applied to a nondiversity channel. This factor is relative to the probability of a system outage in the "worst fading month", which was determined to be approximately $1 \times 10^{-3}$. This performance value was based on measurements performed on an 8 GHz, 91.04 Mb/s QPRS system, operating over a 51 km path. The base line for system outage was with reference to long-haul availability of 99.98%; requiring an outage probability per loop of $<1.43 \times 10^{-6}$ in the "worst fading month". These authors point out that the non-diversity link performance (probability of outage) was 700 times worse than the long-haul availability

objective. With the use of space diversity (phase adaptive IF combining) this factor was reduced to the order of 18. The combination of adaptive equalization and space diversity provided a combined improvement factor on the order of 20; adequate to reduce the probability of outage to a value "compatible with long-haul availability objectives".

The second reported improvement based on in-band adaptive processing has been reported informally by Rockwell International (Marketing Bulletin, MW-63A, Sept. 6, 1978; private communication). In this case, an adaptive equalizer has been designed and laboratory tested in the IF amplifier modules of digital receivers. The reported results include a correction of up to 14 dB of linear tilt in the IF bandpass of 30 MHz width; a slope of 0.47 dB/MHz. We note that this represents an improvement factor on the order of 2.5 over the in-band slope distortion reported to be critical in Barnett's (1978) measurements. In addition, the equalizer is reported to be very effective against frequency selective fades at or near the bandpass center frequency, and is capable of responding to fade rates as high as 75 dB/s.

It is recommended that the digital SNI-LP link be first engineered on the basis of a nondiversity system, and an estimate of the expected outage time be computed using the techniques suggested by Emshwiller (1978) and/or Prabhu and Greenstein (1978). Multipath values from this report may be used as typical for the link during the worst of the anomalous propagation. The time expected for the latter should be estimated from previous meteorological data and experience, and should include the expected conditions for December as well as the dominant months of August and September. The nondiveristy performance (outage) estimate can then be used to calculate the expected outage or availability time for the system as implemented with space and frequency diversity, and including the improvement factor for the recommended adaptive in-band processing. These methods should provide a reasonable and fairly

reliable performance estimate for the implemented digital system. In this process, it is implied that the nondiversity performance calculation be based on known statistics of the fading encountered over the link for the present analog system, and using deviations from the theoretical performance curves given in the literature for the modulation techniques used (i.e., QPSK, 8-PSK, QPRS, etc.).

## 6. ACKNOWLEDGEMENTS

The author wishes to acknowledge the following individuals for their noted contributions to this project:

Mr. Jim Weblemo and Mr. Jim Kaness of PMTC for their support and interest in the project. Mr. Kaness served as project monitor.

Mr. Jim Ordner and Mr. Henry Merhoff of PMTC for their interest, support, and background information relative to the project. ITS also owes a great deal of thanks to other personnel in the Range Communications Division for their technical assistance during the conduct of the experiment.

Mr. Robert Bowker of PMTC for his excellent assistance in making the necessary logistic and technical support arrangements.

Mr. Lauren Pratt and Mr. John Wood of ITS for their efforts in both installing the equipment, and performing the measurements at Pt. Mugu. Their assistance in the data analyses and summaries is also appreciated.

Mrs. Olive Fritz of ITS for preparation of the manuscript.

## 7. REFERENCES


Anderson, C.W., S. Barber, and R. Patel (1978), The effect of selective fading on digital radio, International Communications Conference, Toronto, Ontario, Canada, June.

Barnett, W.I. (1978), Measured performance of a high capacity 6 GHz digital radio system, International Communications Conference, Toronto, Ontario, Canada, June.

Dougherty, H.T. (1967), Microwave fading with airborne terminals, ESSA Tech. Rept. IER 58-ITSA 55, October.

Dougherty, H.T., and W.J. Hartman (1977), Performance of a 400 Mbit/s system over a line of sight path, IEEE Trans. on Comm., Vol. COM-25, No. 4, April.

Emshwiller, M. (1978), Characterization of the performance of PSK digital radio transmission in the presence of multipath fading, International Communications Conference, Toronto, Ontario, Canada, June.

Gallager, R.G. (1964), Characterization and measurement of time and frequency spread channels, MIT Lincoln Laboratory, Lexington, MA, Report 352.

Hartman, W.J., and D. Smith (1975), Titlting antennas to reduce line-of-sight microwave link fading, Federal Aviation Administration, Report No. FAA-RD-75-38, February.

Hubbard, R.W. (1977), Measurements in microwave telecommunication systems using a pseudo-random noise (PN) probe, URSI Measurement in Telecommunications, Lannion, France, October.

Linfield, R.F., R.W. Hubbard, and L.E. Pratt (1976), Transmission channel characterization by impulse response measurements, OT Report 76-96, August.

PMTC (1976), Communications Capability, Capabilities Development Department, Pacific Missile Test Center, Pt. Mugu, CA.

Prabhu, V.K., and L.J. Greenstein (1978), Analysis of multipath outage with applications to 90 Mb/s PSK systems at 6 and 11 GHz, IEEE Trans. on Comm., COM-27, No. 1, Janaury.

Rummler, W.D. (1978), A multipath channel model for line-of-sight digital radio systems, International Communications Conference, Toronto, Ontario, Canada, June.

Samson, C.A., A.P. Barsis, and D. Smith (1976), Performance measurement over long line-of-sight microwave links in Colorado, OT Report 76-92, June.

## APPENDIX

This appendix contains a selected summary of the data analyses used to reach the conclusions presented in the main body of this report. Section A is a presentation of the pulse-width distribution analyses performed on the power impulse functions, measured for both channels of the space diversity receiver at Laguna Peak. Section B contains a few selected analyses of the tilted-beam experimental data, showing the probability distribution functions of the RSL for both tilted and untilted receiving antennas. Section C presents some additional analyses that are discussed in relation to each figure, and includes an example of a ray-tracing that depicts the possibility of reflective multipath within a strong duct on the SNI-LP link.

### A. Impulse-Width Distribution Analyses.

The range of multipath delays reported in Section 4 has been determined from the probability functions presented below. The width of the measured impulse responses was analyzed using a time-histogram algorithm in a special digital analyzer. To avoid errors in cases where the impulse response splits due to phase opposition of short-delay components, a trigger circuit was designed to assure full pulse-width distribution analyses. The distributions thus display the probability density (pdf) of the total delay spread over the indicated analysis period.

These distribution functions actually convey two pieces of information about the dynamics of the channel response (see for example Figure A-2). First, the probability of the delay spread is shown in the right half of the function, to the value of the pulse width in excess of the "clear channel" width. The latter is 13.3 ns for the 150 MHz clock rate, and 40 ns for the 50 MHz data. The portion of the function to the left of these values register periods when the response was narrowed due to phase interference between the multipath components or by power fading. It will be noted in some of the functions that the

pulse width has a finite probability density to a pulse width of zero. This characteristic is typical of fading in the channel, and indicates those periods where the phase opposing multipath causes complete cancellation of the received impulse.

Figure A-1 presents the distribution functions for the 5-minute data samples shown in Figures 10 through 13 of Section 4. The maximum delay spread is seen to be on the order of 10 ns, with a fairly high probability of phase interference fading (pulse widths < 40 ns).

Figures A-2 through A-14 present the pdf's of the power impulse width for several data runs during the period 22 August 1978, through 14 September 1978. Specific notes regarding the distributions are included in each figure. A few of the presentations include samples of the RSL records taken during the period of the pdf's. From these, one can see the relation between the impulse width distributions and the signal fading characteristics.

B. Angle Diversity Analysis.

As noted in Section 4, the data indicate that angle diversity does not provide any fade margin improvement for refractive multipath. Although individual fades may be found in all of the data that were less severe on the tilted antenna channel, the converse was also true. The probability density analyses of the RSL have shown that the tilted antenna had a higher probability of a deeper fade. Figures A-15 through A-17 are representative examples of these data, and were chosen to illustrate essentially three different fading characteristics found in the data. Examples of the RSL recording are included in the lower half of each figure.

C. Additional Analyses.

The origin of multipath components is difficult to define for most microwave links, especially when they are derived in an anomalous propagation condition. For example, multipath in a strong ducting environment is no doubt due to refraction/

diffraction through the atmosphere rather than any form of reflection. However, the refractive structure found during the morning hours of 1 September 1978 was stable enough to permit at least a cursory examination of the possibility for a reflection from the ducting layer. The gradient of the duct was severe with a dN/dh of approximately -160N/kft (-525N/km), which is seen to be much greater than a trapping gradient. This steep gradient is equivalent to an effective earth radius factor $k = -0.43$. The boundaries of the ducting layer were also well defined from the refractivity data. The basic propagation conditions are illustrated in Figure A-18, based on a flat-earth model of the LP-SNI link. As seen from Figure A-6(a), the multipath on both diversity channels during the morning hours was on the order of 12 ns maximum. Using a nominal delay of 10 ns, we have plotted the locus (ellipsoid) for a reflected component with this delay. The ellipsoid is distorted on the flat earth profile, but the solid-line locus is the lower half of the ellipse around the $k = -0.43$ ray path (with the duct). In this example there is a possibility that the multipath could be a result of a reflection from the upper boundary of the ducting layer. The evidence is the near tangential relation between the boundary and the reflection locus. The standard atmospheric condition ($k = 4/3$) is included in the figure for reference purposes. An important observation to make is that the multipath with these conditions could not be due to any surface reflections.

Another example of possible reflection multipath from a layer is illustrated in Figure A-19. We note from Table 1 that during the afternoon hours of 1 September 1978, the ducting layer was higher than during the morning, with the lower bound about 500 ft above SNI. The nominal refractive profile from the surface to the layer was substandard with $dN/dh \simeq 0$. This corresponds to a $k = 1$ over most of the path below the duct. Referring to the impulse width distributions for the afternoon of this date shown in Figure A-6(b), we see that the multipath

delays were between 4 and 8 ns. Thus, using a nominal delay of 6 ns, we have plotted the locus for a reflection in Figure A-19. It is apparent that a reflection from the surface would require a specific tilt to a wave, and is thus less likely than a reflection from the lower bound of the layer. The latter can be seen from the tangential relation between the layer boundary and the 6 ns locus curve near 50 miles (80 km) in Figure A-19.

Surface reflections are also of importance in analyzing this link. Under standard atmospheric conditions, the most likely location of surface reflections would be from a point about 40 to 45 miles from the LP terminal. The nominal delay for a surface reflected component would be on the order of 2 to 3 ns. The most significant evidence of the surface component is perhaps shown in the impulse width distributions of Figure A-14(a) for the afternoon of 13 September 1978. Both diversity channels show a higher probability of the impulse width near 15 ns, which would correspond to the surface reflection delay. It is obvious however, that longer delay times were prevalent with the highest probability of delay being approximately 5 ns. This delay was probably caused by a small layer that existed near the LP terminal, but below the LP height.

The best evidence of a surface reflection was observed for the data of 8 September 1978 in the early morning hours before sunrise (Figure A-11). The refractivity structure was super refractive (approaching ducting) with a gradient of -30 N/kft (-98.4 N/km), yielding a $k = 2.7$. Under these conditions a surface component could be observed from a point approximately 50 miles from LP with a delay on the order of 5 ns. The impulse distributions of Figure A-11 indicate a high probability that this component was present.

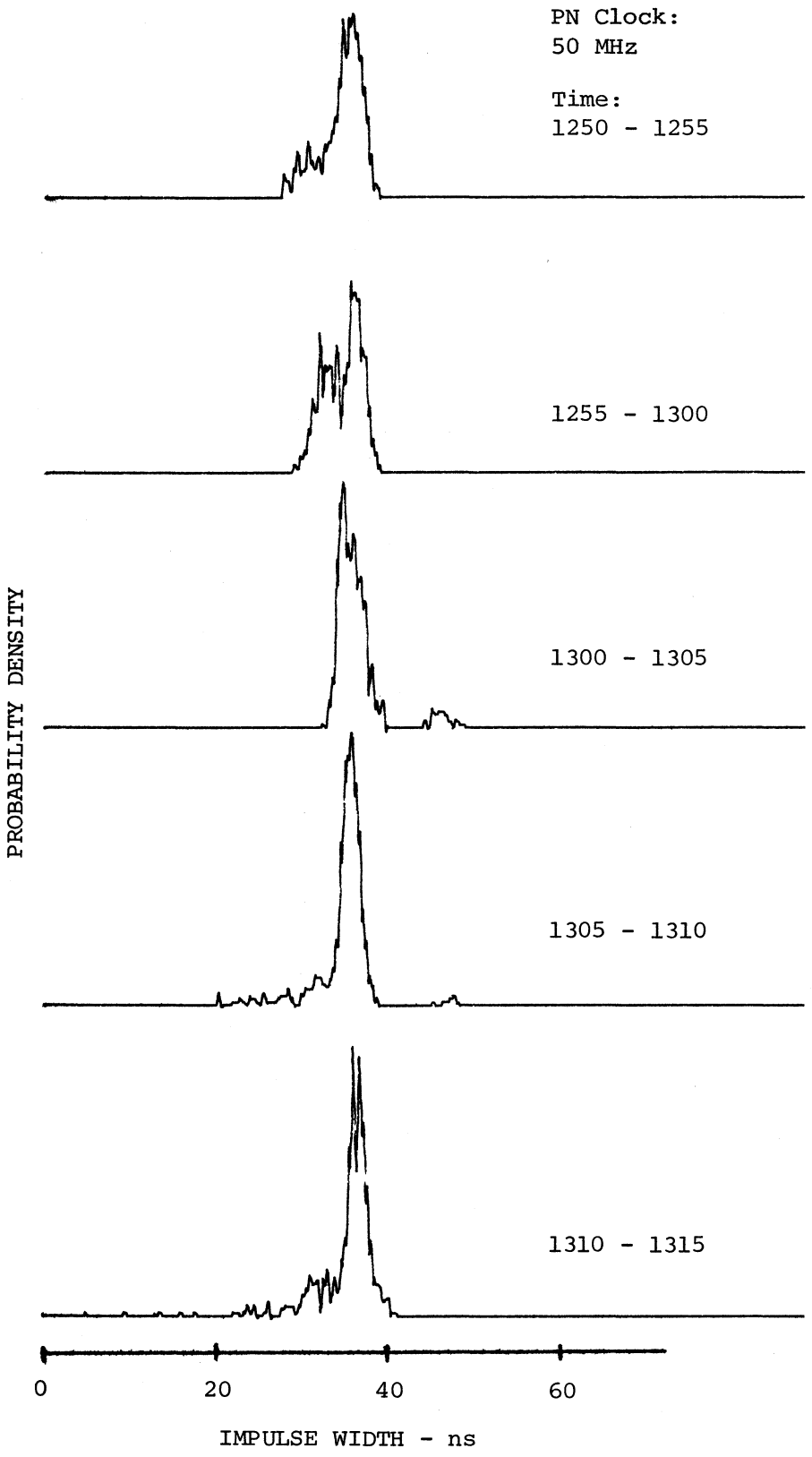


Figure A-1. The probability density functions of the power impulse width for the low antenna on 31 August 1978. These data correspond to Figures 10 through 13.

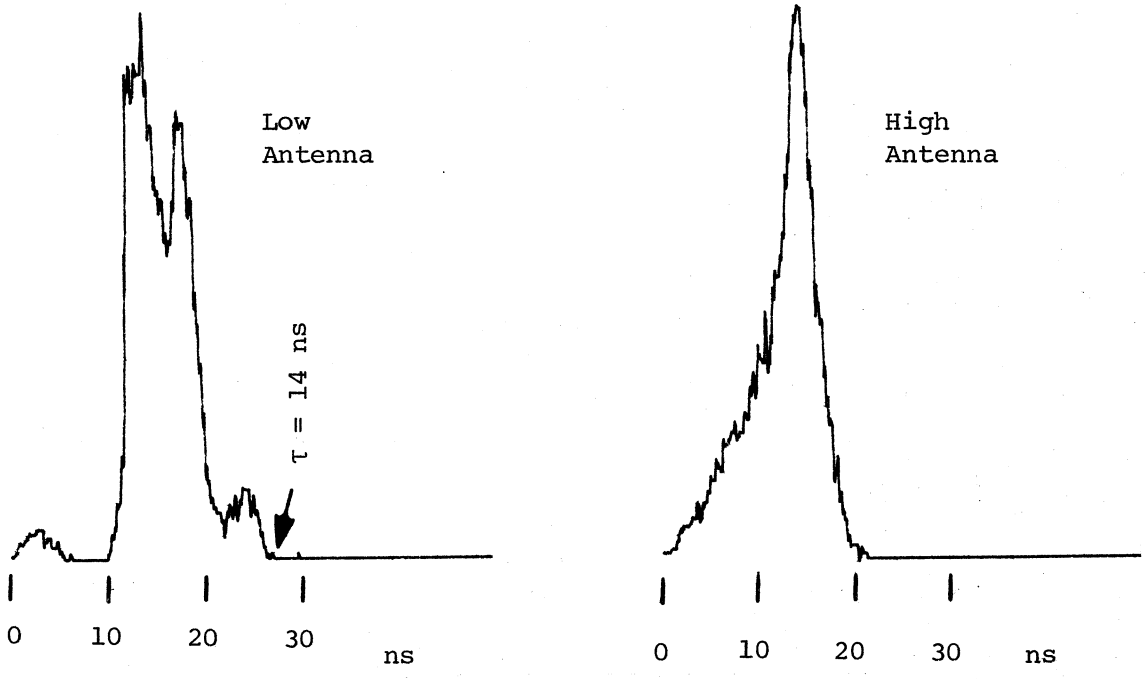


(a) Time: 1550 - 1735 PST PN Clock Rate: 150 MHz

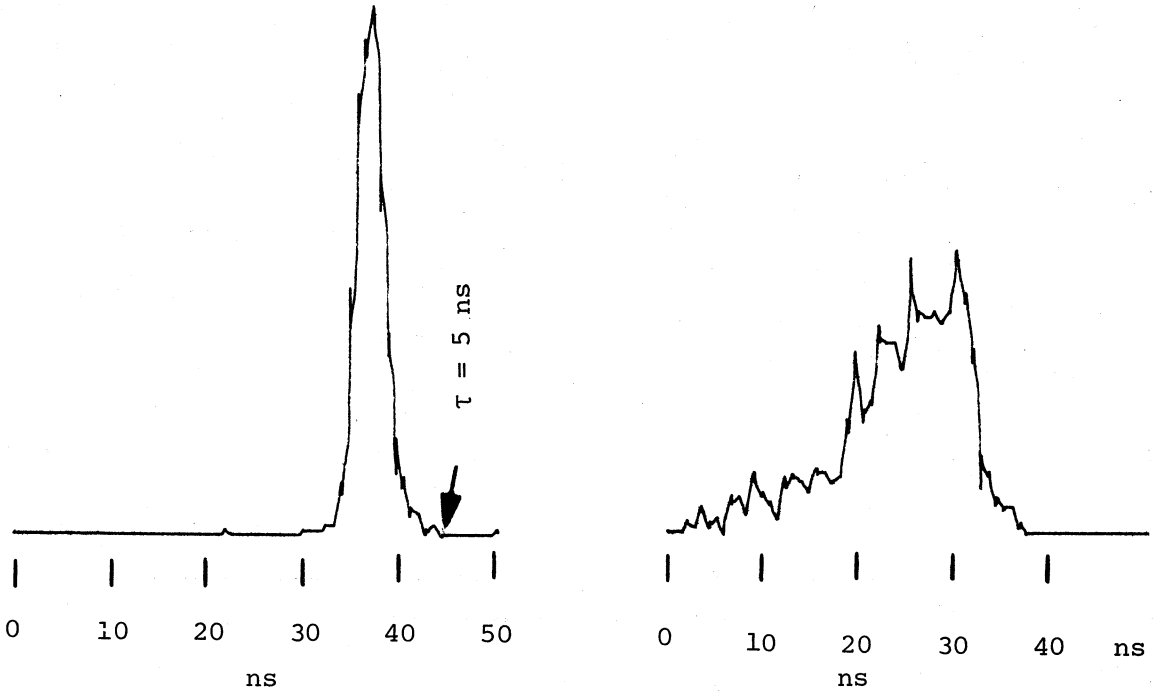


(b) Time: 1740 - 1750 PST PN Clock Rate: 50 MHz

Figure A-2. Power impulse width distributions for 22 August 1978.

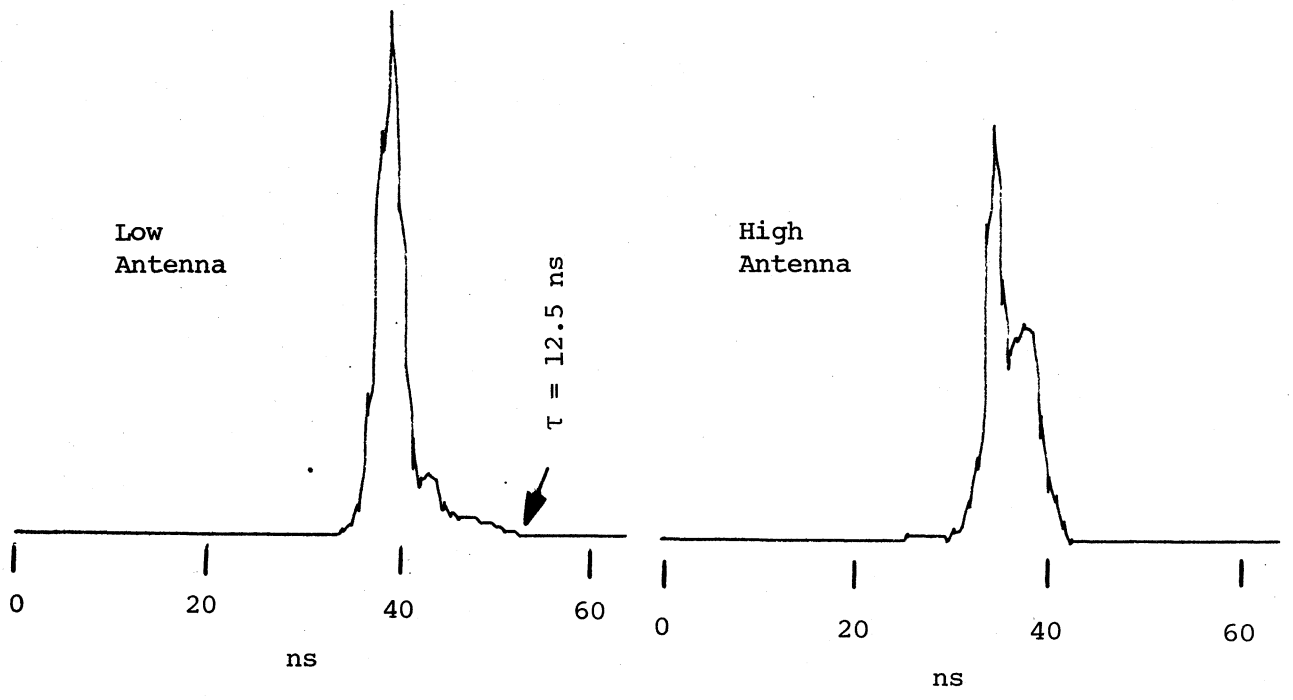


(a) Date & Time: 23 August 1978, 0907 - 0930 PST PN Clock Rate: 50 MHz

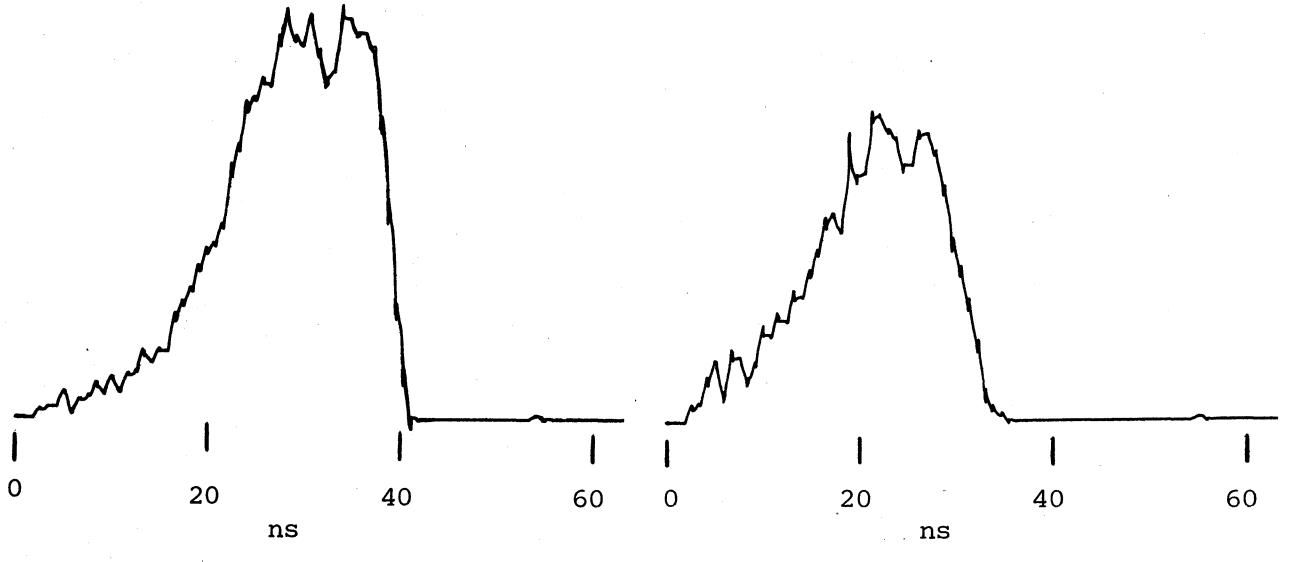


(b) Date & Time: 24 August 1978, 1515 - 1645 PST PN Clock Rate: 50 MHz

Figure A-3. Power impulse width distribution functions.

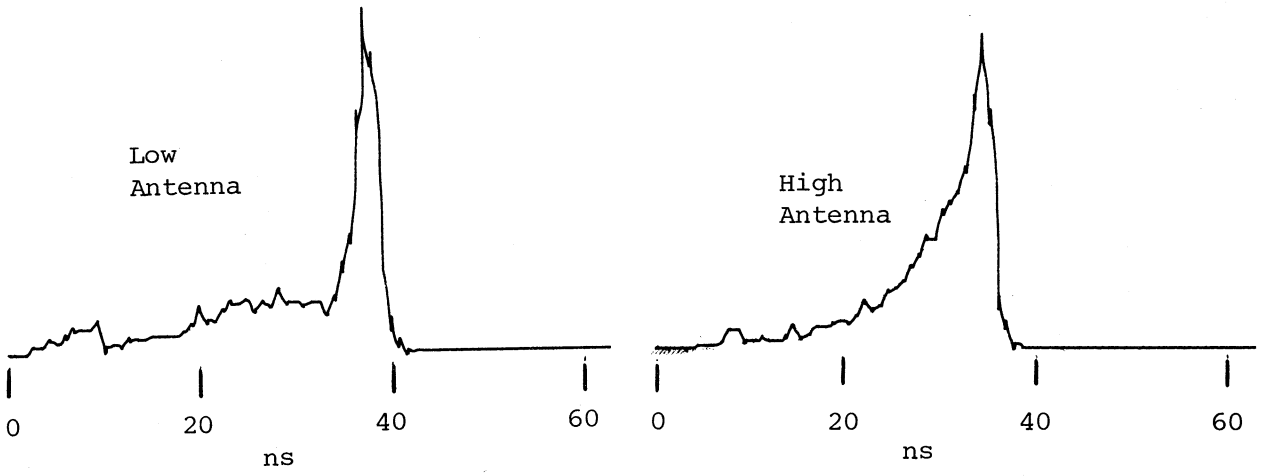


(a) Time: 0900 - 0950 PST PN Clock Rate: 50 MHz

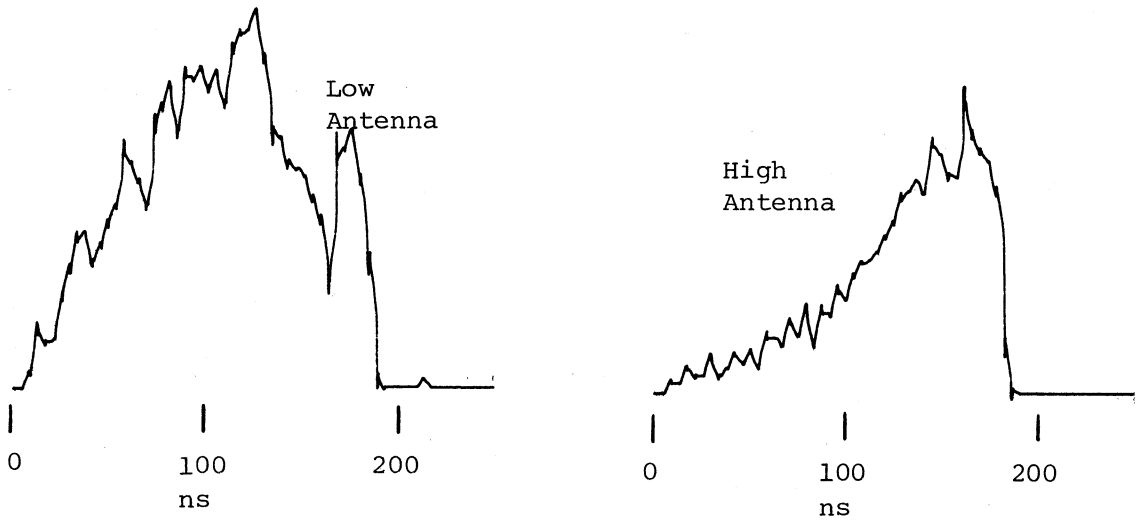


(b) Time: 1530 - 1600 PST PN Clock Rate: 10 MHz

Figure A-4. Power impulse width distributions for 25 August 1978.

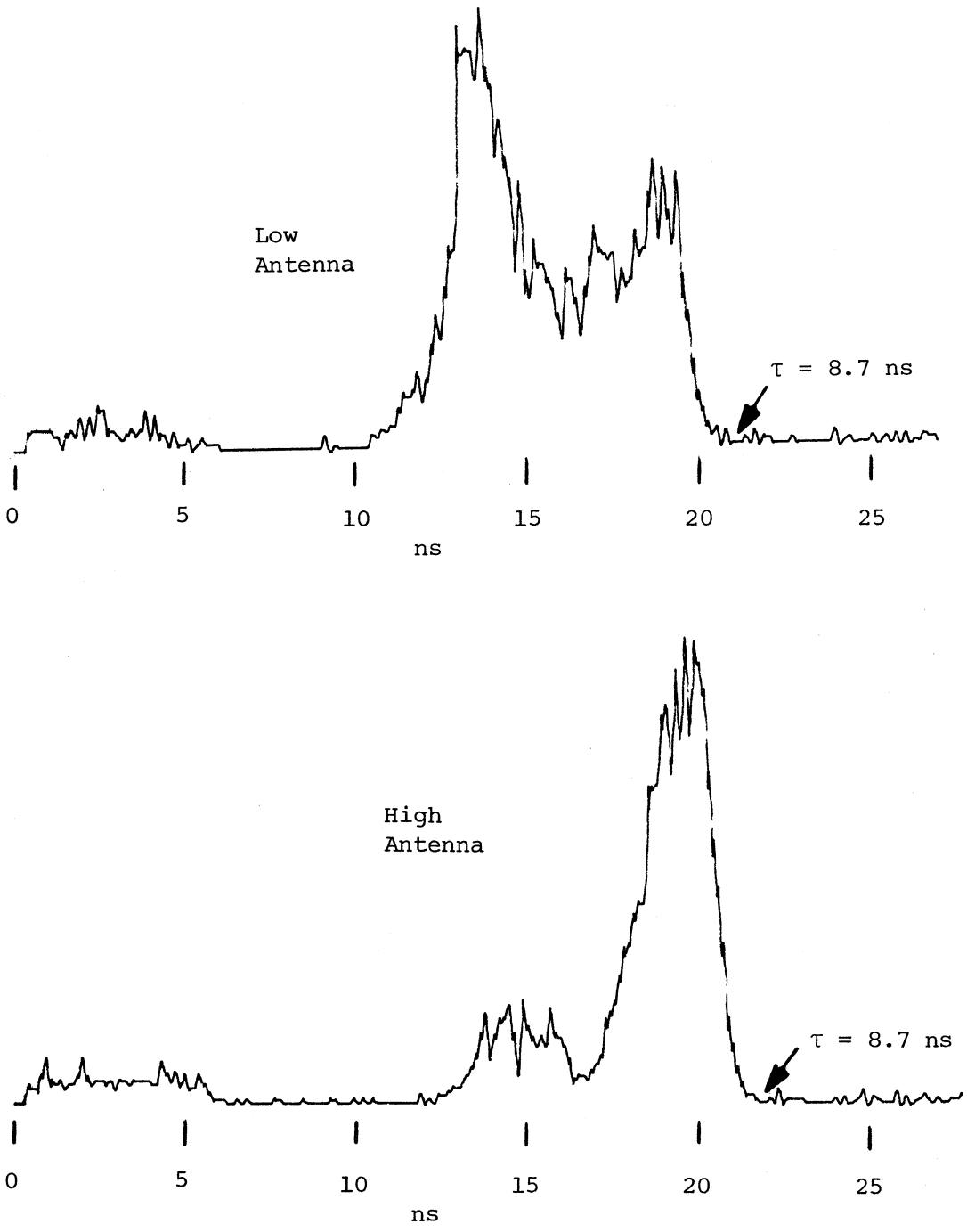


Figure A-5. The power impulse width distribution functions for the data of 31 August 1978. These data were measured between 1112 and 1200 PST at a PN clock rate of 150 MHz, just prior to the period discussed in Section 4.

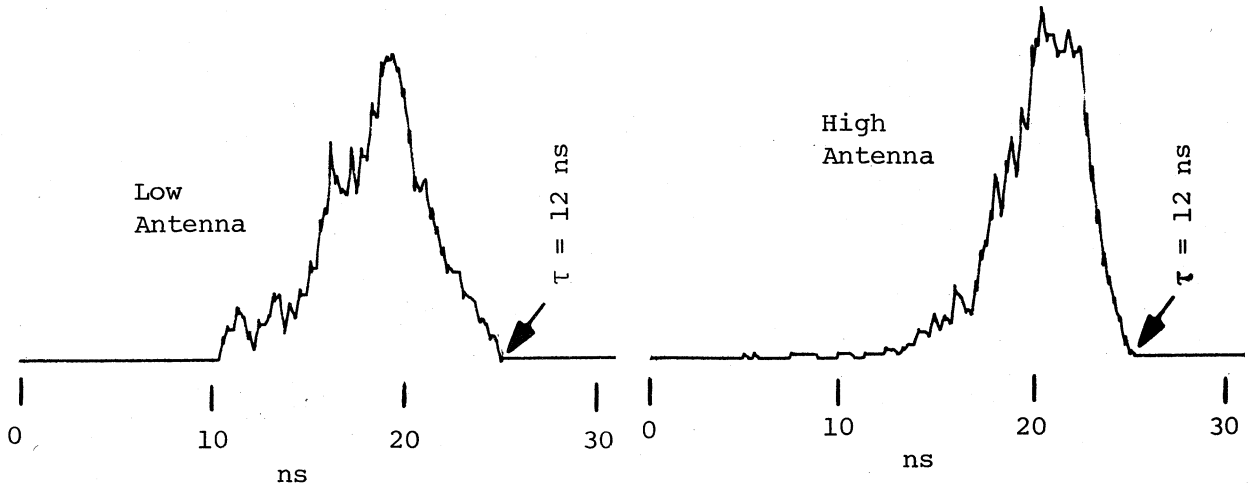


(a) Time: 1005 - 1055 PST PN Clock Rate: 150 MHz

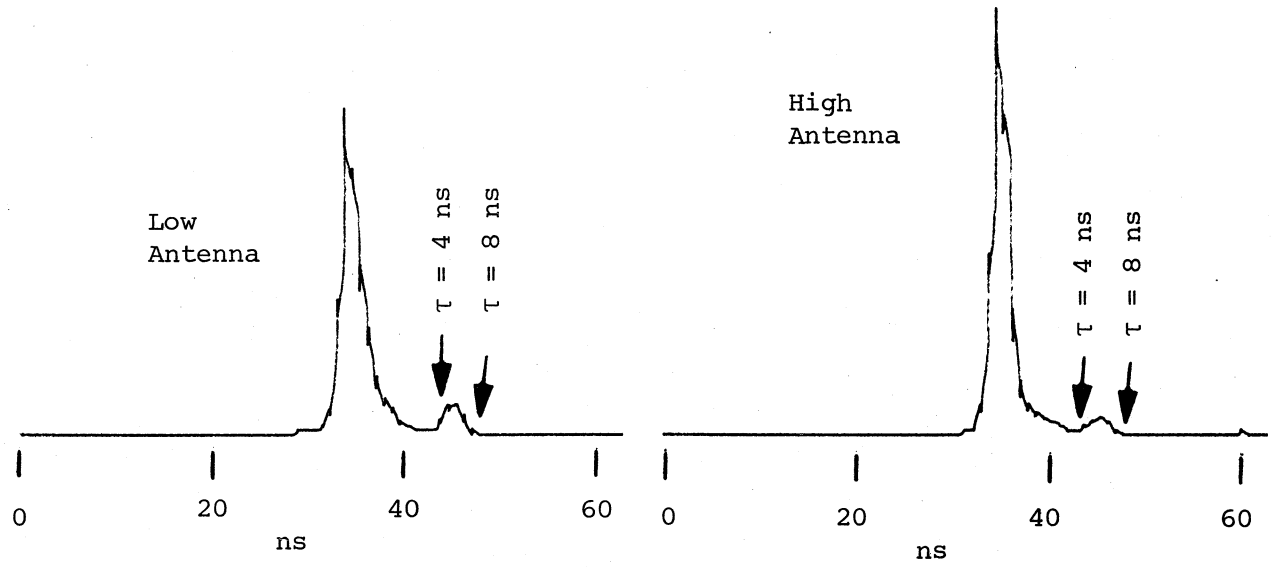


(b) Time: 1155 - 1435 PST PN Clock Rate: 50 MHz

Figure A-6. Power impulse width distributions for 1 September 1978.

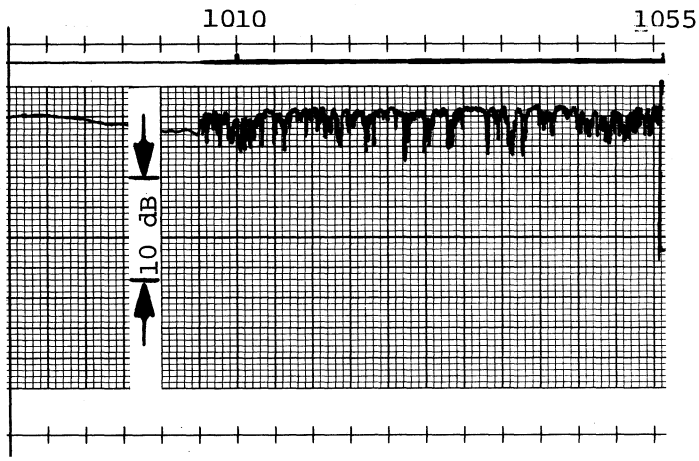


(a) RSL record for 1005 - 1055 PST, 1 September 1978, low antenna.

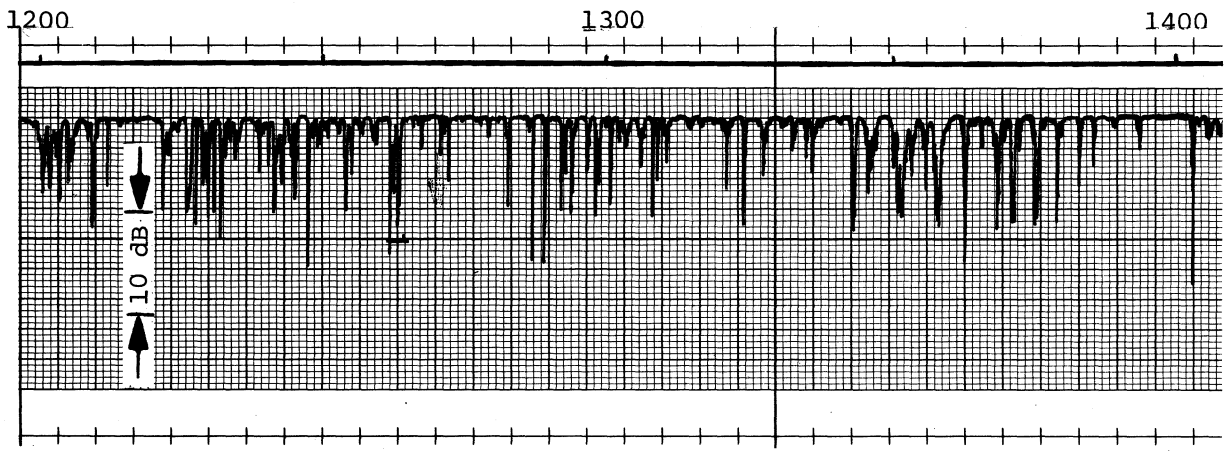


(b) RSL record for 1200 - 1400 PST, 1 September 1978, low antenna.

Figure A-7. Recordings of the PN probe RSL for the multipath conditions depicted by the distribution functions in Figure A-6. Note that the phase interference fading is worse for the afternoon data. This fact is reflected in the higher probability that the power impulse width was less than standard, as shown by the distribution functions of Figure A-6(b).

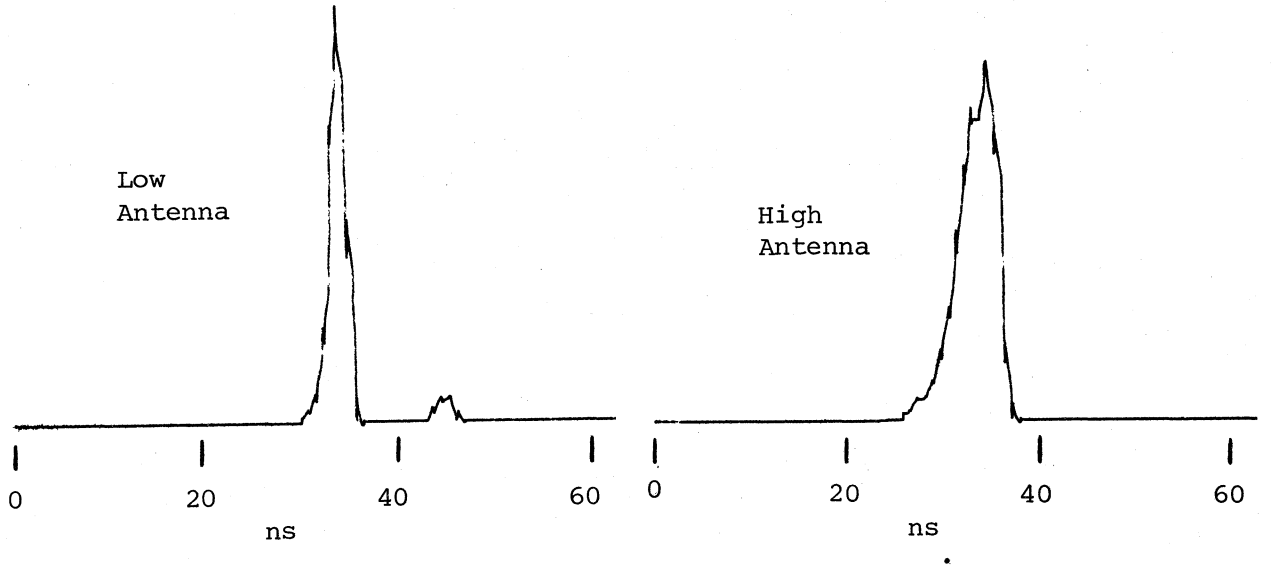


(a) Time: 1705 - 2300 PST PN Clock Rate: 50 MHz

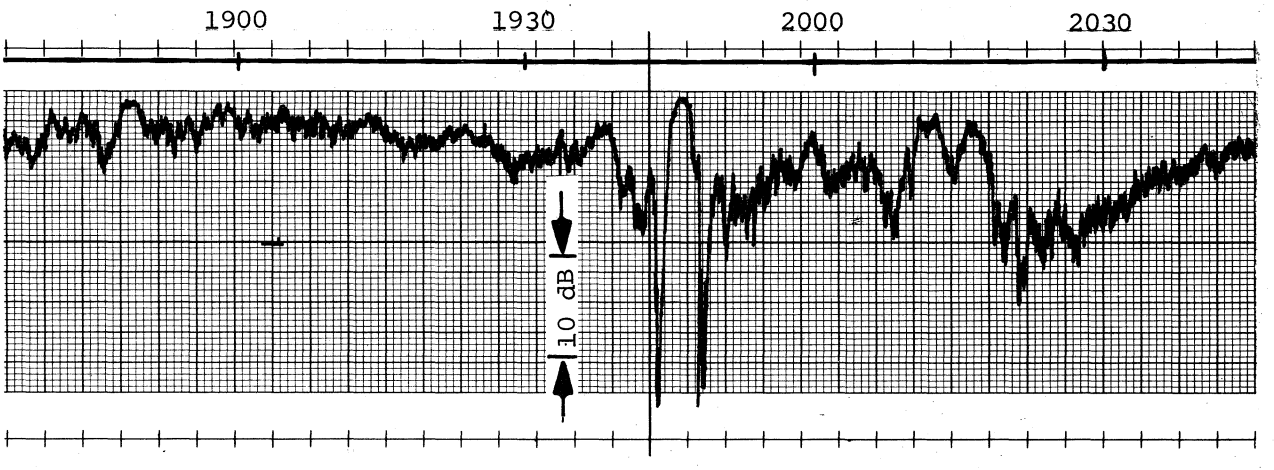


(b) RSL record of the PN signal on the low antenna.

Figure A-8. Power impulse width distributions and RSL record for a night run on 5 September 1978. Note that the distribution function for the impulse data on the low antenna is quite similar to that of Figure A-6. The fading however is much slower, indicating less dynamic change in the multipath components. Two very deep fades are seen around 1945 PST, with a signal enhancement between them.

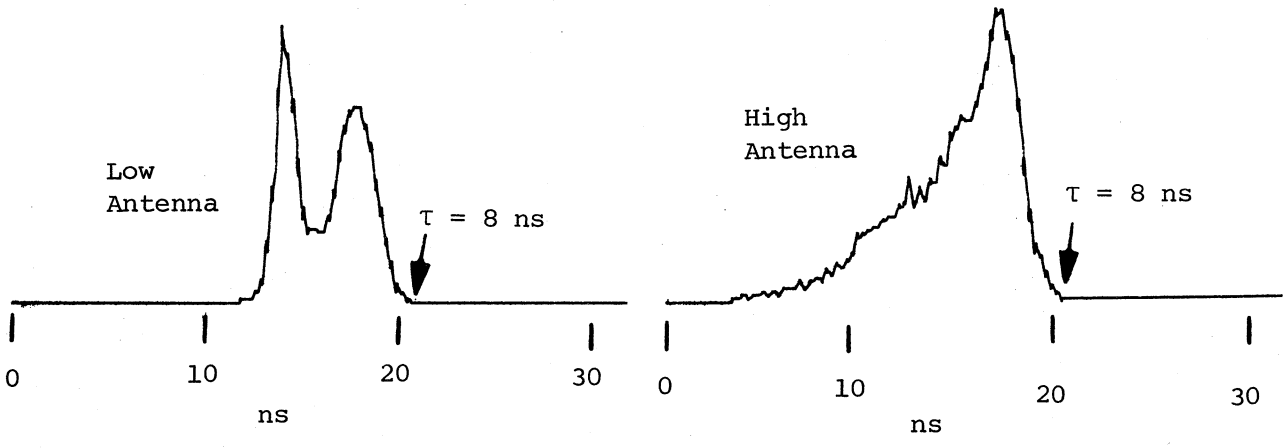


(a) Time: 1635 - 1910 PST PN Clock Rate: 150 MHz

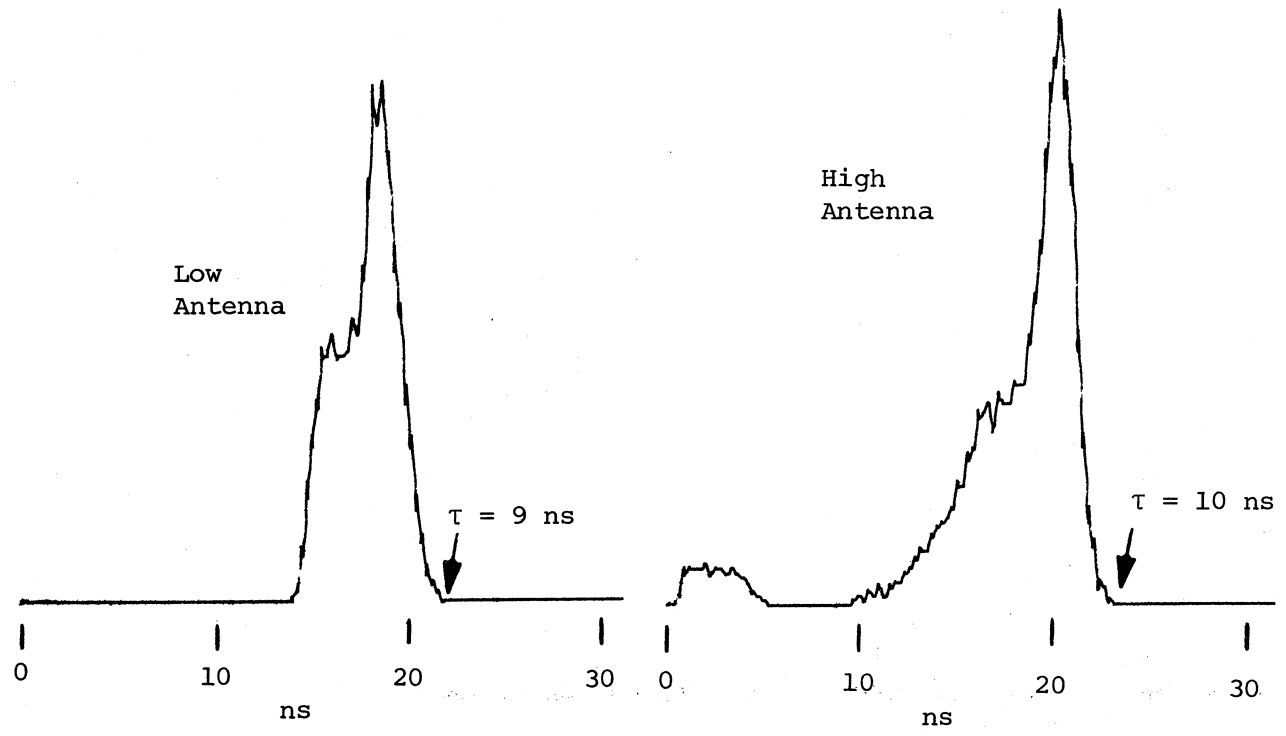


(b) Time: 1957 - 2155 PST PN Clock Rate: 150 MHz

Figure A-9. Power impulse width distributions for 6 September 1978.

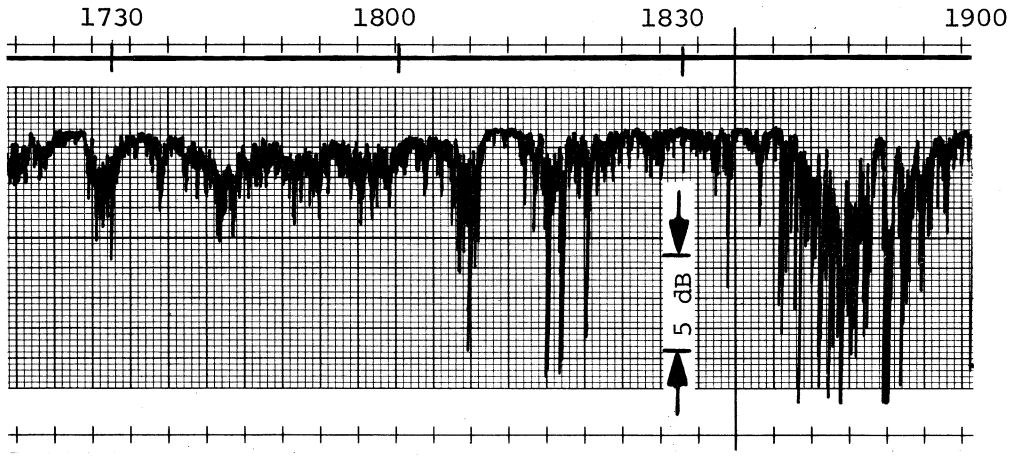


(a) RSL for the period 1730 - 1900 PST, 6 September 1978.

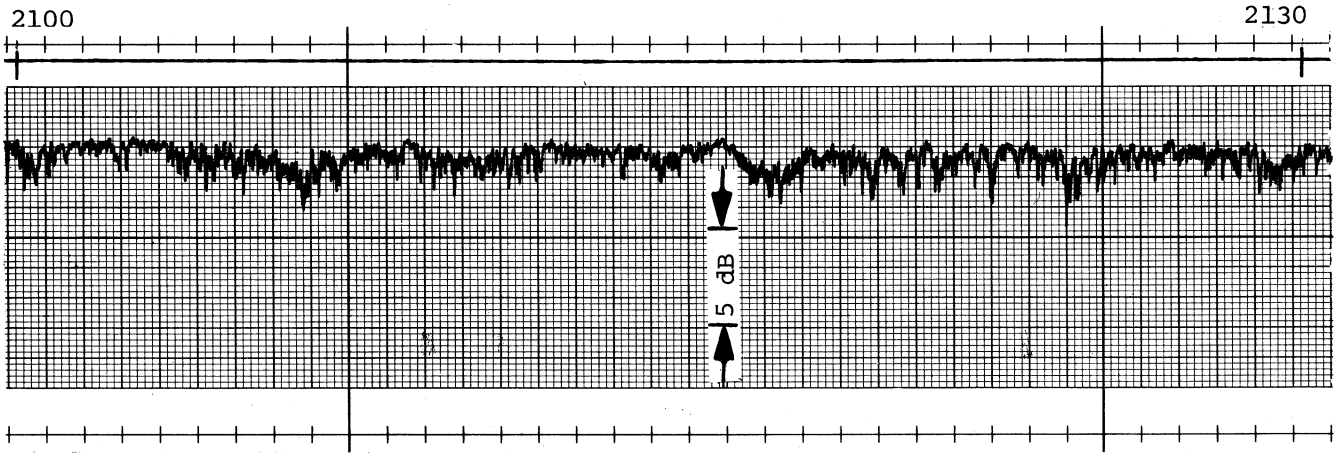


(b) RSL for the period 2100 - 2130 PST, 6 September 1978.

Figure A-10. The RSL records of the PN probe data for the low antenna distributions of Figure A-9. The delay spread of the multipath is similar for each period; however, the dynamics of the channel cause deeper fading over the sunset period.

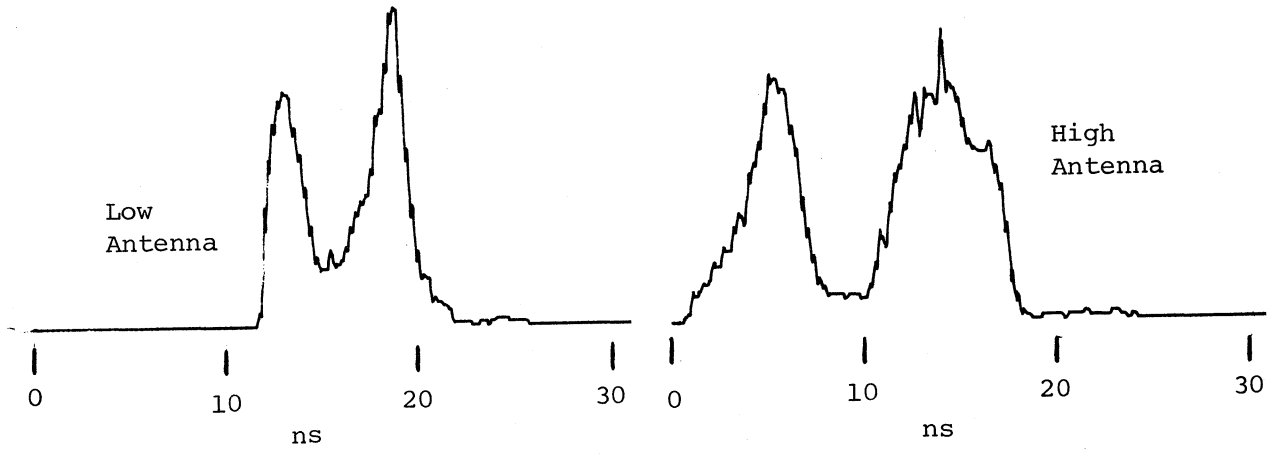


(a) Time: 0030 - 0207 PST PN Clock Rate: 150 MHz

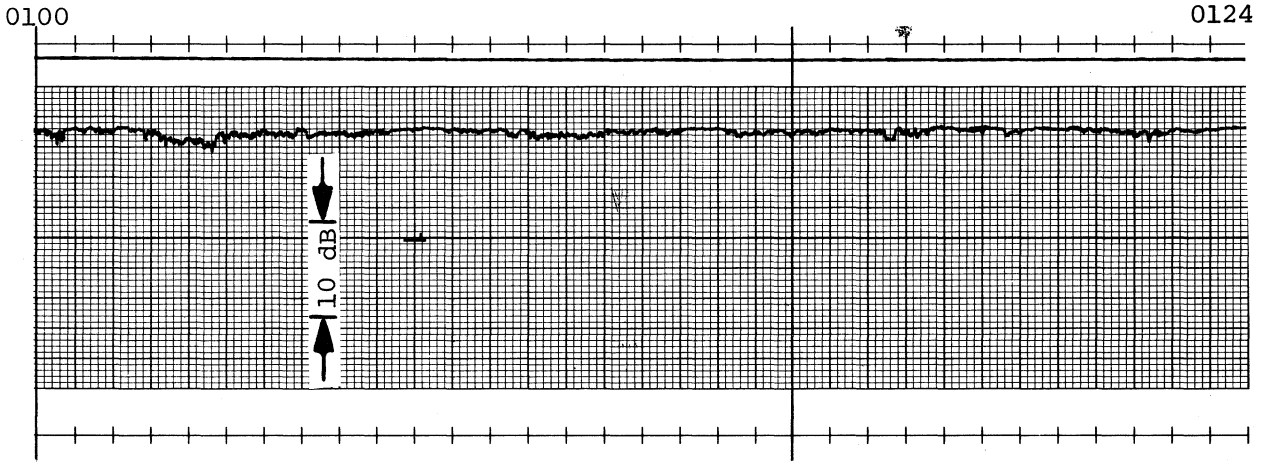


(b) RSL record for the low antenna between 0100 and 0124 PST. The steady signal was typical for the entire night until early morning.

Figure A-11. Power impulse width distributions and the RSL record for an all night run on 7-8 September 1978. The multipath delay was essentially the same for both diversity channels; however, the fading was significantly different. As seen in (b), the low antenna RSL was very stable. The fading in the high antenna channel was severe, as noted from the impulse width distribution in (a).

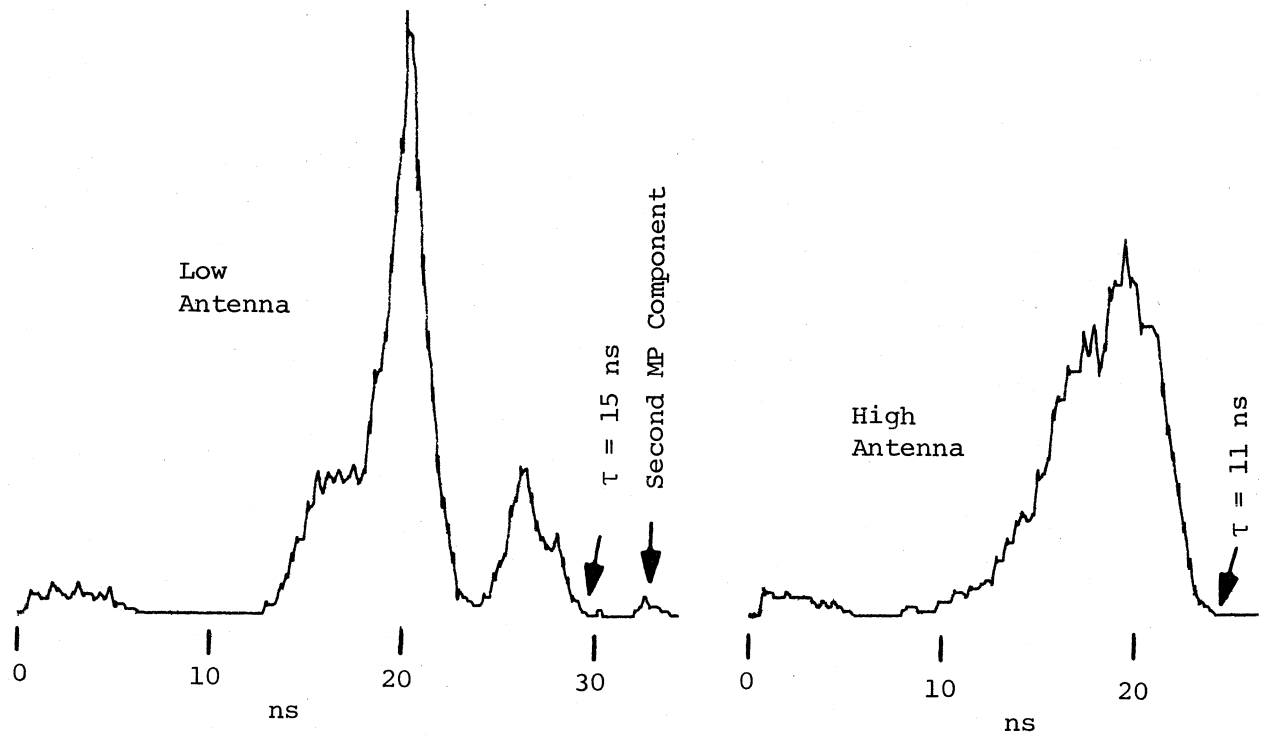


(a) Time: 0445 - 0649 PST PN Clock Rate: 150 MHz

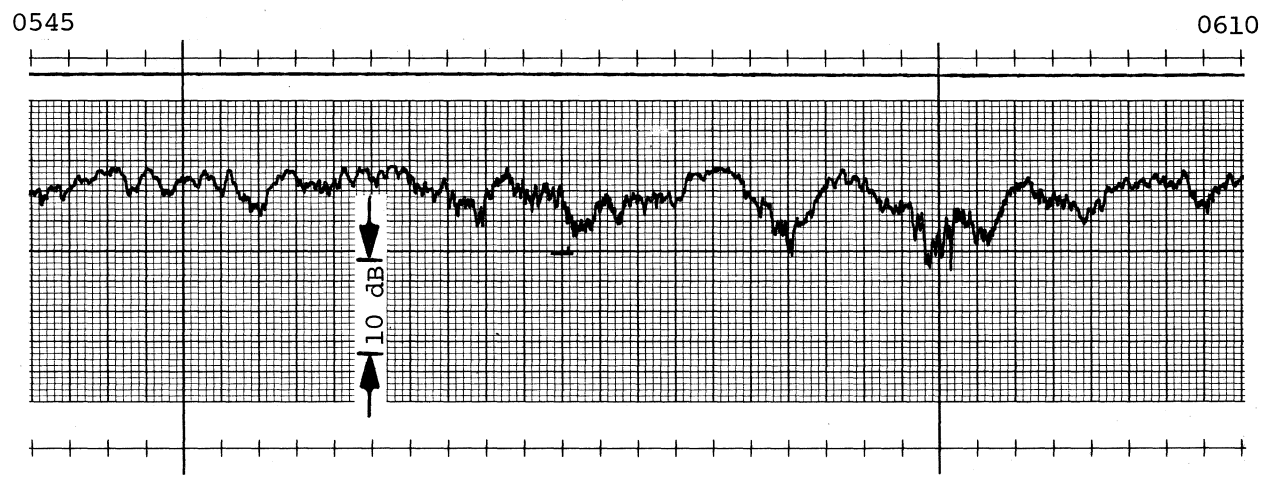


(b) RSL record for the low antenna between 0545 and 0610 PST.

Figure A-12. Power impulse width distributions and the RSL record for the early morning and sunrise period on 8 September 1978. Both channels began to fade during this period, and the impulse response for the low antenna indicated a three-path structure as noted in the distribution function of (a).

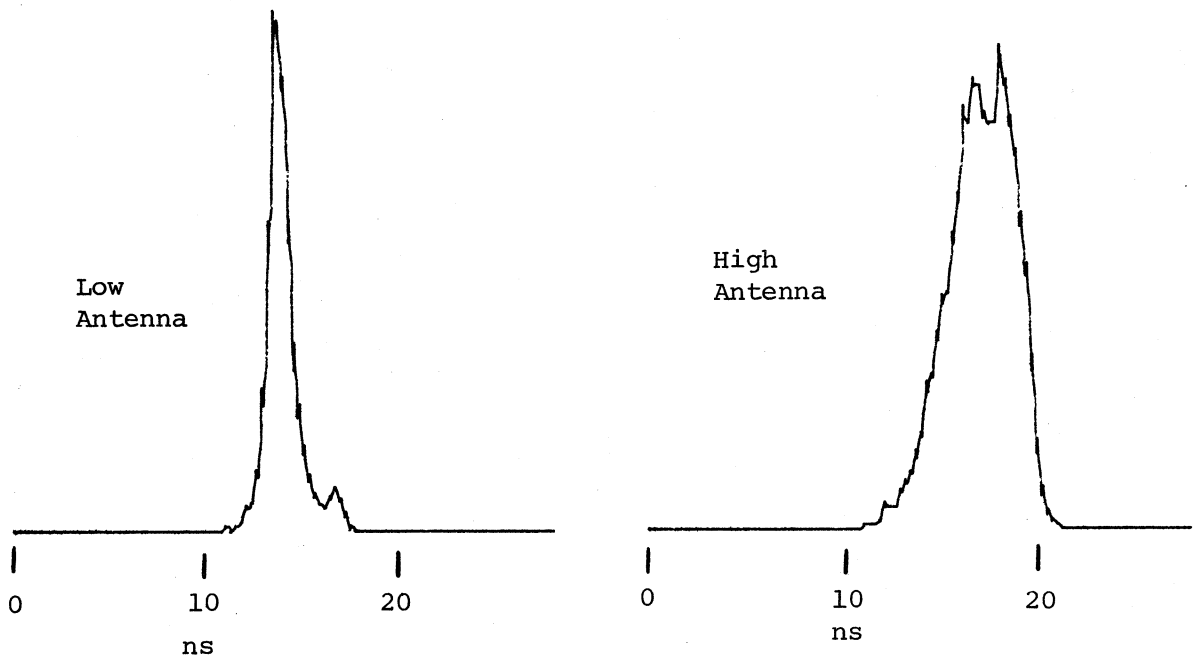


(a) Date & Time: 10 September 1978, 0550 - 0740 PST PN Clock Rate: 150 MHz

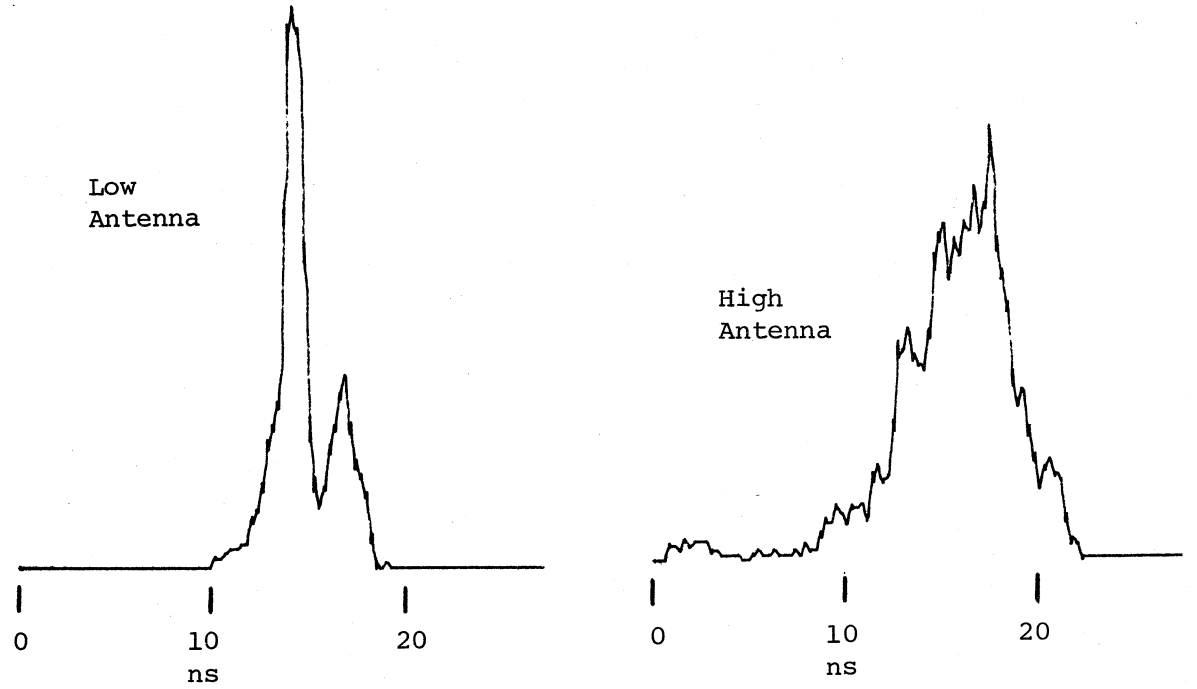


(b) Date & Time: 11 September 1978, 0947 - 1100 PST PN Clock Rate: 150 MHz

Figure A-13. Power impulse width distribution fuunctions for the data of 10 and 11 September 1978. Note that the distribution functions for the low antenna data indicate a near-standard impulse width with high probability.

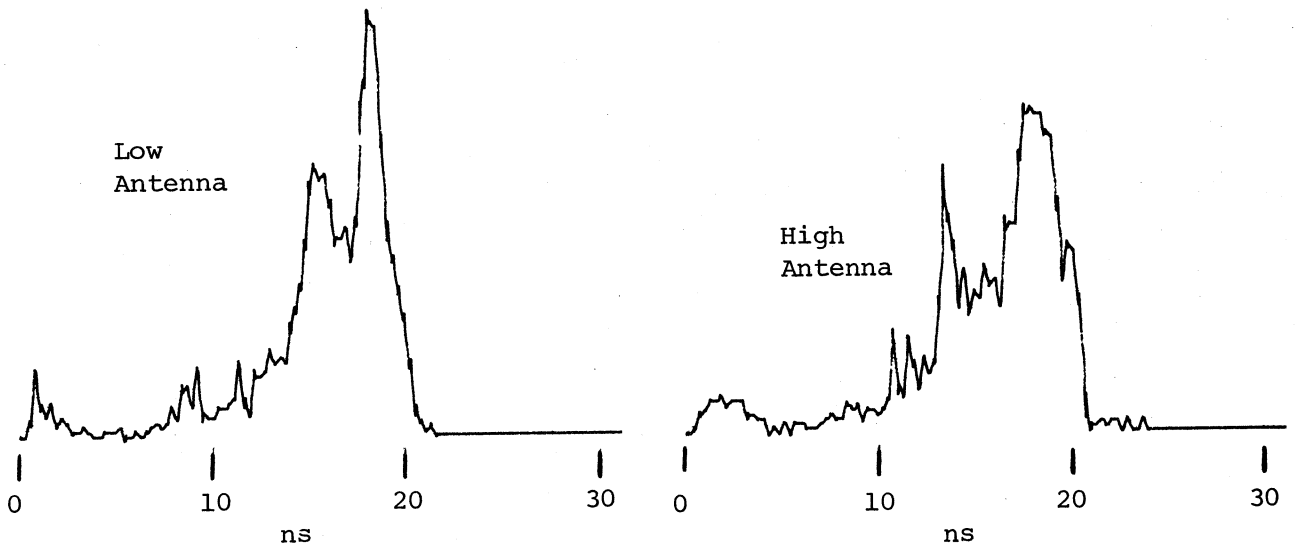


(a) Date & Time: 13 September 1978, 1630 - 1654 PST PN Clock Rate: 150 MHz

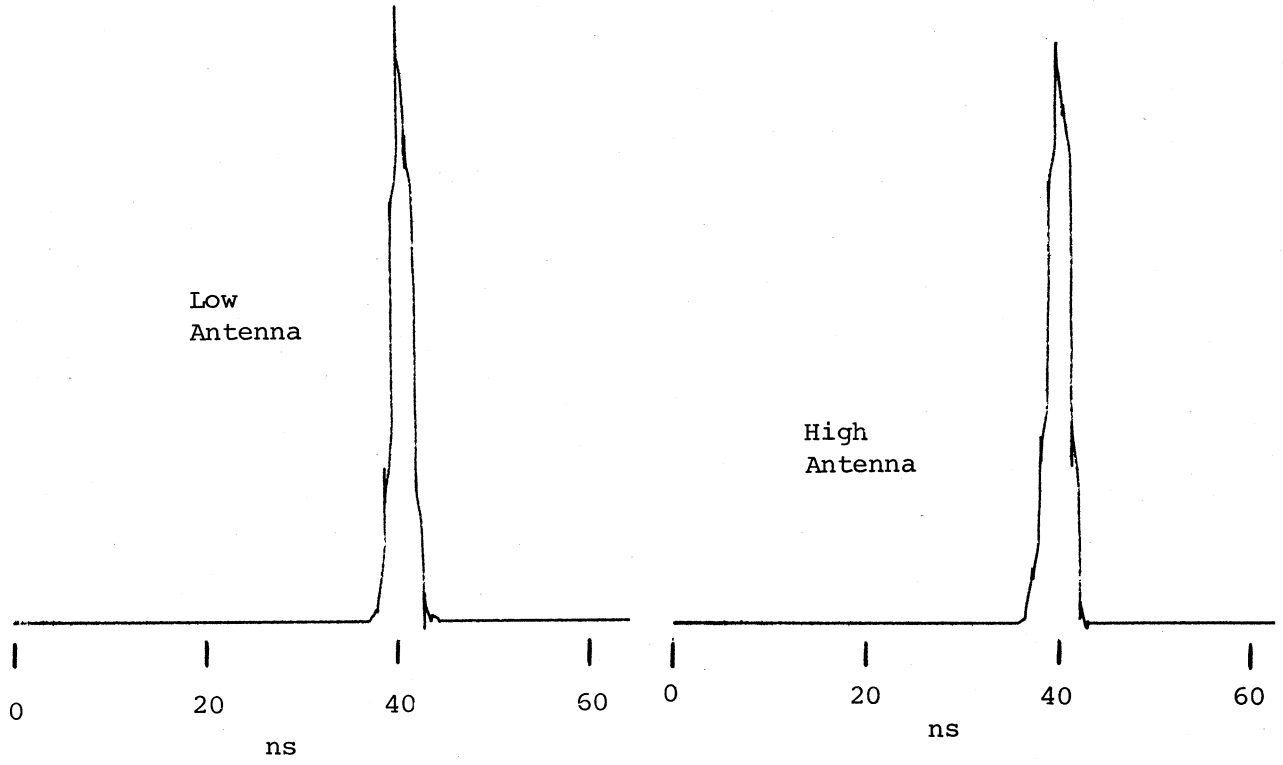


(b) Date & Time: 14 September 1978, 1100 - 1200 PST PN Clock Rate: 50 MHz

Figure A-14. Power impulse width distributions for the data of 13 and 14 September 1978. Minor multipath and moderate fading were characteristic for 13 Sept. Little or no multipath was seen in the final run on 14 Sept.

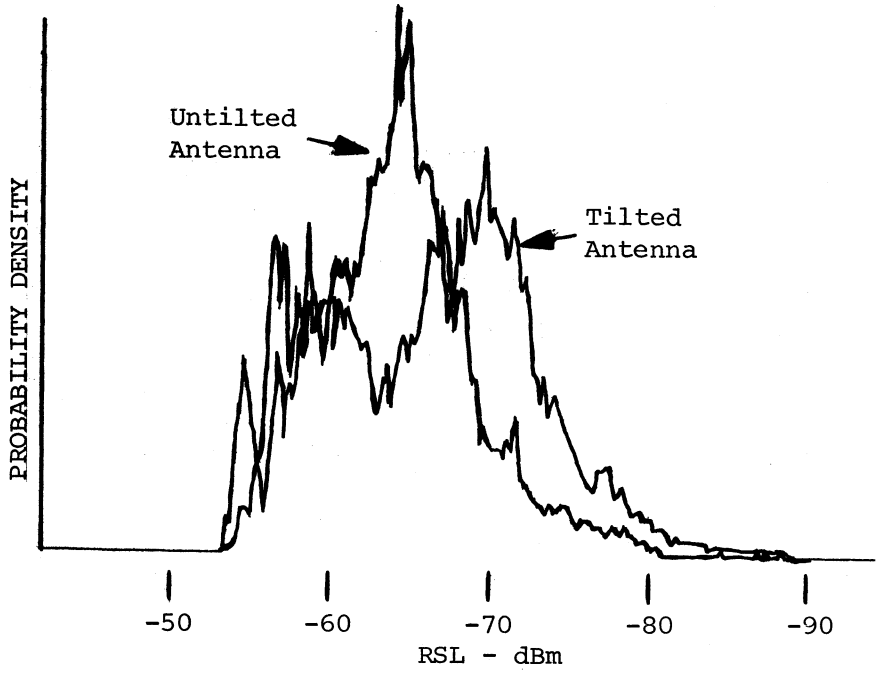


(a) Probability density functions.

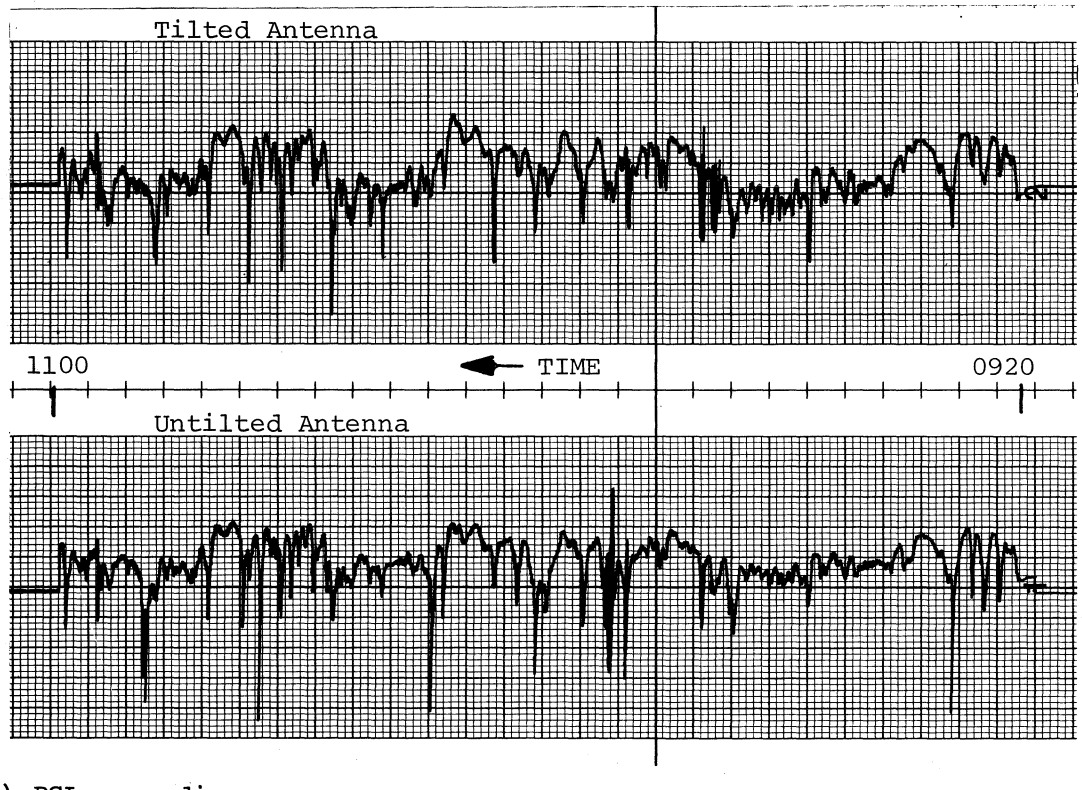


(b) RSL recording.

Figure A-15. Angle diversity data, 0920 to 1100 PST, 31 August 1978.

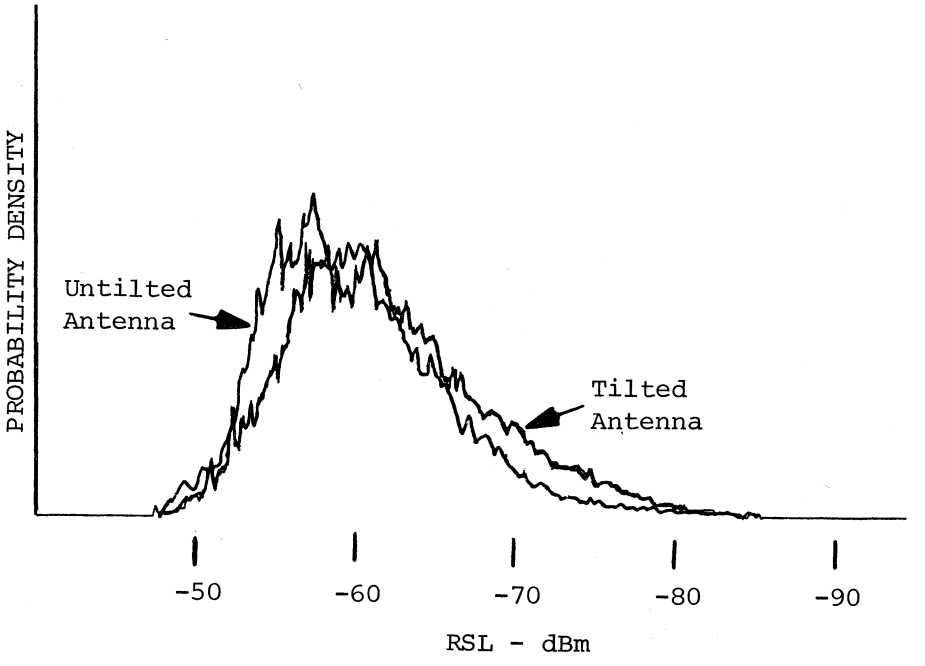


(a) Probability density functions.

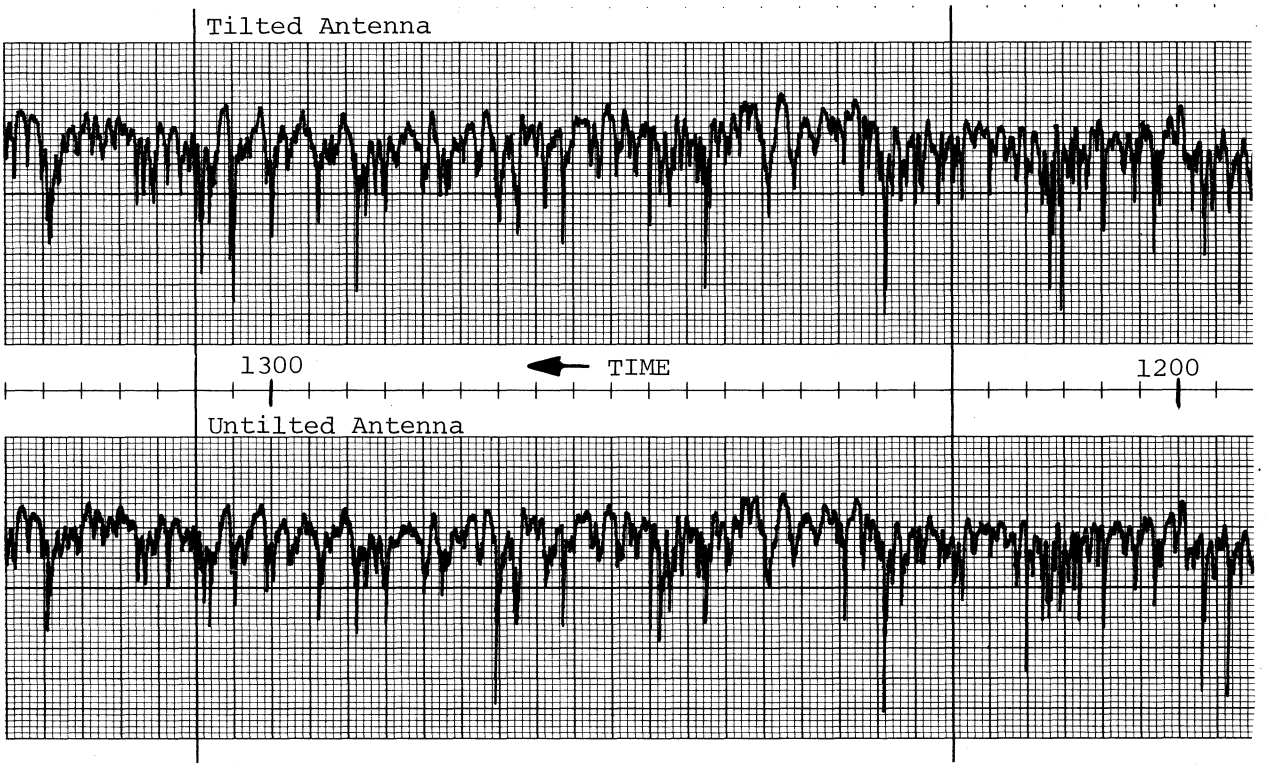


(b) RSL recording.

Figure A-16. Angle diversity data, 1155 to 1435 PST, 1 September 1978.

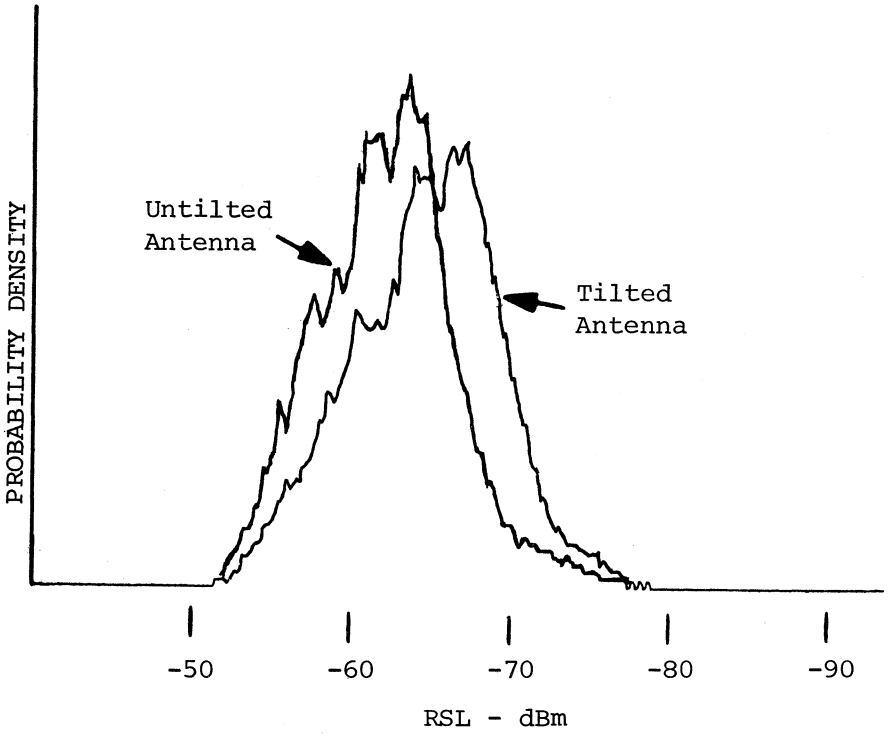


(a) Probability density functions.

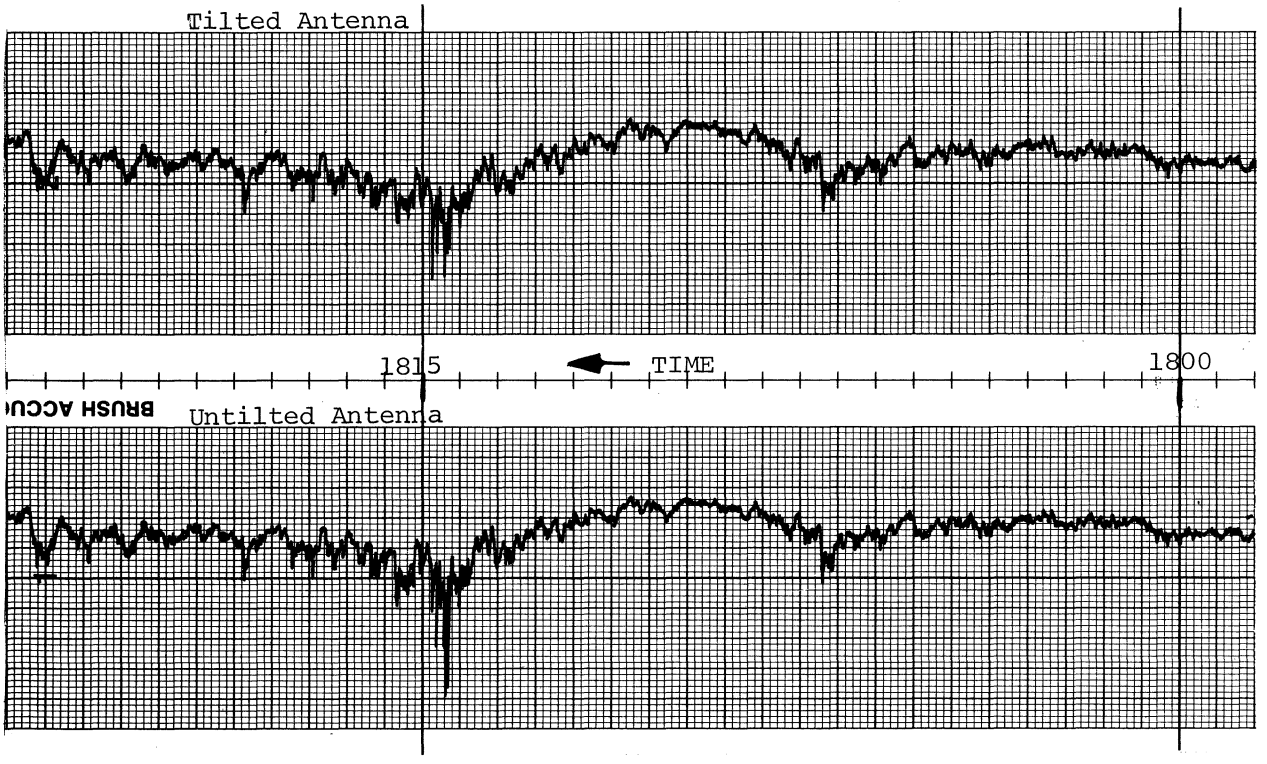


(b) RSL recording.

Figure A-17. Angle diversity data, 1710 to 1910 PST, 5 September 1978.

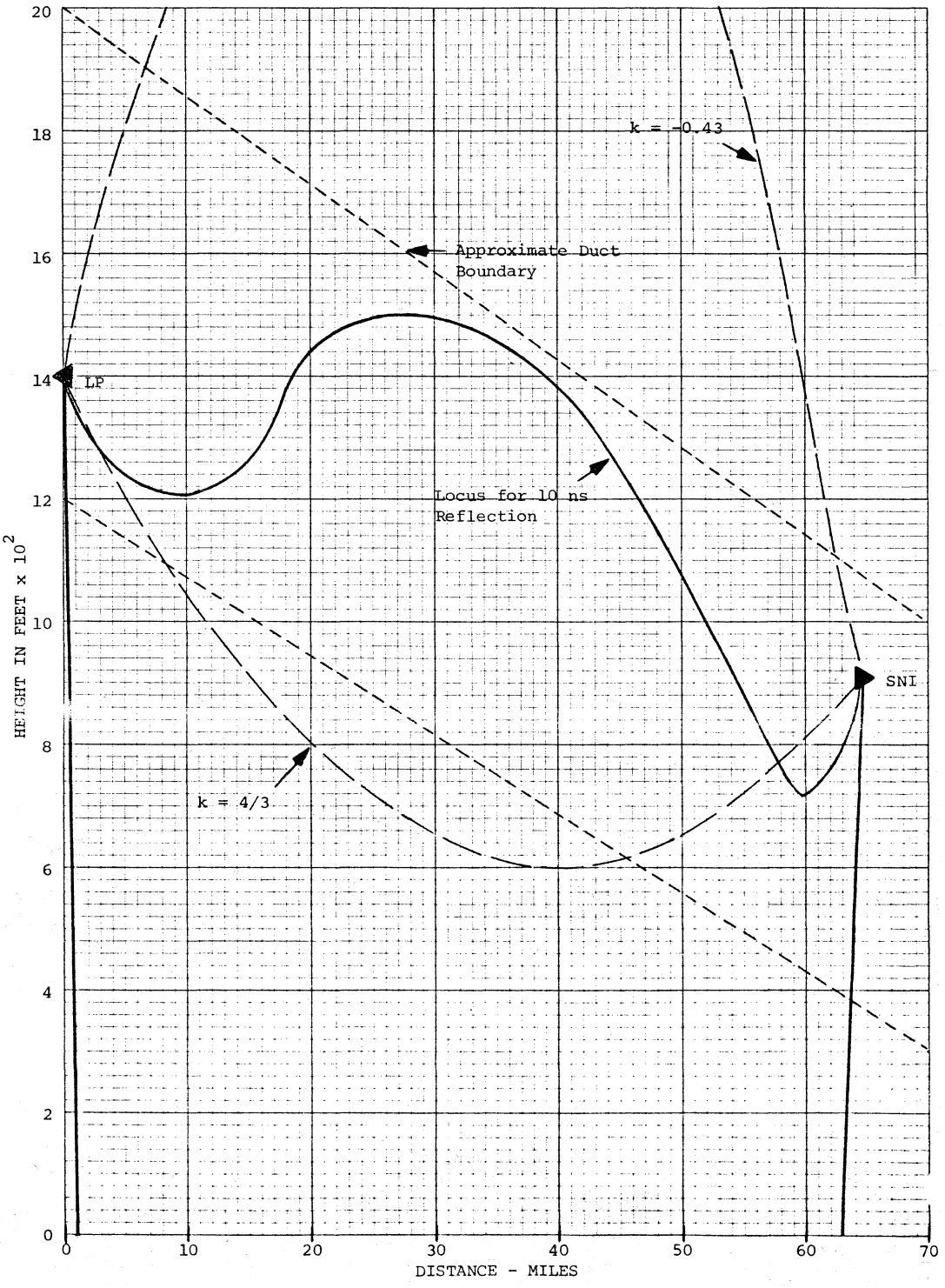


Figure A-18. Illustration of possible reflection type multipath from a strong ducting layer on 1 September 1978.

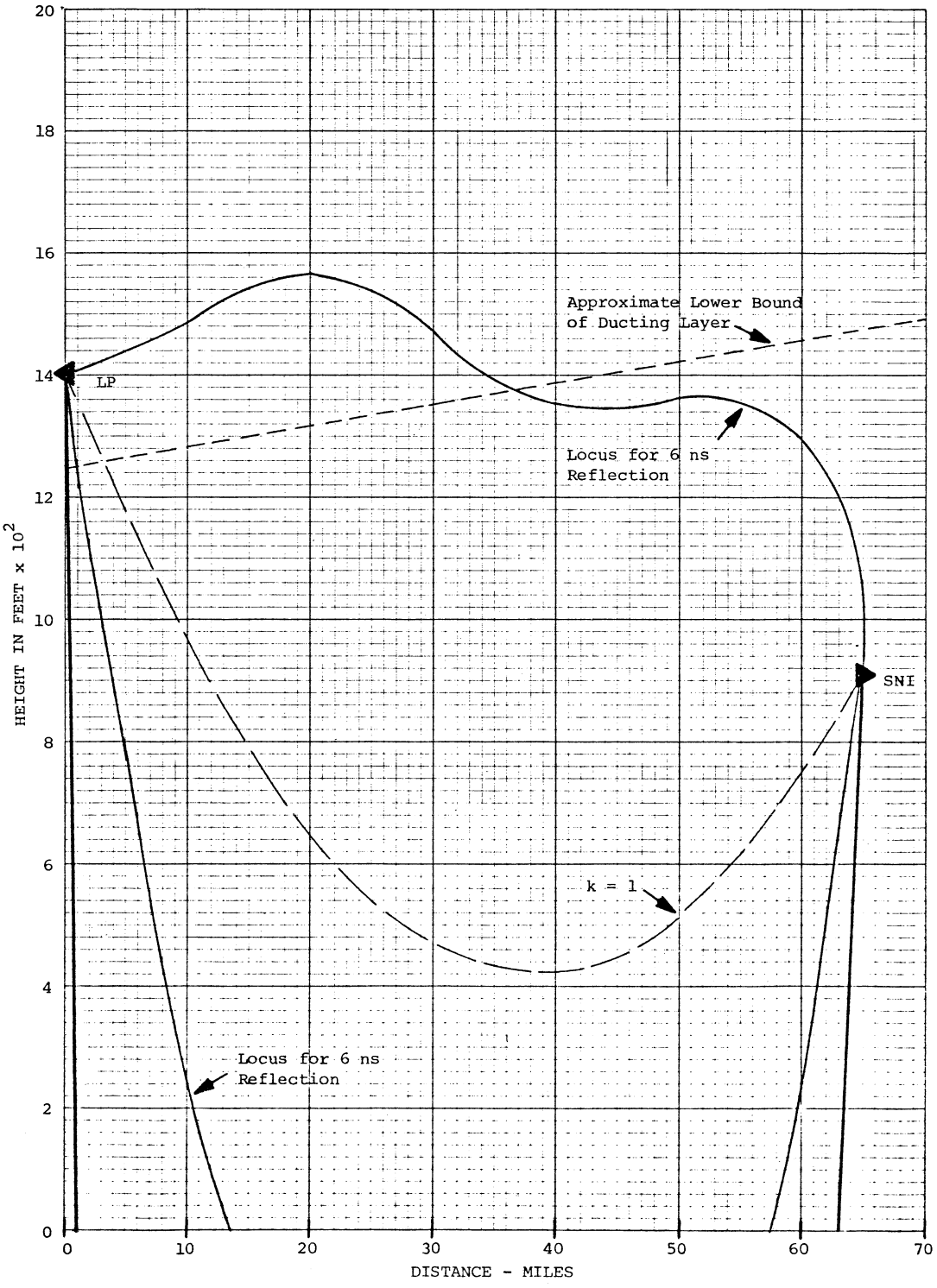


Figure A-19. Illustration of possible reflection type multipath from a strong ducting layer on 1 September 1978.

FORM OT-29
(3-73)

U.S. DEPARTMENT OF COMMERCE
OFFICE OF TELECOMMUNICATIONS

# BIBLIOGRAPHIC DATA SHEET

| | | |
|---|---|---|
| | 1. PUBLICATION OR REPORT NO.<br>NTIA Report 79-24 | 2. Gov't Accession No. |
| 3. Recipient's Accession No. | | |

4. TITLE AND SUBTITLE
Investigation of digital microwave communications in a strong meteorological ducting environment

5. Publication Date
August 1979

6. Performing Organization Code
NTIA/ITS

7. AUTHOR(S)
R.W. Hubbard

9. Project/Task/Work Unit No.
9103543

8. PERFORMING ORGANIZATION NAME AND ADDRESS
Institute for Telecommunication Sciences
National Telecommunications and Information Administration, U.S. Department of Commerce
Boulder, CO 80303

10. Contract/Grant No.
MIPR N6312678MP31106

11. Sponsoring Organization Name and Address
Capabilities Development Department
Pacific Missile Test Center (PMTC)
Point MuGu, CA 93042

12. Type of Report and Period Covered
NTIA Report FY 79

13.

14. SUPPLEMENTARY NOTES

15. ABSTRACT *(A 200-word or less factual summary of most significant information. If document includes a significant bibliography or literature survey, mention it here.)*

This report describes an experiment conducted over a LOS microwave link off the coast of southern California. The objective was to determine the effect of known amomalous propagating conditions, caused by persistent temperature inversions in the atmosphere on a wideband digital communications system. A channel probe was used to measure the effective impulse response of the transmission channel, and bit-error-rate (BER) measurements were made on the same probe test signal. In addition, a dual receiver was used to investigate the application of angle diversity on the reception of signals in this propagation environment.

The results of the experiment indicate that the test link should, if properly configured, support digital transmission at a mission rate on the order of 50 Mb/s. Recommendations for implementing a digital system for the specific link are given in the conclusions.

16. Key words *(Alphabetical order, separated by semicolons)*

Angle diversity; channel characterization; digital microwave communications; impulse response

17. AVAILABILITY STATEMENT

☒ UNLIMITED.

☐ FOR OFFICIAL DISTRIBUTION.

18. Security Class *(This report)*
Unclassified

20. Number of pages
95

19. Security Class *(This page)*
Unclassified

21. Price:

☆U.S. GOVERNMENT PRINTING OFFICE:1979-0-681-284/69

USCOMM-DC 29716-P73